

# **Energy Efficient Iterative Adaptive On-Off Control of Capacitively-Loaded Actuators for Micro-robots**

by

Bongsu Hahn

A dissertation submitted in partial fulfillment  
of the requirements for the degree of  
Doctor of Philosophy  
(Mechanical Engineering)  
in The University of Michigan  
2012

Doctoral Committee:

Assistant Professor Kenn Richard Oldham, Chair  
Professor Jessy W. Grizzle  
Professor Karl Grosh  
Professor Huei Peng

© Bongsu Hahn

---

2012

## TABLE OF CONTENTS

LIST OF FIGURES .....	iv
LIST OF TABLES .....	ix
LIST OF APPENDICES.....	x
ABSTRACT.....	xi
CHAPTER 1 Introduction.....	1
1.1 Motivation .....	1
1.2 Problem Description.....	3
1.3 Literature Review .....	6
1.4 Objective, Approaches, and Scope.....	9
1.5 Contributions.....	11
CHAPTER 2 Power Consumption Estimates for Components of Microscale Servo System.....	13
2.1 Capacitive Actuator and Analog Driving Circuit .....	15
2.2 Switching Drive Circuit .....	17
2.3 Sensing Circuit .....	25
2.4 Summary: Estimated Power Consumption versus Switching Drive Frequencies and Sampling Rates .....	30
CHAPTER 3 Model Free Adaptive On-Off Control .....	33
3.1 Definition of Variables, States, and Dimensions .....	33
3.2 System Description .....	35
3.3 Heuristic Adaptive (HA) On-Off Controller for a Micro-robotic Leg Joints .....	40
3.3.1 Controller Design .....	41
3.3.2 Convergence Analysis Approach.....	44
3.3.3 Convergence Analysis for 2 <sup>nd</sup> Order Microactuator .....	49
3.3.4 Validation by Simulation and Experiment.....	55
3.3.5 Summary of HA On-Off Controller .....	58

3.4 Stochastic Approximation Adaptive (SAA) On-Off Control.....	58
3.4.1 Controller Design .....	59
3.4.2 Convergence Analysis.....	64
3.4.3 Validation by Simulation and Experiment.....	71
3.4.4 Summary of SAA On-Off Controller.....	75
CHAPTER 4 Convergence Rate Estimation for the Adaptive On-Off Controllers and Prediction of Power/Energy Requirement .....	76
4.1 Problem Statement .....	76
4.2 Estimation of Convergence Rate.....	77
4.3 Case Study I: HA On-Off Control .....	83
4.4 Case Study II: SAA on-off control.....	90
4.5 Summary .....	97
CHAPTER 5 Comparison of Performance, Power, and Energy Under Various Control Schemes .....	99
5.1 Description of LQG and PWM Controller.....	99
5.2 Comparison to HA On-Off Control .....	101
5.3 Comparison to SAA On-Off Control.....	106
5.4 Summary .....	111
CHAPTER 6 Discussion and Conclusions .....	112
6.1 Discussion .....	112
6.2 Conclusions and Future Works .....	116
6.3 List of Publications .....	119
APPENDECIES .....	121
BIBLIIOGRAPHY .....	131

## LIST OF FIGURES

Figure 1.1 (a) Concept drawing of an autonomous micro-robot (b) Prototype micro-robotic leg joint, courtesy U.S. Army Research Laboratory .....	2
Figure 2.1 Block diagram of micro servo control system.....	13
Figure 2.2 Definition of $T_{act}$ and $f_d$ for sample analog and switching inputs. ....	15
Figure 2.3 An analog driving circuit for capacitively-loaded actuators.....	16
Figure 2.4 Switching drive circuit based on the basic level shifter with pull-up resistors to limit leakage current .....	18
Figure 2.5 Timing diagram for the circuit of Figure 2.4.....	19
Figure 2.6 RC models of CMOS inverters in Figure 2.4 .....	20
Figure 2.7 (a) Input wave forms and output signal based on Figure 2.5 for the CMOS inverter A of Figure 2.6 and (b) the corresponding short circuit current .....	21
Figure 2.8 (a) Input wave forms and output signal based on Figure 2.5 for the CMOS inverter B of Figure 2.6 and (b) the corresponding short circuit current .....	24
Figure 2.9 A capacitive sensing with differential capacitive sensing circuit amplifier .....	25
Figure 2.10 Noise vs. quiescent current of OP-Amps from Nation Semiconductors [44].....	30
Figure 2.11 Power consumption of two candidate drive circuitries and sensing circuitry with a 1nF capacitive microactuator at with 20V maximum input with respect to sample rates and switching drive frequencies .....	32
Figure 2.12 Total power consumption of sensing and switching drive circuitries with a 1nFcapacitive microactuator at 20V 'On' input with respect to sample rates and switching drive frequencies.....	32

Figure 3.1 General definition of switching instances, measured targets and outputs at each sample instance for on-off input.....	39
Figure 3.2 Definitions of switching times and sample times for a specific step controller .....	42
Figure 3.3 Sample nominal response to a switching input and bounds on uncertainty in output relative to response due to bounded, unknown nonlinearities .....	51
Figure 3.4 (a) Nominal change in output at first measurement point ( $x_p$ ) as a function of first switching time in current iteration ( $\tau_p$ ) and change in first switching time next iteration ( $\delta\tau_p$ ) (b) Magnitude of possible error in estimate of change in output at first measurement point ( $y_p^{k+1} - z_p^{k+1} - y_p^k - z_p^k$ ).....	52
Figure 3.5 Maximum change in second switching time ( $\delta\tau_s$ ) satisfying convergence criteria as a function of switching times $\tau_s$ and $\tau_d$ for $\tau_p = 0.003s$ .....	53
Figure 3.6 (Dotted points) Region of switching times for which some incremental change in switching time satisfies convergence criterion for at least one iteration (Circle points) Closed region of switching times satisfying convergence conditions when $r = 0.5$ .....	54
Figure 3.7 Simulation result of the nominal system (3.31) with model uncertainties.....	55
Figure 3.8 A piezoelectric actuator testbed.....	57
Figure 3.9 Sample experimental responses: (a) converging case and (b) non-converging case.....	57
Figure 3.10 Illustration of input time parameter definitions for SAA on-off controller .....	62
Figure 3.11 Nominal system output as a function of switching times $\tau_2$ and $\tau_3$ for $p = 3$ and $\tau_1=0.5ms$ , and marked regions of possible local minima/maxima when unknown, bounded nonlinearities present. ....	70

Figure 3.12 Sample image of the MEMS leg actuator .....	72
Figure 3.13 Step response and nominal linear dynamics of the experimental system .....	72
Figure 3.14 Simulation result of the nominal system (3.58) with model uncertainties.....	73
Figure 3.15 Experimental results for the system (3.58): (a) for target: 0.3 rad, (b) for target 0.2 rad .....	74
Figure 4.1 Actual Vs. estimated convergence rate for HA on-off controller with 100 Hz sample and driving frequency.....	85
Figure 4.2 Estimated convergence rate with respect to several initial values for the HA on-off controller .....	85
Figure 4.3 Experimental Vs. estimated convergencfe for HA on-off control.....	86
Figure 4.4 Estimated convergence rate with respect to several sample rates for HA on-off controller .....	88
Figure 4.5 Power consumption to reach the target error with respect to sample rates for HA on-off controller .....	88
Figure 4.6 Energy Dissipation to reach the target error with respect to sample rates for HA on-off controller .....	89
Figure 4.7 Energy evolution of HAA on-off control with further iterations after converging with respect to Sample rates.....	89
Figure 4.8 Actual Vs. estimated convergence rate for SAA on-off controller .....	92
Figure 4.9 Several single runs of actual convergence rate for SAA on-off controller .....	92
Figure 4.10 Experimental Vs. estimated convergence rate for SAA on-off controller .....	93
Figure 4.11 Estimated convergence rate with respect to the number of switching for the adaptive controller with SPSA .....	95
Figure 4.12 Power consumption to reach the target error with respect to the number of switching for SAA on-off control.....	95
Figure 4.13 Detail of Figure 4.12.....	96

Figure 4.14 Energy consumption to reach the target error with respect to the number of switching for SAA on-off control .....	96
Figure 4.15 Energy evolution of SAA on-off control with further iterations with respect to the number of switching .....	97
Figure 5.1 PWM generation with a saw tooth carrier wave and a desired signal .....	100
Figure 5.2 LQG controller step response with 1ms measurement sample rate for the system (3.31) with model uncertainties .....	102
Figure 5.3 PWM controller step response with 1ms measurement samples for the system (3.31) with model uncertainties .....	103
Figure 5.4 Control accuracy under various control schemes for the system (3.31) with model uncertainties over several stepping motions .....	104
Figure 5.5 Average power consumption of servo system components under various control schemes for the system (3.31) with model uncertainties.....	105
Figure 5.6 Energy dissipation under various control schemes for the system (3.31) with model uncertainties over several stepping motions .....	105
Figure 5.7 LQG controller step response with single measurement for the system (3.58) with model uncertainties.....	107
Figure 5.8 PWM controller step response with single measurement for the system (3.58) with model uncertainties.....	108
Figure 5.9 Control accuracy under various control schemes for the system (3.69) with model uncertainties over several stepping motions .....	109
Figure 5.10 Average power consumption under various control schemes for the system (3.58) with model uncertainties .....	110
Figure 5.11 Energy dissipation under various control schemes for the system (3.58) with model uncertainties over several stepping motions .....	110
Figure 6.1 Comparison of sensing power consumption between the state-of-the-art circuit and the conventional configuration .....	114



Figure 6.2 Comparison of power consumption using (a) conventional  
circuit to (b) state-of-the art one for HA on-off control case ..... 114

Figure 6.3 Comparison of power consumption using (a) conventional  
circuit to (b) state-of-the art one for SAA on-off control case ..... 115

## LIST OF TABLES

Table 1.1 Characteristics of various microactuator types [13] .....	3
Table 1.2 MEMS parameters and cause of uncertainty [17].....	5
Table 2.1 Coefficient of noise and power model of (2.31) and (2.32) for the case of Figure 2.9 .....	29
Table 3.1 Measurement errors as $k$ goes to infinity at Figure 3.9 (a).....	58
Table 3.2 Nominal system coefficients and bounds on corresponding nonlinearities deviating from these coefficients.....	71
Table 5.1 The summary of estimated power and energy required to achieve a desired performance under various control schemes with typical switching instances and sample rate to control the system (3.31) with model uncertainties.....	106
Table 5.2 The summary of estimated power and energy required to achieve a desired performance under various control schemes with typical switching instances and sample rate to control the system (3.58) with model uncertainties.....	111

## LIST OF APPENDICES

APPENDIX A. VOLTAGE OUTPUT AT EACH FUNCTIONAL COMPONENT IN FIGURE 2.9..	121
APPENDIX B. EFFECTS OF CHANGES TO SWITCHING TIMES IN THE HA ON-OFF CONTROL .....	121
APPENDIX C. RANGES OF POSSIBLE $\partial y_f / \partial \tau_Q$ DURING SAA ON-OFF CONTROL FOR A 2ND- ORDER NONLINEAR SYSTEM .....	127

## ABSTRACT

This dissertation proposes a pair of strategies for model-free, iteratively adaptive ‘on-off’ switching control of capacitive micro-actuators with limited sensing rates and significant model uncertainty. A desired actuator motion is to be repeated many times, with the ability to adjust the input sequence between movements. These strategies are intended to limit power consumption of a servo control system for capacitively-loaded piezoelectric micro-actuators of autonomous walking micro-robots.

The first strategy is based on a heuristic dynamic search algorithm that iteratively searches for optimal switching instances, while the second uses a stochastic gradient approximation algorithm. The first method uses simple adaptation laws based on known, general feature of the dynamic behavior of the actuators and a small number of measurements taken during each iteration. The second method adjusts switching instances to minimize an objective function using simultaneously perturbed stochastic approximation (SPSA). The SPSA estimates the gradient of the objective function and uses just a single sensor measurement in each iteration of actuator movement.

Both approaches can be implemented with much lower sensing and driving circuit power than would be needed to implement a conventional control structure such as pulse-width-modulation (PWM) or analog driving with real-time feedback. Energy savings are verified by comparison to the conventional control structure, using power estimates for the components of the servo system. Methods of convergence analysis and conditions are also proposed for predicting convergence speed and stability of both approaches, and applied to sample target piezoelectric actuators. In addition, the controllers are tested in simulation and experimentally on various piezoelectric actuator test beds, and related to future research needs for realization of highly-mobile micro-robots.

# CHAPTER 1

## INTRODUCTION

### 1.1 Motivation

Miniaturization of sensors and actuators through developments in the field of Microelectromechanical Systems (MEMS) can enable very low-power, small footprint implementation of a variety of engineered systems. However, power consumption of microscale servo systems for autonomous or portable applications can still be challenging to manage. In these applications, power consumption must be strictly limited since the micro-devices are to be self-powered from an embedded battery without any physical connection to an external power source. Hence, low-power design with respect to energy management has been a popular research subject for micro-autonomous or portable MEMS applications [1, 2].

When autonomous micro-systems rely on some form of servo control, power requirements are influenced by all components of servo system such as microprocessor units (MPUs), actuators, sensors, and other supporting circuitry. Meanwhile, the power budget is limited by lifetimes of batteries and the payload or size of the micro-system in terms of its mass and volume [1]. Most previous research has focused on developing miniature power sources [3], improving efficiency of voltage converters [4], providing low-power sensing circuitry [5], or creating high-performance but low-power MPUs [4, 6]. In the contrast, studies of how best to use such technologies for energy efficient actuator control, incorporating appropriate sensing and driving strategies, have been relatively sparse.

One motivating application where power consumption of microactuator control systems must be strictly limited is the development of autonomous micro-robots, such as that shown conceptually in Figure 1.1. This example robot is operated by leg joints consisting of thin-film piezoelectric actuators. Candidate high-force, low-power

microactuators for millimeter-scale, high-mobility micro-robots are thin-film piezoelectric microactuators [7] or contractive electrostatic actuators [8].

These actuators act as capacitive loads and typically feature capacitances of just a few nanofarads or smaller, equating to a few microjoules of energy consumption or tens of microwatt of power consumption each time they are charged. The current best case performance of individual actuator has been to generate up to  $3 \times 10^{-9}$  N·m of work and 3 degrees or more rotational motion in a  $500\mu\text{m} \times 100\mu\text{m}$  area [9]. The resulting maximum angle of a leg joint with 8 actuators is 24 degrees [10]. The payload capacities for a high-mobility microrobot based on these actuators are in the range of 5 to 50mg [10]. With state-of-the-art battery power densities of approximately 80W/kg at this scale [11], this corresponds to power and energy availability to all robot systems on the order of only 0.4 to 4 mW and 0.8 to 8mW·h, respectively, even neglecting other uses of available body mass. Meanwhile power consumption of sensing and driving circuitry can easily exceed actuator power or even total power availability when conventional techniques are used to implement motion control (as to produce a robot's walking gait) in a practical system [12].

Under these conditions, it is very important to identify control strategies that could provide effective servo control under an extremely constrained power budget. This emphasizes the need for extremely low power servo systems accounting for power consumption of not just actuators, but also power electronics and sensors.

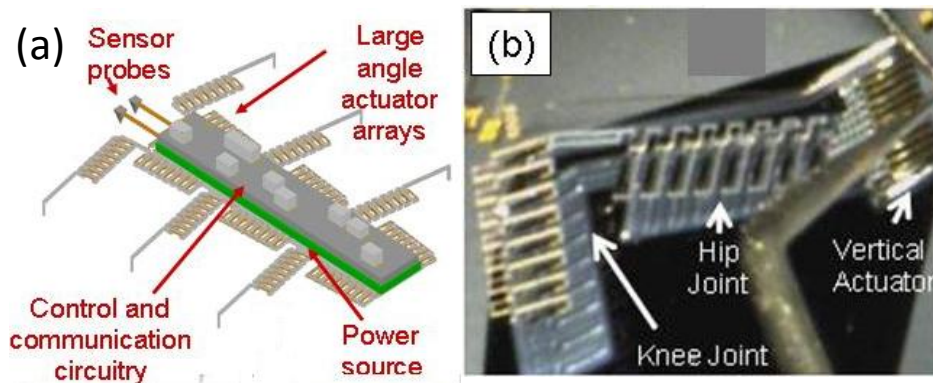


Figure 1.1 (a) Concept drawing of an autonomous micro-robot (b) Prototype micro-robotic leg joint, courtesy U.S. Army Research Laboratory

## 1.2 Problem Description

### 1.2.1 Power Consumption of Driving and Sensing Techniques for Capacitive Actuator Control

Table 1.1 shows characteristics of various types of actuators commonly used in the MEMS field. As can be seen, the efficiency of capacitive microactuators is much higher than the efficiency other types of actuators. This advantage of the capacitive actuators, along with fast response times and, in the case of piezoelectric actuation, large deflection and force capabilities, may be useful to for autonomous microsystems.

Table 1.1 Characteristics of various microactuator types [13]

Actuator		Maximum deflection	Maximum force	Speed of actuation	Efficiency (%)
Capacitive	Electrostatic	Low	Low	Very fast	> 90
	Piezoelectric	High	Medium	Fast	10 – 30
Thermal		Medium	Very high	Slow	< 5
Shape memory alloy		High	Very high	Slow	< 5

However, even when capacitive microactuators are power efficient, other servo component around the actuators may not satisfy a strictly limited power budget of an autonomous microsystem. Commonly used driving methods for micro-scale capacitive actuators are analog or pulse-width modulation (PWM) driving schemes implemented with operational amplifiers or electric switches, respectively. To operate at full force and/or displacement, capacitive actuators require relatively high voltages (20 to 30 V for piezoelectric actuation, generally higher for electrostatic actuation).

This results in both conventional analog and PWM driving circuitry being very inefficient. Under an analog drive, for example, typically 95% of all servo system power usage for the actuators is wasted in amplifiers [14]. The resulting power consumption of the amplifiers, thus, is on the order of hundreds of microwatts to a few milliwatts. While this typically drives system designers to PWM techniques, even these approaches may

require excessive power usage, due to the repeated charging and discharging of the capacitive load at high-frequencies. For instance, a 1 nF piezoelectric actuator and switching circuit consumes  $400\mu\text{W}$  of power when PWM techniques are used at a typically driving frequency on the order of 20kHz. Both methods, hence, may be infeasible for energy efficient control.

When the capacitive actuators operate with feedback, power consumption of sensors and sensing circuitry also can rival or exceed the power budget of the system. Among various possible scenarios, sensing power often outweighs actuation power when position sensing from micro-scale sensors is desired during the actuator operation. Furthermore, sensing circuit power, particularly for capacitive sensing circuits, rises dramatically with sample rate [15]. For instance, even at relatively low sampling rates, on the order of 10-100 Hz, the power consumption of capacitive sensing circuits, commonly used in MEMS devices, is typically on the order of about 1 to 2mW, according to the power estimates presented in Chapter 2 of this dissertation. Most feedback systems for microactuators with full measurement of dynamics (i.e., full observability, sampling above the Nyquist sample rate) use even faster sample rates.

These conditions, then, make it very difficult to use position sensing in conventional real-time feedback control under the limited power budget of a microrobot. It is, however, important in many applications to provide robustness and precision with feedback position sensing, especially when there exist system uncertainties or nonlinearities, as will be discussed in more detail in the following section.

### **1.2.2 System Uncertainties and Nonlinearity in Micro Servo Systems**

When the dynamics of the system to be controlled are well known mathematically, sensor measurements may be omitted and open-loop input sequences used, including for open-loop energy minimization. Unfortunately, it may not be easy to achieve an accurate mathematical model of a microscale system due to lack of consistency of the system parameters resulting from fabrication variation and a lack of analytical modeling methods for many MEMS applications [16]. Changes in environmental conditions can also be severe for microscale systems and cause



uncertainties during operation. Some possible uncertain parameters and causes of the uncertainty in MEMS applications are presented in [17] as shown in Table 1.2.

Table 1.2 MEMS parameters and cause of uncertainty [17]

Physical Parameter	Cause of Uncertainty
Mass	<ul style="list-style-type: none"> <li>• Moisture absorbance</li> <li>• Line width and thickness errors</li> <li>• Material density inconsistency</li> </ul>
Spring Constant	<ul style="list-style-type: none"> <li>• Flexure width and thickness errors</li> <li>• Thin-film material constants inconsistency</li> </ul>
Damping	<ul style="list-style-type: none"> <li>• Varying humidity, pressure, and temperature</li> <li>• Gap error</li> </ul>

Among capacitive microactuators, while thin-film piezoelectric actuators have smaller hysteresis than most piezoelectric actuators, they do display both some hysteresis, nonlinear gains, and damping behavior that are difficult to predict or model. In addition, when a micro-robot locomotes, terrain roughness, ground contact force or friction, and other obstacles around the robot may grow large relative to the robotic size scale [18]. In order to overcome these scenarios, it may be desirable to implement a feedback control system that is robust or can adapt an input sequence applied to the system using feedback. This requirement, however, may dramatically increase power consumption of micro-servo systems when a real-time feedback control is applied as discussed previously. Therefore, it may be very desirable to design a control strategy to overcome the microsystem uncertainties with reduced sample rates

To summarize, an ideal controller, for capacitive actuators in micro-robots with model uncertainties and/or nonlinearities under a strict power budget, would have the following features;

- (1) Few switching events that charge actuators,
- (2) Minimal standby or leakage current when driving the actuators,
- (3) Low frequency sampling rates,
- (4) Ability adapting to model uncertainties and/or nonlinearities,
- (5) Simple computation algorithms.

This dissertation, therefore, focuses on a pair of controllers with the features discussed above. Related works to these types of controllers are presented in the next section.

## 1.3 Literature Review

### 1.3.1 Locomotion Control of Microrobots

Various control approaches for micro-robotic locomotion have been proposed in the literature. These are related to walking, jumping, flapping, and other forms of locomotion. From a viewpoint of handling power consumption and system uncertainties in microscale servo control systems, these approaches can be classified into three categories: (1) open loop control without consideration of power limitations, (2) open loop control with consideration of power consumption, and (3) closed loop control without consideration of power consumption.

Researchers in the first category have proposed mechanical structures for robots with thermal actuation [19], electromagnetic actuation [20], piezoelectric actuation [21], and electrostatic actuation [22], respectively. In these works, the researchers in [19, 20], and [21] demonstrated gait motions with simple input signal into the actuators to operate the robots. The inputs utilized different resonance frequencies [19], switched sequential logic [20] for each leg, or shifting resonance frequencies for body [21]. One other work, [22], showed an untethered mechanism to deliver power and/or control signals, but the robot needed to be operated on a capacitively-coupled substrate. Without control, these prior robots could not move to specific target locations or with precise gaits, and have had to be operated on specific ideal surfaces. In addition, these researchers did not consider how much power would be consumed within the control circuitry and actuators to implement their robots.

The works in the second category, [23 – 26], implemented successful power-limited circuits for power delivery, actuation control, and power source management (a solar cell) on the robot body. To overcome power and payload limitations, very simple control input sequence were analyzed and embedded in a basically functional MPU of clocking registers. In addition, a CMOS level shifter [24], which is broadly used in IC

technology and PWM control schemes [26], was used to drive high voltage operated actuators to reduce actuation power usage. The algorithm did not use any feedback measurement to identify system dynamics, and the controller was not designed with an accurate dynamic model.

Very useful methods were proposed to overcome uncertainties and nonlinearity and, thus, achieve precise position control of the microrobots in [27 – 30], which are included in the last category. Flapping motion for a micromechanical flight insect was controlled in [27 – 29]. In these works, the authors utilized PWM switching control to drive piezoelectric actuators more efficiently than with an analog controller. The switching input was generated by a state estimator including nonlinear and time-varying terms for the actuator, stochastic model of the noise and disturbances, and wing force sensing. In another work, an adaptive control approach was recently announced to control an endoscopic capsular microrobot [30]. This was model reference adaptive control (MRAC) with a known structure but unknown model parameters. To add robustness and accuracy, the authors accounted for uncertainties in parameters, surface forces modeled with sliding friction and surface adhesion, and closed-loop behavior in simulation. These works showed successful locomotion with a well designed control architecture when encountering uncertainty and nonlinearity of the system. However, the authors did not consider carefully how to schedule or reduce sensing measurements, which may be constrained in use due to power budget when the robot is untethered.

### **1.3.2 Control Strategies for Handling Low Power Consumption with Model Uncertainty and/or Nonlinearity**

In fields beyond micro-robotics, power amplifiers to drive capacitive actuators have been a topical subject for mitigating power dissipation of servo systems in both micro- and macro-scale applications. Among candidate approaches, switching amplifiers [14], [31, 32] have been proposed to implement PWM control but these can still require unacceptable power consumption for high-speed microactuators due to high frequency of operation. Charge recovery methods [33 – 35] have also been proposed to further reduce power consumption of the drive by recovering stored energy in the capacitive actuator to

a storage capacitor when it is turned off, but power usage is still primarily dictated by switching frequency. Meanwhile, on the sensing side, ultra low power interfaces for capacitive sensors were designed in [15] and [36 – 38]. While the power consumption of their circuitries was in the range of a few microwatts or even in a few nanowatts, this low power is guaranteed only for low sample frequencies on the order of hundreds of hertz or less.

Control algorithms, hence, should ideally be adapted to utilize slow switching inputs and low-frequency sensing, in order to make fullest use of available power limiting techniques. In related work to limit energy use in slow switching control, researchers have studied optimal on-off control methods to minimize fuel consumption in spacecraft [39, 40]. However, their methods were not directly applicable to the capacitively-loaded actuation, where power consumption is dictated by the rate at which the actuator is switched ‘on’, rather than the amount of time spent in the ‘on’ state. Various on-off control algorithms have also been suggested to estimate optimal switching instances. However, most existing on-off control algorithms rely on mathematically accurate knowledge of system dynamics [7], [41 – 46], for open-loop situations or comparatively high-frequency sensing in order to implement decision rules on feedback measurements [47].

Previous controllers oriented towards adaptive on-off control, as well as most other adaptive switching controllers, rely on model-based adaptation schemes, where the form of the system dynamics was known but not all of the parameters [48 – 51]. There are also significant works on model-free control of unknown, nonlinear systems in [52, 53], but these have not been applied to on-off control. Other, model-free adaptive controllers organized around neural nets [54 – 56], could potentially perform function estimation in the on-off context as well, though the assumption of an affine dependence on input in most cases prevents existing algorithms from being directly applicable when switching time is the input being adapted. Alternate, related adaptive controllers utilize fuzzy logic or sliding mode control, but to date these controllers were used to adapt a single control parameter [57, 58]. Most of all, the adaptive control approaches discussed in this paragraph were necessarily operated with comparatively high-frequency sensing measurement.

## 1.4 Objective, Approaches, and Scope

The main objective of this dissertation is to design low power controllers with a very low frequency on-off switching inputs and limited sensor measurements for microactuators with unknown nonlinear contributions to the system dynamics. The target application is capacitive piezoelectric microactuators in an autonomous microrobot. Only control strategies covering sensing and driving power consumption are evaluated although there are several other, less significant, components consuming power in such microsystems. Two elements are utilized to meet the constraints on controller capabilities and, thus, achieve the objective: (1) on-off switching control and (2) iterative adaptation of the switching instances without explicit model information, although a nominal model is used to select controller parameters.

On-off controllers are often used by engineering systems with only basic actuator capabilities, limited computation resources, and/or tight energy constraints as shown in the section of literature review. On-off control, in which only a few switching transitions between ‘on’ and ‘off’ states are used to guide actuator motion, can dramatically reduce power consumption of capacitive actuators by reducing the number of times that the actuator is charged. In return, on-off control entails a degradation of system performance, due to oscillations between switches and excitation of high-frequency dynamics. Nonetheless, under extreme power constraints, such as those on an autonomous microrobot, this trade-off may be acceptable.

In theory, with sufficient sampling speed on the output displacement, system identification techniques may be used to identify the system model or uncertainty. From there, optimal on-off switching times may be computed to produce desired motions using integer programming or other optimization techniques. However, this optimization is computationally intensive, and the high sampling rate is required for effective system identification. As discussed in the section of problem description, power consumption of sensing transducers and circuitry used in MEMS devices, such as capacitive position sensors, increases greatly with sampling rate. This makes it very difficult to implement any control strategy based on real-time feedback for an autonomous microsystem.

Fortunately, in the case of terrestrial micro-robotics which are motivating applications, actuator motions are expected to repeat many times, as in walking or running gaits. This allows for measurement at lower sampling frequencies, which can be compared over several iterations of a given movement, to guide on-off switching sequences producing a desired displacement or trajectory. For certain classes of system, this can be performed without any model of the system in the controller itself, which further simplifies computational requirements from the microrobot. Therefore, the second aspect of the controllers presented here is the use of step-to-step, or iterative, adaptations of the on-off switching sequence to adjust for unknown dynamics with relatively low sensor sampling rates.

This dissertation examines two types of iterative adaptive structures for capacitively-loaded micro-robotic leg joints, one based on deterministic heuristic switching rules and the other based on a stochastic gradient approximation to determine proper switching instances. The heuristic method is targeted for control of micro-robotic steps, by directly adapting specific time periods within an on-off sequence using measurements taken over successive iterations. In this controller, the sample times may optionally be slower than Nyquist, although this limits feasible outcomes of the adaptation; all behavior of a system may not be observed but a limited number of measurements may be available and outputs at those instance potentially regulated. The second, stochastic gradient approximation based approach is for the problem of selecting transition times of an on-off input sequence, based on the simultaneous perturbation stochastic approximation (SPSA) developed by Spall et al. [59 – 62]. This method poses several benefits for power minimization in micro-robotics, including a need for only one sensor measurement each iteration an individual actuator moves through a desired motion, the ability to perform computation between iterations to reduce processor requirements, and effectiveness in the presence of noisy sensors.

In both cases, the controllers are performed without any stored model of system dynamics in the controller, but convergence range is analyzed with some knowledge of general system behavior such as bounded nonlinearity with respect to a known nominal linear model. Eventual convergence of switching times to at least locally optimal values is guaranteed for some limited range of initial switching instances selections and

adaptation gains. The detail methods of convergence analysis are studied and examined for specific 2<sup>nd</sup> order systems of microrobot leg actuators. In addition, this dissertation investigates how fast an object function or output error reaches zero or a desired error level in order to predict total energy required to identify the optimal switching time. This type of investigation is generally known as analysis of convergence rate of output error. Here, a limited approach to convergence rate estimation is implemented that makes use of the binary nature of on-off inputs (0 or 1) and knowledge about behavior in the known regions of convergence.

Then, using compiled power estimates of servo system components, the proposed control strategies are compared to conventional linear-quadratic-Gaussian (LQG) with analog and PWM implementation in terms of power/energy dissipation and performance, to provide insight of advantages and limitations of the proposed controllers.

## **1.5 Contributions**

The main contributions of this dissertation are the analysis of power consumption related to components of microscale servo systems, design of model-free iterative low power control using on-off switching drive and minimum measurements, and development of a convergence rate methodology for an iterative switching adaptation.

Based on the analysis of power consumption in servo system components, primary factors and mutual correlations related to power consumption and noise are examined and compared. This examination provides proper insight and understanding of how to approach controller design to reduce power consumption of an autonomous microsystem under appropriate performance constraints.

The developed controllers make it possible for control to be implemented at much lower overall power and energy levels than would be needed to implement a conventional control strategy such as through LQG and PWM with real-time feedback. In addition, a method for predicting convergence range of systems with nominally linear dynamics and unknown, bounded nonlinearities is described, and applied to sample target capacitive microactuators. In turn, the proposed methodologies provide a unique perspective on

managing energy losses in feedback control of microactuators and some analytical techniques for examining behavior of the resulting system.

Finally, a proposed method for predicting convergence rate provides an ability to identify strategies for reducing total energy usage of control system when identifying optimal input sequences for repeated actuator motions, using predicted convergence behavior for various selections of adaptation gains, the number of switching instances, and sampling times. Error in measured outputs is estimated using upper bounds on output error, as a function of error in on-off switching times, and lower bounds on the change in switching times from iteration to iteration. Using the upper bound on error provided in this work, simulation and experimental results from the test case of a capacitively-loaded microrobotic leg joint indicate reasonable agreement between estimated error and full controller behavior.

The on-off iterative adaptive schemes to be described in this dissertation are targeted for control of micro-robotic steps, by directly adapting specific time periods within an on-off sequence using measurements taken over successive iterations, without any model of system dynamics. This requires limiting the desired motion to specific profiles (in these cases, smooth steps to various reference levels) and only transient performance may be predicted reliably. However, the benefit is an extremely simple control law to implement, with guarantees on convergence to certain final positions for systems with bounded nonlinearity and much lower power and energy level than conventional control schemes.



## CHAPTER 2

### POWER CONSUMPTION ESTIMATES FOR COMPONENTS OF MICROSCALE SERVO SYSTEM

To design a low-power controller for a micro-actuator, it is important to understand the sources of power consumption in the potential control system. Figure 2.1 shows the basic structure of the type of microscale servo control system under discussion. Power in the system is consumed by the actuator, driving circuitry, sensing circuitry, and control circuitry from a given battery power source. In addition, inefficiency in the voltage converter introduces a power loss when converting low voltage of a battery to high voltage for the actuator.

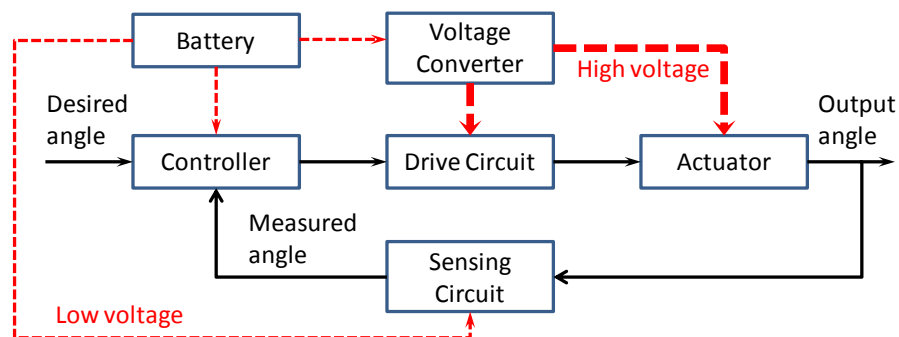


Figure 2.1 Block diagram of micro servo control system  
(dashed lines: power flows: solid lines: signal flows)

The most important components of the proposed control system are actuators and driving and sensing interfaces, which cause the largest portion of the power losses and noise generation for microscale servo control [10]. Hence, it is important to be able to predict these effects for incorporation into controller design, as well as to improve performance of the overall system. It should be noted that control (computation) circuitry and the voltage converter may need a relatively large amount of power in this microscale

system, as well; for instance, a state-of-the art DSP, TMS320C5000 [63], consumes up to 150 $\mu$ W at standby mode and adds 150 $\mu$ W per MHz operation. However, for the most part this is smaller than actuator and sensor power consumption, and voltage converter and control circuitry are considered out of the scope of this work. The aim of this work will be specifically to study an optimized low power control strategy accounting for sensing, driving, and actuators.

In this chapter, to estimate certain components' power consumption quantitatively, a capacitive actuator, two types of actuator driving circuits, and a sensing circuit are analyzed. One of the driving circuits is an analog driving circuit based on power op-amps, which is appropriate to use continuous input control, and the other is a switching drive circuit based on CMOS, which is used for a switching control such as PWM or on-off control. However, the analog driving circuit is included to compare power usage of switching versus analog control methodologies. Both circuits were designed specifically for a low-power, small capacitance architecture.

The sensing technique under discussion is taken to be capacitive sensing. Capacitive sensing is considered suitable for autonomous microsystems because capacitive sensors typically offer higher sensitivity but consume less power than other types of sensors, such as inductive, piezoresistive, and resistive sensors at that scale [64]. Although piezoelectric sensors can offer high sensitivity and similar properties of power consumption, this sensing technique is not ideal for position control systems since the piezoelectric sensors cannot be used for static measurement. Hence, an interface circuit for capacitive sensor is analyzed to determine power dissipation. A common type of the capacitive sensing interface is a differential capacitive sensing circuit [65]. This configuration consists of several op-amps. Since the op-amps in such a circuit dominate power dissipation, careful selection is taken in this work to reduce sensing power usage by proper circuit analysis.

Based on the following analysis, the primary factors related to power consumption and noise are examined and compared. This examination may provide proper insight how to approach controller design to reduce power consumption with appropriate system performance.

## 2.1 Capacitive Actuator and Analog Driving Circuit

### 2.1.1 Power Consumption of Capacitive Actuator

Average actuator power can be estimated as the amount of energy during charging and discharging over the course of motion, multiplied by the frequency that the actuator is charged, as in

$$P_{act} = \frac{C_{act}}{2T_{act}} \int_0^{T_{act}} u^2(t) dt \quad (2.1a)$$

$$P_{act} = C_{act} V^2 f_d \quad (2.1b)$$

where,  $u(t)$  and  $V$  are the voltage input used to charge the actuator at time  $t$ ,  $C_{act}$  is actuator capacitance, and  $T_{act}$  and  $f_d$  are the time period of actuator charging as shown schematically in Figure 2.2. Equations (2.1a) and (2.1b) are applicable for when the actuator is driven by analog input and switching input, respectively, with  $f_d$  equal to the frequency of individual motions ( $1/T_{act}$ ) multiplied the number of times the actuator is charged during each motion.

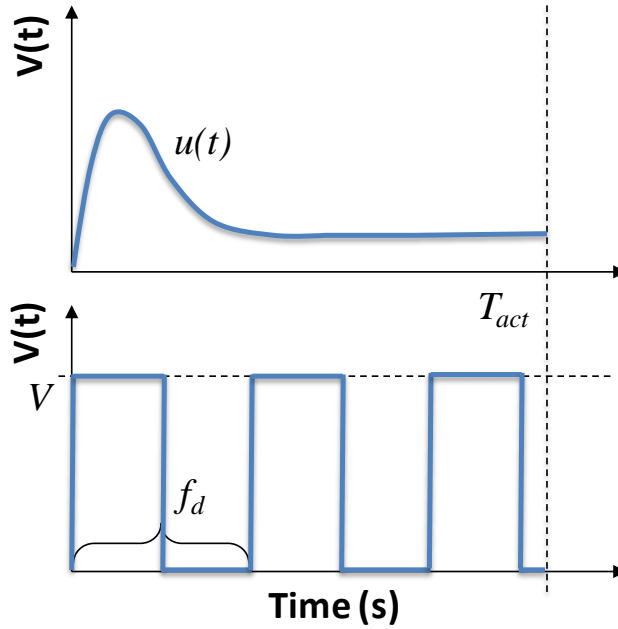


Figure 2.2 Definition of  $T_{act}$  and  $f_d$  for sample analog and switching inputs.

### 2.1.2 Analog Circuit Description and Power Consumption

Power op-amps are traditionally used to drive capacitively-loaded actuators when a continuous analog input is to be applied. Since capacitive loads can affect an op-amp's linear response, unexpected results may be produced. For instance, they change the transfer function, which affects the system's AC and step response [66]. However, this type of approach is still broadly used because of its simplicity to implement and use, with appropriate methods such as series resistor or shunt resistor compensation added to mitigate the above drawbacks.

Figure 2.3 is a basic driving circuit with inverting amplification and is used to estimate power dissipation of an analog driving circuit. Power consumption of the circuit is dominated by the op amp's quiescent current,  $I_{q,op}$ , and actuator capacitance,  $C_L$ , at low frequencies, while the series resistor,  $R_{iso}$ , will dominate at high frequencies as follows,

$$P_{an} = (V_s - (-V_s)) \left( I_{q,op} + 2V_o C_L f_a \right), \text{ if } f_a \ll \frac{1}{2\pi R_{iso} C_L} \quad (2.2)$$

$$P_{an} = (V_s - (-V_s)) \left( I_{q,op} + \frac{V_o}{\pi R_{iso} C_L} \right) - \frac{V_o^2}{R_{iso}}, \text{ if } f_a \gg \frac{1}{2\pi R_{iso} C_L} \quad (2.3)$$

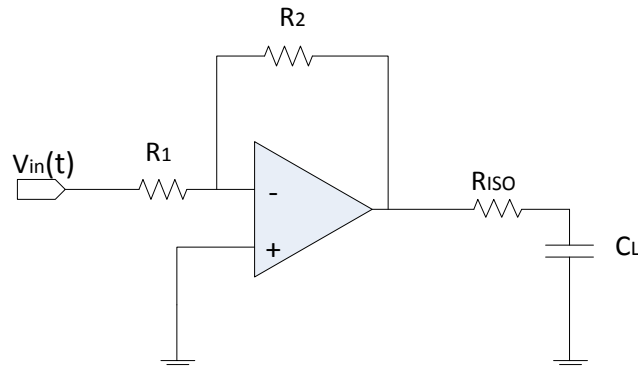


Figure 2.3 An analog driving circuit for capacitively-loaded actuators

where,  $V_s$ ,  $I_{q,op}$ , and  $V_o$  are supply voltage, quiescent current, and output voltage of the op amp, respectively, and  $f_a$  is the frequency of the analog command input to the actuator.

Since for micro-scale systems the value of  $V_s$  and  $I_{q,op}$  are larger than those of other components regardless of  $f_a$ , power dissipation by the circuit itself can be estimated as

$$P_{an} \approx (V_s - (-V_s))I_{q,op} \quad (2.4)$$

Existing low-power op-amps, such as the Analog Device OP490 [97], may require approximately 400 $\mu$ W with 10 nA quiescent current and  $\pm 20$ V supply voltage for the circuit in Figure 2.3.

## 2.2 Switching Drive Circuit

### 2.2.1 Circuit Description

An alternative method for providing voltage inputs to a microactuator is with a switching drive circuit. To limit switching losses in the interface between a low-voltage controller and the comparatively high-voltage actuators, a low power switching circuit was designed to interface the two elements. The switching circuit designed for the micro-capacitively-loaded actuators consists of CMOS inverters with a level shifter. CMOS inverters are a commonly used switching circuit configuration in the integrated circuit design field for reducing power consumption because in the ideal case, there is no static current and power is consumed only at the “on” or “off” transition time.

However, a CMOS inverter alone cannot be used directly for driving the actuators. While the actuator should be driven at 20 to 30 V or more, most IC circuits, as are typically used to implement a control law, operate at 5 V, 3.3 V, or less. Therefore, a level shifter based on the CMOS inverter was designed to interface between a high voltage and a conventional IC process [31, 67]. In order to reduce the power consumption

of the circuit, two resistors are added to the basic-level shifter. The conceptual circuit is shown in Figure 2.4.

Note that the addition of these resistors to the inverter helps to reduce peak leakage current during the switching transitions. While this loss is typically of little consequence when using larger actuators, it can be a substantial portion of energy consumption when working with microscale capacitive load actuators having comparatively small capacitance. Since these resistors can be equivalent to an RC circuit with a load capacitor of  $C_l$  or  $C_m$ , they can affect the rise and fall time of on-off signal. Therefore a proper value of the resistors should be selected to satisfy both the power consumption and the driving performance.

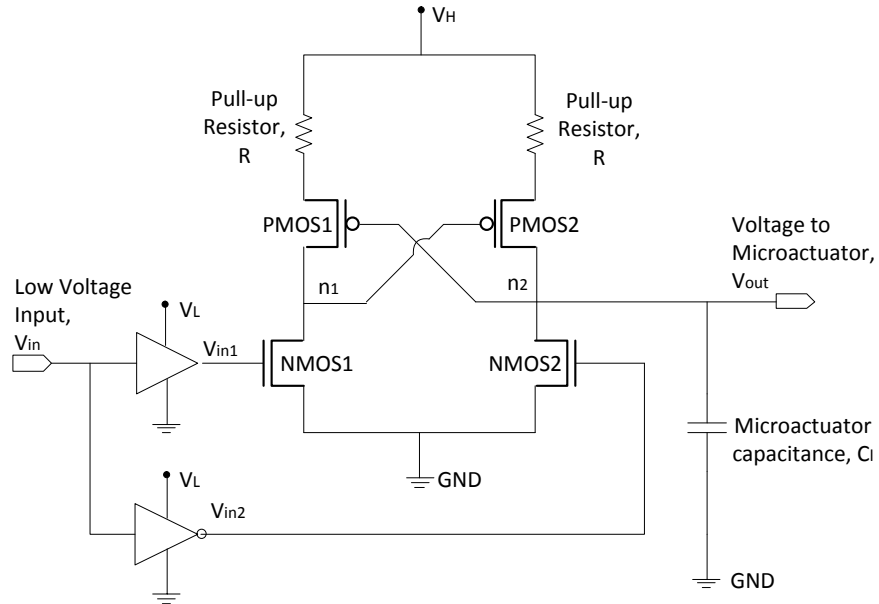


Figure 2.4 Switching drive circuit based on the basic level shifter with pull-up resistors to limit leakage current

The operation of the circuit can be explained through the timing diagram shown in Figure 2.5.  $V_H$  is a higher voltage than  $V_L$  so that  $V_{in}$  is converted from a low voltage level,  $V_L$ , to a high voltage level,  $V_H$ . The procedure of converting proceeds:

When  $V_{in}$  is high (equal to the  $V_L$  value), low voltage transistor  $V_{in1}$  also goes to the input voltage level,  $V_L$  value while  $V_{in2}$  falls down to the GND.

Due to these two input operation, NMOS1 turns on and thus pulls  $n_1$  to GND ('a' of Figure 2.5) while NMOS2 turns off.

(1) This causes PMOS2 to turn on and hence  $n_2$  is pulled up to  $V_H$  ('b' of Figure 2.5), causing PMOS1 to be turned off.

(2) Now when the  $V_{in}$  falls,  $V_{in2}$  goes to  $V_L$  and  $V_{in1}$  falls to the GND.

(3) In this phase, NMOS2 and PMOS1 are turned on while NMOS1 and PMOS2 are turned off.

(4) This leads  $n_2$  to be pulled down to GND ('c' of Figure 2.5) and  $n_1$  to be pulled up to  $V_H$  ('d' of Figure 2.5).

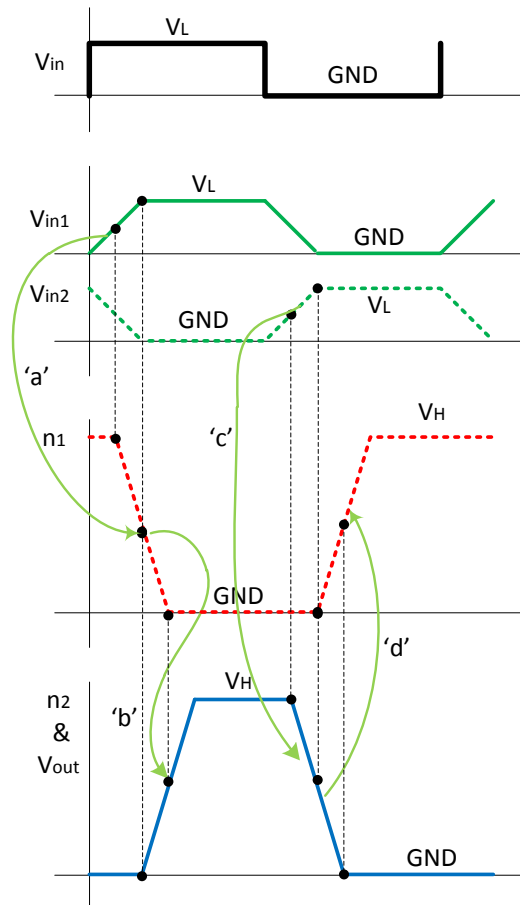


Figure 2.5 Timing diagram for the circuit of Figure 2.4

### 2.2.2 Power Dissipation of the Circuit

The two CMOS inverters of the on-off circuit in Figure 2.4 are considered as RC circuits as shown in Figure 2.6 in order to estimate power dissipation. In Figure 2.6,  $R_p$  and  $R_n$  are a pMOSFET and nMOSFET equivalent resistance, respectively, and  $C_m$  is an equivalent capacitance of the MOSFETs. There are two primary components that make up the power dissipation in the CMOS inverter: dynamic power and short circuit power dissipation [68].

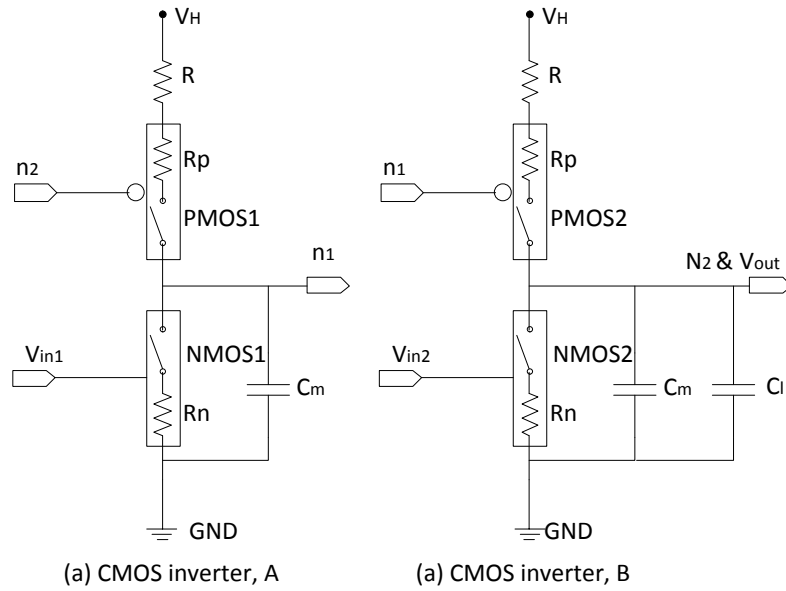


Figure 2.6 RC models of CMOS inverters in Figure 2.4

Dynamic power is the power needed to charge and discharge the capacitance of  $C_m$ . Therefore the dynamic power dissipation can be estimated by a similar approach to that used to calculate the energy stored in a capacitor after the transition completes and the capacitor is fully charged to a voltage level. Assuming that the CMOS inverters in Figure 2.6 are switched on and off in a  $1/f_d$  time period, then the average dynamic power,  $P_{C_m}$ , dissipated by two capacitors of  $C_m$  is equal to

$$P_{C_m} = 2C_m V_H^2 f_d \quad (2.5)$$



The short circuit power dissipation happens during the time when both the nMOSFET and pMOSFET are turned on and hence current can flow from the power supply to ground. From a DC point of view, the short circuit current flows in the inverter as long as its input voltage is between  $V_{TN}$  and  $V_H - |V_{TP}|$  where  $V_{TN}$  and  $V_{TP}$  are threshold voltages of nMOSFET and pMOSFET, respectively. This phenomenon cannot be avoided using CMOS level shift.

Consider the CMOS inverter A of Figure 2.6 and the timing diagram of Figure 2.5. Figure 2.7 (a) shows rearranged input wave forms driving NMOS1 and PMOS1 along with the output signal. Figure 2.7 (b) shows the short circuit current of the inverter for this transition. In the rising transition of input, the current remains at zero when input  $V_{in1}$  is less than  $V_{TN}$  or input  $n_2$  is greater than  $V_H - |V_{TP}|$  because either NMOS1 or PMOS1 is off. The NMOS1 is saturated from  $t_1$  to  $t_2$ , while the PMOS1 is saturated from  $t_2$  to  $t_3$ . Here,  $t_1$  is the time when  $V_{in1}$  becomes  $V_{TN}$ ,  $t_2$  is the time when the current reaches its maximum,  $i_{max}$ , and  $t_3$  is the time when  $n_2$  reaches at  $V_H - |V_{TP}|$ . In the falling transition of input, however, it is assumed that the short circuit current is negligible since the on time of both NMOS1 and PMOS1 is much shorter than the during the rising transition.

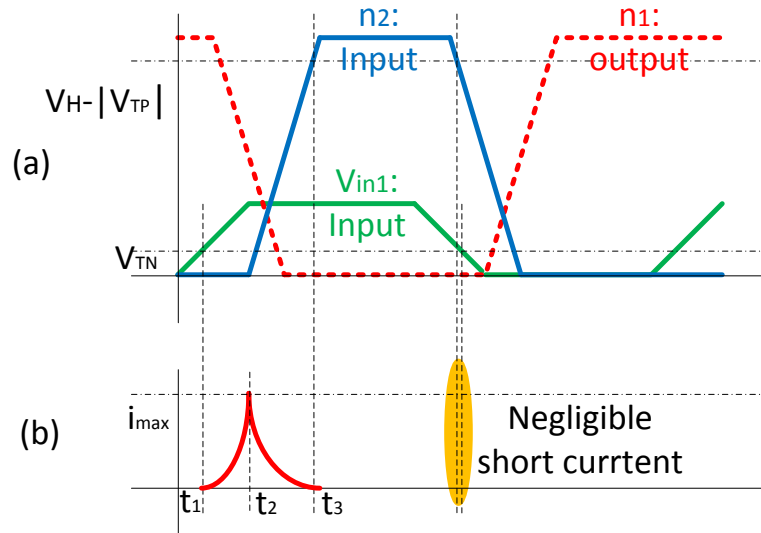


Figure 2.7 (a) Input wave forms and output signal based on Figure 2.5 for the CMOS inverter A of Figure 2.6 and (b) the corresponding short circuit current

Using an RC model for the inverter and buffer, the input signals,  $n_2$  and  $V_{in1}$  are given at any instant during transition as

$$\begin{aligned} n_2(t) &= V_H \left( 1 - e^{-\frac{1}{(R + \beta_p^0)(C_i + C_m)}t} \right) \\ &= V_H \left( 1 - e^{-\frac{1}{R(C_i + C_m)}t} \right) \end{aligned} \quad (2.6)$$

$$V_{in1}(t) = V_L \left( 1 - e^{-\frac{1}{R_i C_i}t} \right) \quad (2.7)$$

where  $R_p$  can be neglected due to its relatively small value compared to the pull-up resistor,  $R$  and  $R_i$  and  $C_i$  are an equivalent resistance and capacitance of buffer, respectively. Hence, the current  $i_{DP}$  and  $i_{DN}$  flowed through PMOS1 and NMOS1, respectively, is obtained as

$$i_{DP}(t) = \frac{V_H - n_2(t) - |V_{TP}|}{K_g R} \quad (2.8)$$

$$i_{DN}(t) = \frac{i_{\max}}{V_L - V_{TN}} (V_{in1}(t) - V_{TN}) \quad (2.9)$$

where  $K_g$  is a gain coefficient of a MOSFET. (2.8) and (2.9) can be given from the standard drain current equations for pMOSFET and nMOSFET. Since the peak current is generated when  $n_2$  reaches about  $0.9V_L$ ,  $i_{\max}$  can be obtained from (2.8) as follows:

$$i_{\max} = \frac{V_H - 0.9V_L - |V_{TP}|}{K_g R} \quad (2.10)$$

While the current behavior between  $t_1$  and  $t_2$  is dominated by input  $V_{in1}$ , the one during the time period from  $t_2$  to  $t_3$  depends on the input  $n_2$ . Note that the value  $t_2$  can be

influenced by both  $V_{in1}$  and  $n_2$ . Hence, a time point  $t_2'$  between  $t_2$  and  $t_3$ , is defined for the  $n_2$  dominant period. Therefore,  $t_1$ ,  $t_2$ ,  $t_2'$ , and  $t_3$  can be achieved from (2.6) and (2.7) such that

$$t_1 = -R_i C_i \log \left( 1 - \frac{V_{TN}}{V_L} \right) \quad (2.11)$$

$$t_2 = 2.3026 R_i C_i \quad (2.12)$$

$$t_2' = -R(C_l + C_m) \log \left( 1 - \frac{0.9V_L}{V_H} \right) \quad (2.13)$$

$$t_3 = -R(C_l + C_m) \log \left( 1 - \frac{V_H - |V_{TP}|}{V_H} \right) \quad (2.14)$$

The short circuit power dissipation of the CMOS inverter A,  $P_{SA}$ , can be obtained as follows

$$\begin{aligned} P_{SA} &= \left[ \int_{t_1}^{t_2} i_{DN}(t) dt + \int_{t_2}^{t_3} i_{DP}(t) dt \right] V_H f_d \\ &= \left\{ -\frac{(V_H - 0.9V_L - |V_{TP}|) V_L R_i C_i \left( \frac{V_{TN}}{V_L} - 0.9 \right)}{K_g R (V_L - V_{TN})} \right. \\ &\quad \left. + \frac{C_m}{K_g} \left[ V_H - 0.9V_L - V_{TP} - |V_{TP}| \log \left( \frac{V_H - 0.9V_L}{V_{TP}} \right) \right] \right\} V_H f_d \end{aligned} \quad (2.15)$$

Using the same method as for CMOS inverter A and with the sequence in Figure 2.8, the short circuit power dissipation of CMOS inverter B can be obtained such that

$$\begin{aligned} P_{SB} &= \left\{ -\frac{(V_H - 0.9V_L - |V_{TP}|) V_L R_i C_i \left( \frac{V_{TN}}{V_L} - 0.9 \right)}{K_g R (V_L - V_{TN})} \right. \\ &\quad \left. + \frac{(C_m + C_l)}{K_g} \left[ V_H - 0.9V_L - V_{TP} - |V_{TP}| \log \left( \frac{V_H - 0.9V_L}{V_{TP}} \right) \right] \right\} V_H f_d \end{aligned} \quad (2.16)$$

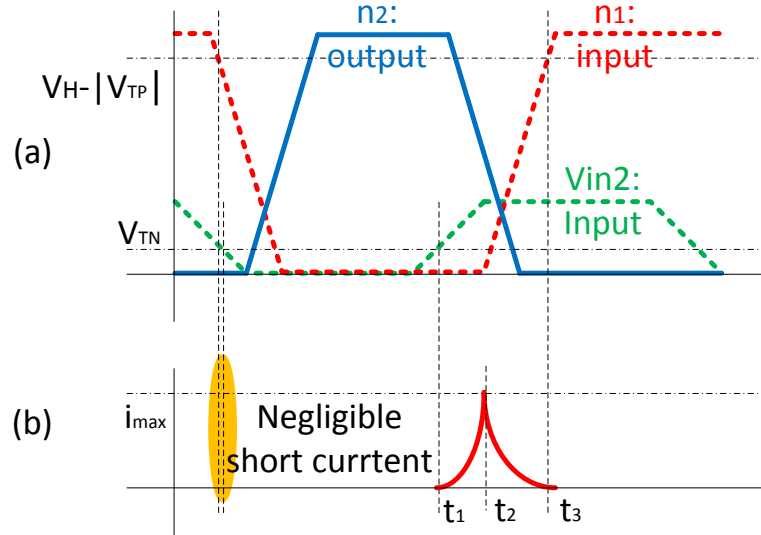


Figure 2.8 (a) Input wave forms and output signal based on Figure 2.5 for the CMOS inverter B of Figure 2.6 and (b) the corresponding short circuit current

Therefore, the total power dissipation,  $P_{switch}$ , of the on-off driving circuit is equal to

$$P_{switch} = P_{SA} + P_{SB} + P_{C_m} = E_{switch} f_d \quad (2.17)$$

where  $E_{switch}$  is a constant of switching power consumption dictated by resistors, capacitors, and other circuit components based on (2.5), (2.15), and (2.16) and same as energy dissipation of the circuit. Choosing state-of-the-art values of the components such as ultra-low-power MEM Relays [69],  $E_{switch}$  is obtained as  $0.15\mu\text{J}$ . In detail, the relay had capacitance of  $0.5\text{fF}$ , gain coefficient of 1.99, and threshold voltage of 1V. Pull-up resistors of 100 and  $1000\Omega$ , respectively, were adjusted to balance response time of the circuit with low-power consumption.

## 2.3 Sensing Circuit

### 2.3.1 Sensing Circuit Description

A capacitive sensing circuit was designed to determine the motion of microscale actuators by measuring the change in capacitance caused by actuator deflection. A common type of sensing technique for miniature or micro-scale systems is capacitive sensing with a differential capacitive sensing circuit. One example of such a circuit (when only one side of the time varying capacitance may be accessed directly) is shown in Figure 2.9.

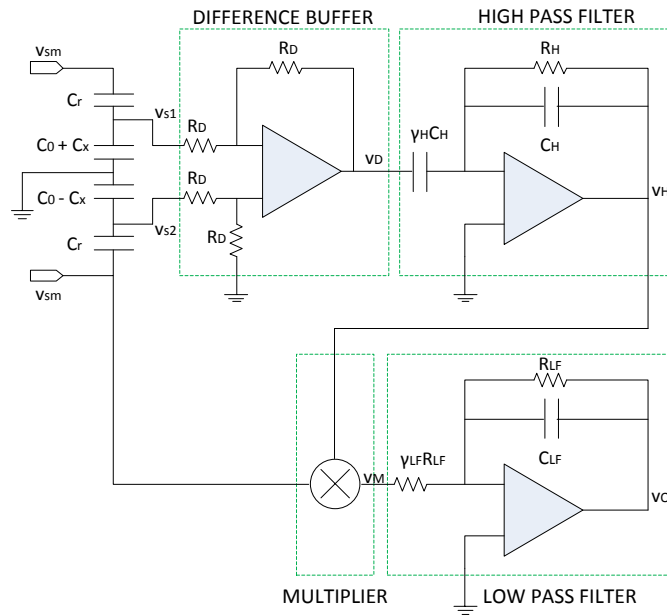


Figure 2.9 A capacitive sensing with differential capacitive sensing circuit amplifier

The circuit consists of capacitive sensors with a nominal capacitance,  $C_0$ , and capacitance change,  $C_x$ , along with a difference buffer, High Pass Filter (HPF), multiplier, and Low Pass Filter (LPF).

The sensor signals,  $v_{s1}$  and  $v_{s2}$ , are first modulated by a signal,  $v_{sm}$ , with amplitude  $V_{sm}$  and frequency  $f_{sm}$ . These signals are then subtracted by the difference buffer to generate output  $v_D$  and finally the true sensor output is demodulated through the HPF,

multiplier, and LPF. The offset error and  $1/f$  noise of the sensing circuit can be reduced through this modulation/demodulation process.

It is assumed that operational frequencies of the circuit have the following relation, as:

$$\begin{aligned}
f_a &= \frac{1}{\kappa_a} f_s, \\
f_{LF} &= \kappa_{LF} f_s, \\
f_H &= \kappa_H f_s, \\
f_{sm} &= \kappa_{sm} f_s, \\
0 &< \kappa_a < \kappa_{LF} < \kappa_H < \kappa_{sm}
\end{aligned} \tag{2.18}$$

Where  $f_a$ ,  $f_s$ ,  $f_{LF}$ ,  $f_H$ , and  $f_{sm}$  are actuator stepping motion frequency, AD sample frequency, LPF and HPF cutoff frequency, and modulating frequency respectively, and  $\kappa_a$ ,  $\kappa_{LF}$ ,  $\kappa_H$ , and  $\kappa_{sm}$ , are constant gains for the relation.

### 2.3.2 Power Dissipation of the Circuit

Assuming that all gains,  $\gamma_H$ ,  $\gamma_M$ , and  $\gamma_{LF}$  of the circuit have the value of one, the power consumption of the each component can be calculated by the definition of power as follows,

$$\begin{aligned}
P_D &= I_{q,op} \left[ V_{s,op} - (-V_{s,op}) \right] + \frac{(\bar{v}_2 - \bar{v}_1 + \bar{v}_2)^2}{2R_D} + \frac{2\bar{v}_1^2}{R_D} \\
&= 2I_{q,op} V_{s,op} + \frac{5\bar{v}_1^2 + 4\bar{v}_2^2 - 2\bar{v}_1\bar{v}_2}{2R_D}
\end{aligned} \tag{2.19}$$

$$P_H = 2I_{q,op} V_{s,op} + \frac{\bar{v}_H^2}{R_H} + C_H \bar{v}_H^2 f_{sm} + \gamma_H C_H \bar{v}_D^2 f_{sm} \tag{2.20}$$

$$P_M = 2I_{q,multi} V_{s,multi} \tag{2.21}$$

$$P_{LF} = 2I_{q,op}V_{s,op} + \frac{\bar{v}_O^2}{\gamma_{LF}R_{LF}} + C_{LF}\bar{v}_O^2 f_a + \frac{\bar{v}_M^2}{R_{LF}} \quad (2.22)$$

where,  $P_D$ ,  $P_H$ ,  $P_M$ , and  $P_{LF}$  are the power dissipation by difference buffer, HPF, multiplier, and LPF respectively,  $V_{s,op}$ ,  $V_{s,multi}$ , and  $I_{q,multi}$  are a supply voltage and a quiescent current of the op-amp and the multiplier respectively, and the nomenclature with a bar over a character represents an RMS value of each of the functional components. The total power dissipation of the circuit can be obtained as

$$P_{sen} = P_D + P_H + P_M + P_{LF} \quad (2.23)$$

It is noted that if non-unity gains of  $\gamma_H$ ,  $\gamma_M$ , and  $\gamma_{LF}$  are used, the power consumption of the circuit would be increased for larger gains or decreased for smaller gains than unity since the values of  $v_H$ ,  $v_M$ , and  $v_{LF}$  in (2.19) to (2.22) would be affected by the values of the gains. The detailed equations of the output are presented in Appendix. A.

### 2.3.3 Noise Analysis

Although the main emphasis of this chapter is power dissipation, when controller performance is evaluated, noise levels in the sensing circuit have a significant influence. This section discusses the noise generated within the circuit. There are three main noise sources in the circuit: voltage and current noise in op-amps and Johnson noise from external resistors or capacitors. However, in practice op-amp circuits are designed with low source impedance on the inputs so that only the voltage noise is important for the low source impedance inputs [70]. Hence the current noise from the op-amps is not considered in this work.

If (2.18) holds and the values of all gains in the circuit are one, the noise,  $v_{n,s1}$  and  $v_{n,s2}$  of capacitive sensors,  $v_{n,D}$  of difference buffer,  $v_{n,H}$  of HPF, and  $v_{n,LF}$  of LPF, can be estimated by

$$v_{n,s1}^2 = \frac{k_B T}{C_r + C_0 - C_x} K_n \kappa_4 f_s \quad (2.24)$$

$$v_{n,s2}^2 = \frac{k_B T}{C_r + C_0 + C_x} K_n \kappa_4 f_s \quad (2.25)$$

$$v_{n,D}^2 = (10k_B T R_D + v_{n,op}^2) K_n \kappa_4 f_s \quad (2.26)$$

$$v_{n,H}^2 = \left( 4k_B T R_H + \frac{2k_B T}{C_H} + v_{n,op}^2 \right) K_n \kappa_4 f_s \quad (2.27)$$

$$v_{n,M}^2 = v_{n,multi}^2 K_n \kappa_4 f_s \quad (2.28)$$

$$v_{n,LF}^2 = \left( 8k_B T R_{LF} + \frac{k_B T}{C_{LF}} + v_{n,op}^2 \right) K_n \kappa_2 f_s \quad (2.29)$$

where  $k_B$  is the Boltzman constant,  $v_{n,op}$  and  $v_{n,multi}$  are voltage noise spectral densities of an op-amp and a multiplier respectively,  $T$  is the absolute temperature in kelvins, and  $K_n$  is the brick wall conversion factor with respect to the number of poles in an op-amp filter or amplifier [96].

Therefore, the total noise in the circuit is equal to,

$$v_n^2 = v_{n,s1}^2 + v_{n,s2}^2 + v_{n,D}^2 + v_{n,H}^2 + v_{n,M}^2 + v_{n,LF}^2 \quad (2.30)$$

As with power, it is noted that if non-unity gains of  $\gamma_H$ ,  $\gamma_M$ , and  $\gamma_{LF}$  are used, the noise of the circuit would be increased for larger gains or decreased for smaller gains than unity since the noise in (2.24) to (2.29) would be amplified by the values of the gains; however, the effect of increasing or decreasing the measurement signal strength would also have to be included in controller performance analysis.

### 2.3.4 Power Dissipation versus Noise Property for Sensing

Under many circumstances, particularly when sensing capacitance is large compared to parasitic capacitances and sampling frequency is low, the power



consumption and noise generated are highly dependent on a selected sample frequency.

To examine this relationship, (2.23) and (2.30) are rearranged and simplified to the forms

$$P_{sen} = p_1 I_{q,op} + p_2 \frac{1}{T_s} + p_3 \quad (2.31)$$

$$v_n^2 = v_{n1} \frac{1}{T_s} + v_{n2} v_{n,op}^2 (I_{q,op}) \frac{1}{T_s} \quad (2.32)$$

where,  $p_1$ ,  $p_2$ , and  $p_3$  are constants of power consumption and  $v_{n1}$  and  $v_{n2}$  are constants of noise generation dictated by resistors, capacitors, and other circuit components based on (2.19) to (2.22) and (2.24) to (2.29). Using estimated capacitance of a capacitive sensor and specific values of the components in Figure 2.9, the coefficients of (2.31) and (2.32) were obtained as shown in Table 2.1. The properties of op-amps and multiplier are obtained from [71 – 73]. It is worth noting that even though only a capacitive sensing approach is evaluated here, an affine, positive dependence of sensing power upon sampling rate is typical of micro-scale sensing schemes, though the coefficients in (2.31) would be different (and generally higher) for other sensing techniques.

Table 2.1 Coefficient of noise and power model of (2.31) and (2.32) for the case of Figure 2.9

Coefficient	Specific Values
$v_{n1} (V^2_{rms}/Hz)$	$9.7 \times 10^{-9}$
$v_{n2}$	$3.15 \times 10^3$
$p_1 (V)$	15
$p_2 (W/Hz)$	$1.6 \times 10^{-6}$
$p_3 (W)$	$1.06 \times 10^{-4}$

As shown in (2.31) and (2.32), the noise model for  $v_n$  and power consumption,  $P_{sen}$ , for the circuit depend on the voltage noise spectral density,  $v_{n,op}$ , and the quiescent

current,  $I_{q,op}$ , of an operational-amplifier used for filtering and signal amplification, as well as the selected sample frequency,  $T_s$ . For instance,  $v_{n,op}$  of commercially available op-amps is roughly inversely proportional to the quiescent current of the op-amp,  $I_{q,op}$ , as shown in Figure 2.10 [71]. Based on the data in Figure 2.10, the  $v_{n,op}$  with respect to  $I_{q,op}$  can be approximately fitted as

$$v_{n,op} = 7.67 \times 10^{27} I_{q,op}^{15} - 0.43 \times 10^{27} I_{q,op}^{14} + 0.01 \times 10^{27} I_{q,op}^{13} \quad (2.33)$$

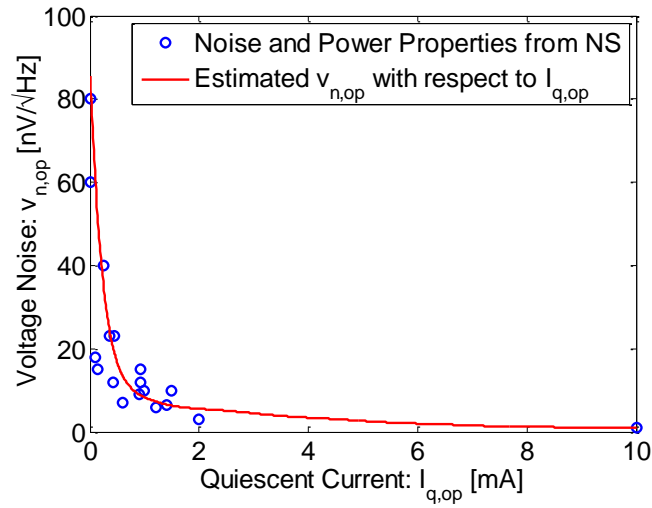


Figure 2.10 Noise vs. quiescent current of OP-Amps from Nation Semiconductors [44]

## 2.4 Summary: Estimated Power Consumption versus Switching Drive Frequencies and Sampling Rates

Given the capacitive actuator and the circuit capabilities discussed above, it is possible to preliminarily illustrate power consumption in terms of switching drive frequencies and sampling rates potentially used by a control system. In this preliminary estimation, it is assumed that the capacitance of the the microactuator is 1nF (a typical order of magnitude for thin-film piezoelectric actuators), that the motion of actuator is slower than the switching drive frequencies or sample rates tested, and the maximum ‘ON’ voltage is 20V for the switching drive. For the analog driving circuit, the charging

energy of the actuator should be integrated from the input voltage command using (2.1). However, the command can be assumed to be a DC value due to very slow motion of actuator so that power consumption by the actuator is taken as  $6.9 \mu\text{W}$  from quiescent and resistive currents in the amplifier [10].

Figure 2.11 shows average power dissipation of each component with actuator power usage. Figure 2.12 illustrates total average power consumption of the actuator and switching drive and sensing circuitries based on (2.1), (2.4), (2.17), and (2.37), assuming that the frequency of actuator stepping motion is 1Hz. From the point-of-view of the actuator, while the analog drive circuit unfortunately consumes a large amount of power as already noted in [14, 32] regardless of switching frequency or sample rates., the switching drive circuit dissipates much less than the analog one at frequency ranges of 0 to 20 kHz although at higher frequency than 20 kHz, power usage increases more rapidly than for the analog circuit. It is noted that a higher frequency than 20 kHz is generally used for PWM control of fast microactuators.

Thus, only switching drive architectures with a slow switching frequency are utilized for the low power control schemes to be introduced in this work. Meanwhile, power usage by the sensing circuit is exponentially increased with respect to faster sample rates, which are generally necessary to use position sensing in true real-time feedback control. Since feedback position sensing will be important in the microscale control application to add robustness or precision, it is also considered useful in this work to study strategies for reducing sample rates of feedback control strategies.

To summarize, Figures 2.11 and 2.12 suggest that control architectures with slow switching input and reduced sample rate may be useful to limit or minimize power dissipation of micro servo system. As the figures show, even with slow sampling and driving frequencies, power consumption of a actuator servo system can be a substantial portion of the available power budget. Further reductions in power consumption may rely on advances in sensing circuitry and actuator energy density, though the trends identified by the analysis in this section are regarded as representative.

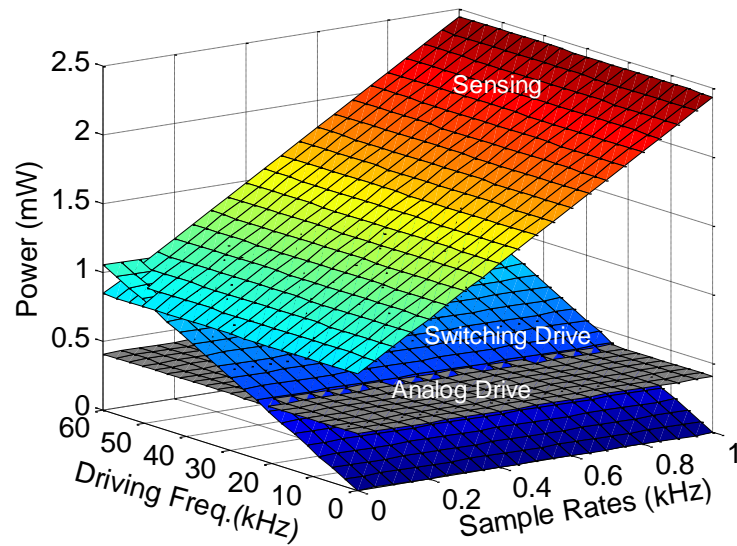


Figure 2.11 Power consumption of two candidate drive circuitries and sensing circuitry with a 1nF capacitive microactuator at with 20V maximum input with respect to sample rates and switching drive frequencies

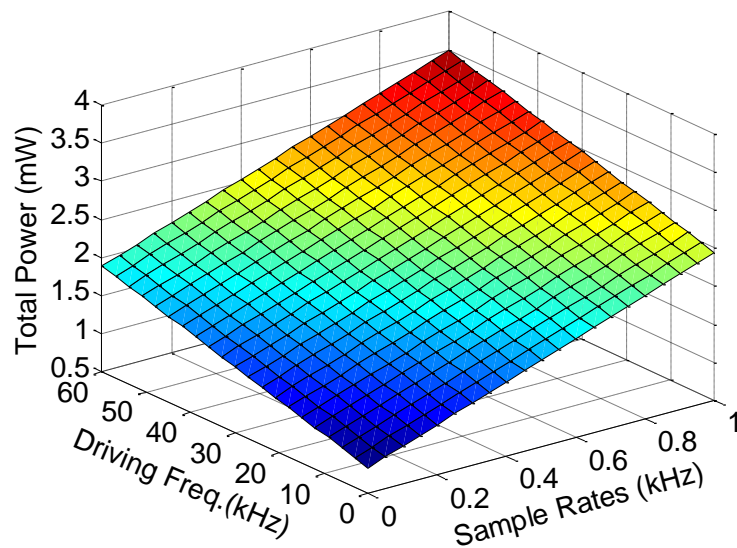


Figure 2.12 Total power consumption of sensing and switching drive circuitries with a 1nFcapacitive microactuator at 20V 'On' input with respect to sample rates and switching drive frequencies

## **CHAPTER 3**

### **MODEL FREE ADAPTIVE ON-OFF CONTROL**

A candidate low-power approach for controlling actuator motion, when actuator motions can be expected to repeat many times, is to perform iterative adaptive on-off control with limited sensor measurements. This allows for lower sampling frequency measurements, compared over several iterations of a given movement, to guide input sequences producing a desired displacement or trajectory.

For certain classes of system, this can be performed without any model of the system in the controller itself, which further simplifies computational requirements on a micro-robot. A fixed number of time instances at which the input to the actuator is turned on or off are adapted using feedback from a few sensor measurements, with the timing of the on-off transitions adjusted from one iteration of an appendage motion to the next. In the case of terrestrial micro-robotics, actuator motions are expected to repeat many times, as in walking or running gaits.

Two types of iterative adaptive control structures for thin-film piezoelectric micro-robotic leg joints are presented in this chapter, one based on stochastic gradient approximation and the other based on deterministic heuristic switching rules. In both cases, eventual convergence of switching times to at least locally optimal values are analyzed for some limited range of initial switching time selections and adaptation gains.

#### **3.1 Definition of Variables, States, and Dimensions**

Since this chapter deals with several variables, states, and dimensions, it is useful to define nomenclatures. The defined nomenclatures and corresponding meanings of dimensions used through this chapter are:

- $k$ : a sequential iteration number of iterative adaptive control

- $q$ : an index for elements of the vector defining the switching instances of on-off inputs
- $Q$ : the maximum number of switching instances of an on-off input between measurements
- $n$ : an index for the elements of a measurement vector
- $N$ : the maximum number of measurements
- $m$ : an element of dynamic state vector.
- $M$ : the maximum order of the system dynamic.

Based on the indexes above, several variables and states are denoted as

- $r$ : a vector with target output values, such that  $r \in \mathbf{R}$
- $\mathbf{x}$ : a known nominal state vector of system dynamics, such that  $\mathbf{x} \in \mathbf{R}^M$
- $\mathbf{x}_b$ : an unknown, nonlinear state vector of system dynamics, such that  $\mathbf{x}_b \in \mathbf{R}^M$
- $\mathbf{x}_e$ : the error state vector defined as  $\mathbf{x}_e = \mathbf{x}_b - \mathbf{x}$ , such that  $\mathbf{x}_e \in \mathbf{R}^M$
- $z$ : a nominal position output response, such that  $z \in \mathbf{R}$
- $z_b$ : an unknown position output response, such that  $z_b \in \mathbf{R}$
- $\mathbf{y}$ : a measured output vector of  $z_b$ , such that  $\mathbf{y} \in \mathbf{R}^{N+1}$
- $\boldsymbol{\varepsilon}$ : the error vector of output, such that  $\boldsymbol{\varepsilon} \in \mathbf{R}^{M+1}$  and  $\boldsymbol{\varepsilon} = \mathbf{y} - \mathbf{r}$
- $\boldsymbol{\tau}$ : a vector of switching input parameter, such as  $\boldsymbol{\tau} \in \mathbf{R}^{Q \times N}$

Since a response to switching inputs of time duration  $t_f$  (with  $t_f = t_N$ , the final measurement time) are to be produced many times, all variables and states defined above at the  $k$ -th iteration are denoted by a superscript of  $k$  such as  $\mathbf{y}^k$  and  $\boldsymbol{\tau}^k$  which mean the measurement and input vector at the  $k$ -th iteration. A numbered subscript put on the variables or states denotes an element number of sampled variables or states. For instance,  $y_n^k$  means the  $n$ -th measurement output at the  $k$ -th iteration and  $\tau_1^k$  means the first element of the switching vector  $\boldsymbol{\tau}^k$ . A numbered subscript with parentheses put on the states represents the element number of states:  $x_{(m)}^k$  indicates the  $m$ -th state at the  $k$ -th iteration.

## 3.2 System Description

### 3.2.1 System Dynamics and Conditions

The dynamic system for application of the adaptive on-off controller is taken to be a nonlinear, single-input-single-output (SISO), time-invariant system, with unknown nonlinearities bounded in magnitude from a known, linear, and stable nominal system. The nominal system with the state vector,  $\mathbf{x}^k$ , can be described as,

$$\begin{aligned}\dot{\mathbf{x}}^k(t) &= \mathbf{A}\mathbf{x}^k(t) + \mathbf{B}u^k(t) \\ z(t) &= \mathbf{C}\mathbf{x}(t)\end{aligned}\quad (3.1)$$

for all  $k$ , where  $\mathbf{A}$  is an  $M \times M$  state matrix,  $\mathbf{B}$  is an  $M \times 1$  input matrix,  $\mathbf{C}$  is  $1 \times M$  output matrix, and  $u^k(t)$  is the controlled input to the system.

The real, unknown system is denoted by a separate state vector,  $\mathbf{x}_b^k$ , and taken to have dynamics of the form

$$\begin{aligned}\dot{\mathbf{x}}_b^k(t) &= \left[ \mathbf{A}\mathbf{x}_b^k(t) + \mathbf{f}_{\mathbf{x}_b}(\mathbf{x}_b^k(t)) \right] + \left[ \mathbf{B} + \mathbf{f}_u(\mathbf{x}_b^k(t)) \right] u^k(t) \\ &= \begin{cases} \mathbf{l}_0(\mathbf{x}_b^k(t)), u^k(t) = 0 \\ \mathbf{l}_1(\mathbf{x}_b^k(t)), u^k(t) = 1 \end{cases}\end{aligned}\quad (3.2)$$

where  $\mathbf{f}_{\mathbf{x}_b}(\cdot)$  and  $\mathbf{f}_u(\cdot)$  are vectors of unknown, Lipschitz continuous, and potentially nonlinear functions of the states, which are denoted as  $\mathbf{f}_{\mathbf{x}_b} = [f_{\mathbf{x}_b1}, f_{\mathbf{x}_b2}, \dots, f_{\mathbf{x}_bM}]^T$ ,  $\mathbf{f}_u = [f_{u1}, f_{u2}, \dots, f_{uM}]^T$ . Then  $\mathbf{l}_0(\cdot)$  and  $\mathbf{l}_1(\cdot)$  are two alternate functions for the ‘off’ state and ‘on’ state, respectively. The nonlinear portions of (3.2) are assumed to be bounded as a function of both absolute and relative magnitudes of the states, according to

$$\begin{aligned}\left| \mathbf{f}_{\mathbf{x}_b}(\mathbf{x}_b^{k+1}(t)) - \mathbf{f}_{\mathbf{x}_b}(\mathbf{x}_b^k(t)) \right| &\leq \mathbf{C}'_{\mathbf{x}_b} \left| \mathbf{x}_b^{k+1}(t) - \mathbf{x}_b^k(t) \right| \\ \left| \mathbf{f}_u(\mathbf{x}_b^{k+1}(t)) - \mathbf{f}_u(\mathbf{x}_b^k(t)) \right| &\leq \mathbf{C}'_u \left| \mathbf{x}_b^{k+1}(t) - \mathbf{x}_b^k(t) \right|\end{aligned}\quad (3.3)$$

$$\begin{aligned} |\mathbf{f}_{x_b}(\mathbf{x}_b^k(t))| &\leq \mathbf{C}_{x_b} |\mathbf{x}_b^k(t)| \\ |\mathbf{f}_u(\mathbf{x}_b^k(t))| &\leq \mathbf{C}_u |\mathbf{x}_b^k(t)| \end{aligned} \quad (3.4)$$

where  $\mathbf{C}_{x_b}$ ,  $\mathbf{C}_u$ ,  $\mathbf{C}_{x_b}'$ , and  $\mathbf{C}_u'$  are  $M \times M$  matrices with real, non-negative entries. It is noted that all elements of  $\mathbf{C}_{(\cdot)}$  are smaller than elements of  $\mathbf{C}_{(\cdot)}'$  with  $\mathbf{C}_{(\cdot)}$  related to average deviation of the nonlinear responses that is smaller than possible local nonlinear deviation.

Finally, there is a known, linear relationship defined by matrix  $\mathbf{C}$  between unknown states,  $\mathbf{x}_b^k$ , and a output variable,  $z_b^k$ , such as

$$z_b^k(t) = \mathbf{C}\mathbf{x}_b^k(t) + d_v(t) \quad (3.5)$$

where  $d_v(t)$  is white, Gaussian, zero-mean measurement noise.

Measured outputs at each sample instances can be given from (3.5), as:

$$y_n^k = z_b^k(t_n) \quad (3.6)$$

The systems in (3.1) and (3.2) are assumed to be asymptotically stable with equilibrium points  $r_{eq}$  and 0 with on and off conditions satisfying:

$$\begin{cases} \mathbf{l}_1(\mathbf{x}_b^k(t)) = 0, & \text{iff } \mathbf{x}_b^k = [\mathbf{r}_{eq} \quad 0 \quad \dots \quad 0]^T \\ \mathbf{l}_0(\mathbf{x}_b^k(t)) = 0, & \text{iff } \mathbf{x}_b^k = [0 \quad 0 \quad \dots \quad 0]^T \end{cases} \quad (3.7)$$

In addition, we assume that there is sufficient time between iterations to treat,

$$t_0 = 0 \text{ and } \mathbf{x}_b^k(0) = \mathbf{0} \quad (3.8)$$

due to the stability of the system with zero input and an assumption of satisfactory time between motions for the system to return to its 'off' equilibrium state. Hence, all switching and measurement times are relative to the start of the iteration marked.



The differential equation (3.2) is taken to have a real, though unknown, solution,  $\Psi_{\mathbf{x}_b}$ , that may be written as functions of the states at a given starting time,  $t_0$ , the current time, and the input, which may be further simplified to solutions  $\Psi_0$  and  $\Psi_1$  over periods in which the system is subject solely to an ‘off’ or ‘on’ input, respectively:

$$\begin{aligned} \mathbf{x}_b^k(t) &= \Psi_{\mathbf{x}_b}(t-t_0, \mathbf{x}_b^k(t_0), u^k(t)) \\ &= \begin{cases} \Psi_0(t-t_0, \mathbf{x}_b^k(t_0)), & u(t) = 0 \quad \forall t > t_0 \\ \Psi_1(t-t_1, \mathbf{x}_b^k(t_0)), & u(t) = 1 \quad \forall t > t_0 \end{cases} \end{aligned} \quad (3.9)$$

While in general it is difficult to make statements about the response of an unknown, nonlinear system to a switching input, with certain assumptions about the size of the unknown nonlinearity relative to a nominal system, a number of facts may be concluded about the system response. In contrast, the nominal linear system evolves according to a known state transition matrix,  $\Phi$ . We combine this with forcing effects to denote the total responses as a function of time and initial conditions when the system is purely in an ‘off’ or ‘on’ state for a specific period, respectively, as in

$$\begin{aligned} \mathbf{x}^k(t) &= \Phi(t-t_0)\mathbf{x}^k(t_0) + \int_0^t e^{A(t-s)}\mathbf{B}u^k(s)ds \\ &= \begin{cases} \Phi(t-t_0)\mathbf{x}^k(t_0), & u = 0 \quad \forall t > t_0 \\ \Phi(t-t_0)\mathbf{x}^k(t_0) + \int_0^t e^{A(t-s)}\mathbf{B}ds, & u = 1 \quad \forall t > t_0 \end{cases} \end{aligned} \quad (3.10)$$

Finally, we assume that an upper bound,  $\mathbf{x}_{\max}$ , on the maximum values of the states is known, or

$$|\mathbf{x}| < \mathbf{x}_{\max} \quad (3.11)$$

This bound does not need to be known very accurately, and is used only to provide a starting point for a numerical integration during convergence analysis.

The model described in (3.3), (3.7), (3.8), and (3.9) provides a good representation of the capacitively-loaded microactuators motivating this work, among

other dynamic systems. Piezoelectric micro-robotic actuators, the primary motivating example for this work, consist of continuous flexible structures with differentiable behavior in mechanical dynamics and piezoelectric response. The system inputs are limited to ‘on’ and ‘off’ voltages supplied by an ultra-low-power switching circuit. While the piezoelectric actuation gain, structural stiffness, and damping effects may be nonlinear functions of system states, equilibrium positions at voltages of 0 (off state) and  $V_{max}$  (on state) exist and are easily measured.

Finally, we anticipate there being sufficient time (for example, while other legs are propelling the robot body) for individual actuators to return to their original position before being actuated again, and experimental testing indicates that the high stiffness of silicon flexures in comparison to the piezoelectric materials results in negligible variation in initial conditions due to any hysteresis in the piezoelectric response.

### 3.2.2 General Controller Structure

On-off iterative adaptive controllers with relatively sparse measurement are considered to investigate for ultra low-power control. In the case of an on-off control, the system has only two possible input values of “ON” state ( $u = 1$ ) and “OFF” state ( $u = 0$ ) such that

$$u^k(t) \in \{0, 1\} \quad \forall t \quad (3.12)$$

The on-off control input switches at  $(Q \times N)$  switching times for all  $k$  recorded in vector  $\boldsymbol{\tau}^k$ ,

$$\begin{aligned} \boldsymbol{\tau}^k &= \left[ \tau_{1,1}^k \quad \cdots \quad \tau_{Q,1}^k \quad \tau_{1,1}^k \quad \cdots \quad \tau_{Q,2}^k \quad \cdots \quad \tau_{1,N}^k \quad \cdots \quad \tau_{Q,N}^k \right]^T \\ 0 &\leq \tau_{1,1}^k \\ \tau_{q-1,n}^k &\leq \tau_{q,n}^k, \quad q = 2, \dots, Q \text{ and } n = 1, \dots, Q \\ \tau_{q,n-1}^k &\leq \tau_{q,n}^k, \quad n = 2, \dots, N \text{ and } q = 1, \dots, Q \\ \tau_{Q,n}^k &\leq \tau_{1,n+1}^k, \quad n = 1, \dots, N-1 \end{aligned} \quad (3.13)$$

which, as illustrated in Figure 3.1, results in the input to the system being described over time by

$$u^k(t) = \begin{cases} 1, & t_n < t < \tau_{1,n+1}^k, \quad n = 0, \dots, N-1 \\ 0, & \tau_{2q-1,n}^k < t < \tau_{2q,n}^k, \quad q = 1, \dots, Q/2 \text{ and } n = 1, \dots, N \\ 1, & \tau_{2q,n}^k < t < \tau_{2q+1,n}^k, \quad q = 1, \dots, Q/2 \text{ and } n = 1, \dots, N \end{cases} \quad (3.14)$$

where  $t_n$  is a sampling instance between  $t_0$  to  $t_N$ , with a sample period  $T_s$ , to measure system outputs  $\mathbf{y}^k$  and compare them to target values  $\mathbf{r}$ . It is noted that the sample time  $T_s$  may optionally be slower than Nyquist, although this limits feasible outcomes of the adaptation; all behavior of a system may not be observed but a limited number of measurements may be available and outputs at those instance potentially regulated.

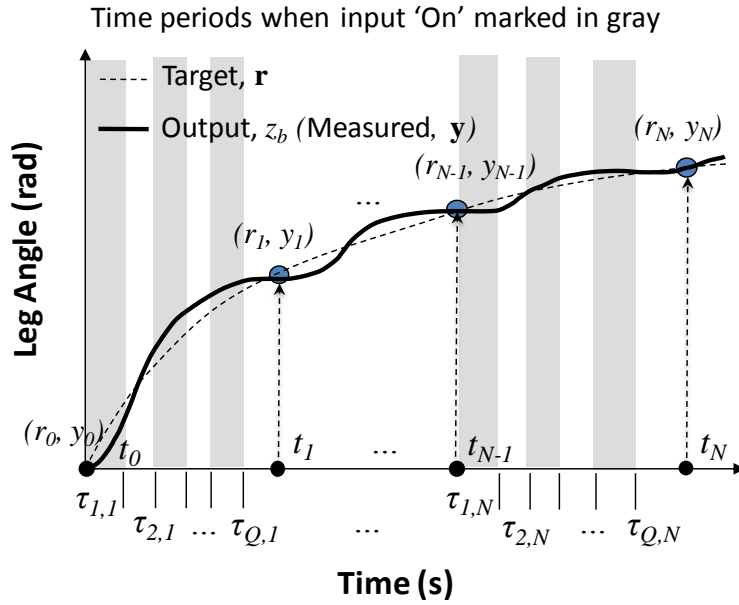


Figure 3.1 General definition of switching instances, measured targets and outputs at each sample instance for on-off input

The on-off iterative adaptive controllers to be considered are model-free online searching algorithms for the control input vector (3.13),  $\tau^k$ , to be adjusted over multiple

iterations of a desired motion. For a known or measured  $\mathbf{y}^k$  and target  $\mathbf{r}$ , an object function is utilized to search the proper  $\boldsymbol{\tau}^k$  as described in

$$\min_{\boldsymbol{\tau}^k} \left[ J^k(\boldsymbol{\tau}^k) \equiv h(\boldsymbol{\varepsilon}^k(\boldsymbol{\tau}^k)) \right] \quad (3.15)$$

One formulation of the on-off adaptive controller considered in this paper can be then described as

$$\boldsymbol{\tau}^{k+1} = \boldsymbol{\tau}^k + \mathbf{T}^k(\boldsymbol{\varepsilon}_1^k, \boldsymbol{\varepsilon}_2^k, \dots, \boldsymbol{\varepsilon}_N^k) \quad (3.16)$$

Here,  $\mathbf{T}^k$  is a  $(Q \times N) \times 1$  vector of an adaptation law related to the errors and performance metric (3.15). The entries in  $\mathbf{T}^k$  are subject to minimum and maximum bounds as,

$$\begin{aligned} (\mathbf{T}^k)^T &= \left[ \mathbf{T}_{1,1}^k \quad \dots \quad \mathbf{T}_{Q,1}^k \quad \mathbf{T}_{1,2}^k \quad \dots \quad \mathbf{T}_{Q,2}^k \quad \dots \quad \mathbf{T}_{1,N}^k \quad \dots \quad \mathbf{T}_{Q,N}^k \right] \\ (\mathbf{T}_{q,n}^k)_{\min} &\leq \mathbf{T}_{q,n}^k \leq (\mathbf{T}_{q,n}^k)_{\max} \end{aligned} \quad (3.17)$$

which adjusts the difference between tuned and current control parameters. This adaptation rule responds to the difference between attained and desired performance and can be covered by a gradient technique, a constant gain over an individual output error of the object function, or other adaptive approaches to improve the performance.

### 3.3 Heuristic Adaptive (HA) On-Off Controller for a Micro-robotic Leg Joints

The HA on-off controller presented in this section uses simple adaptation rules based on known general behavior of the piezoelectric actuators to adjust on-off switching times to drive the actuators through a desired transient stepping motion. Adaptation laws are based on small numbers of measurements taken during each iteration of the actuator movement. The following sections describe the detailed procedure for use of the HA on-off controller, a method of convergence analysis with bounded nonlinearities, and

examinations for a specific controller for repeated stepping motions of a 2nd-order system.

### 3.3.1 Controller Design

#### 3.3.1.1 Problem Statement

Conceptually, the goal of this first iterative controller for a micro-robotic leg joint is to drive the joint to a desired output angle or displacement,  $r_0 = r_1 = r_2 = \dots = r_N = r$ , with little overshoot or oscillation, despite the availability of only two input levels ('on' and 'off') and relatively sparse position sensor measurements. This is essentially a step-and-hold type of motion, within the constraints on actuation. The controller should use measurements from a previous iteration step or steps to adjust the on-off switching times in the next iteration, and converge over several iterations to a smooth stepping motion. Each iteration of actuator motion under the iterative adaptive controller has duration  $t_N$ , with sufficient time before the next iteration to return to the system's equilibrium position in the 'off' state.

For specifically controlling a smooth stepping motion of the system, only three independent switching times will be adapted. First, there will be an initial pulse length,  $\tau_p = \tau_{1,1}$ , that is intended to drive the value of  $y_l$  to a target output value  $r$  at the first measurement time  $t_1$ , roughly corresponding to the peak level of the response. The second switching time,  $\tau_s = \tau_{1,2}$ , regulates the standby time of the first 'off' period, attempting to keep the output at the second measurement equal to that of the first, before entering a periodic on-off switching pattern initiated and regulated by the third independent switching time,  $\tau_d$ , which may be translated into transition times  $\tau_{1,3}$  to  $\tau_{1,N}$  in the general iterative on-off controller nomenclature. Beginning in this third time period, the input to the system is switched 'on' at a constant frequency,  $f_d$ , and duty cycle determined by  $\tau_d$ , as illustrated in Figure 3.2. After a period  $t_N$ , the input to the system is turned 'off' and the system is then assumed to be allowed sufficient time to return to the equilibrium position with zero ('off') input, and the next iteration begins.

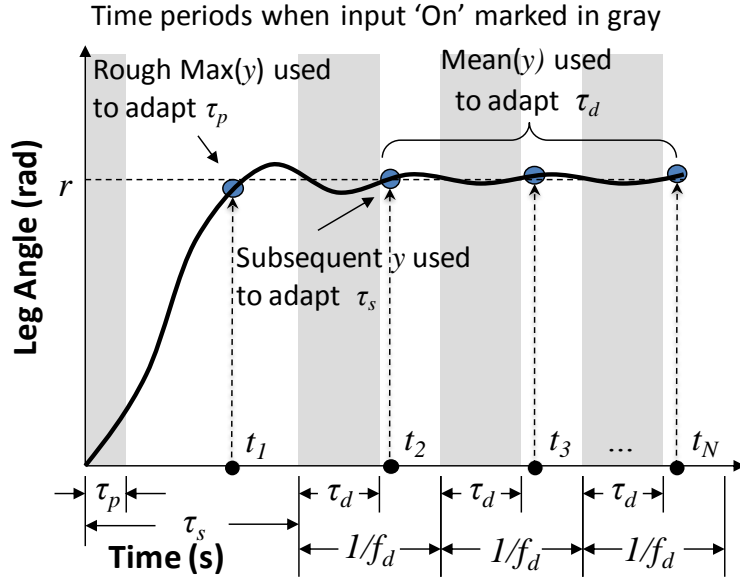


Figure 3.2 Definitions of switching times and sample times for a specific step controller

This generic approach to on-off control provides a simple method for guiding micro-robotic leg joints to a desired motion, while reducing the number of independent switching times to be adapted to three specific time intervals between transitions, each reflecting a phase of step motion.

### 3.3.1.2 Measurement Data

Since only limited sensor measurements are available when maintaining a relatively slow sampling rate, the target outputs for the resulting motion are limited to certain functions of these few measurements. To perform the stepping motion described above, relevant output measurements are selected to represent common phenomena in dynamic system step responses:

$y_p^k$ : The first measurement taken, such that  $y_p^k = z_b^k(t_1)$ , corresponding to the approximate peak value of the output in a single iteration of the stepping motion.

$y_s^k$ : The next sampled value after the apparent peak,  $y_s^k = z_b^k(t_2)$ , when approximately the steady-state “hold” behavior of the controller will have begun.

$y_d^k$ : The average value of the remaining measurements before some final end time  $t_N$ . During this period, an approximately steady state response should occur maintaining the output of the controller near the reference level.

### 3.3.1.3 Adaptation Law

Given the control parameters to be adjusted,  $\tau_p$ ,  $\tau_s$ , and  $\tau_d$ , and measurements,  $y_p$ ,  $y_s$ , and  $y_d$ , a very simple adaptation law,  $\mathbf{T}$  in (3.5) can be implemented to adjust micro-robotic leg motion. In this law, the next set of control parameters for each adaptation cycle can be estimated by current control parameters and current performance measurements as follows:

$$\begin{aligned}\tau_p^{k+1} &= \tau_p^k + \gamma_p (r - y_p^k) \\ \tau_s^{k+1} &= \tau_s^k + \gamma_s (y_s^k - y_p^k) \\ \tau_d^{k+1} &= \tau_d^k + \frac{\gamma_d}{f_d} (r - y_d^k)\end{aligned}\tag{3.18}$$

where  $\gamma_p$ ,  $\gamma_s$ , and  $\gamma_d$  are adaptive control constants and obtained by convergence analysis for the proposed controller, which is described in the next section. (3.18) is related to an objective function for optimization being to minimize

$$\begin{aligned}J(\boldsymbol{\epsilon}^k) &= \text{mean}\left(\left|\boldsymbol{\epsilon}_p^k\right| + \left|\boldsymbol{\epsilon}_s^k\right| + \left|\boldsymbol{\epsilon}_d^k\right|\right) \\ &= \text{mean}\left(\left|y_p^k - r\right| + \left|y_s^k - y_p^k\right| + \left|y_d^k - r\right|\right)\end{aligned}\tag{3.19}$$

This adaptation law was selected to imitate proportional control of the measurements of interest, which allows both extremely simple implementation and tractable, though much more complex, convergence analysis. Other adaptation laws could be tested using more complex functions of the measurements, but the adaptation law in (3.18) has proven to provide sufficient performance for the target micro-robotic application.

The control law is implemented using the on-off decision rule shown in equation (3.3), as:

$$u(t) = \begin{cases} 0 & \text{if } \left\{ \begin{array}{l} \tau_p < t \leq \tau_s \\ \tau_s + (i/f_d + \tau_d) < t \leq \tau_s + (i+1)/f_d \end{array} \right\} \\ 1 & \text{if } \left\{ \begin{array}{l} 0 < t \leq \tau_p \\ \tau_s + (i/f_d) < t \leq \tau_s + (i/f_d + \tau_d) \end{array} \right\} \end{cases} \quad (3.20)$$

where  $f_d$  is a desired switching frequency in the steady-state phase, selected by the controller designer, and  $i$  is a counting variable for the number of steady-state switches,  $i = 0, 1, 2, \dots, i_{\max}$ , occurring before the end time for the iteration,  $t_N$ .

### 3.3.2 Convergence Analysis Approach

#### 3.3.2.1 Requirement for Convergence

The behavior of a system of the type described in (3.1), (3.7), and (3.8) under the adaptation law (3.18) may be viewed as a discrete time dynamic system, with equilibrium points from (3.18) of  $y_p = r$ ,  $y_s = y_p$ , and  $y_d = r$ . It may be possible for the system to converge to these equilibrium points as  $k \rightarrow \infty$  under the given adaptation law if there are some ranges of switching times,  $\tau_p^*$ ,  $\tau_s^*$ , and  $\tau_d^*$ , and maximum allowable changes in switching times,  $\delta\tau_{p,\max} > 0$ ,  $\delta\tau_{s,\max} > 0$ , and  $\delta\tau_{d,\max} > 0$ , such that

$$\begin{cases} \tau_p^k \in \tau_p^*, |\delta\tau_p^{k+1}| < \delta\tau_{p,\max} \\ \tau_s^k \in \tau_s^*, |\delta\tau_s^{k+1}| < \delta\tau_{s,\max} \\ \tau_d^k \in \tau_d^*, |\delta\tau_d^{k+1}| < \delta\tau_{d,\max} \end{cases} \Rightarrow \begin{cases} 0 < \frac{\delta y_p^{k+1}}{\delta\tau_p^{k+1}} < (\delta_p)_{\max} \\ (\delta_s)_{\min} < \frac{\delta y_s^{k+1}}{\delta\tau_s^{k+1}} < (\delta_s)_{\max} & \& 0 < \frac{\delta y_s^{k+1}}{\delta\tau_p^{k+1}} < (\delta_s)_{\max} \\ (\delta_d)_{\min} < \frac{\delta y_d^{k+1}}{\delta\tau_d^{k+1}} < (\delta_d)_{\max} & \& 0 < \frac{\delta y_d^{k+1}}{\delta\tau_s^{k+1}} < (\delta_d)_{\max} \\ & \& 0 < \frac{\delta y_d^{k+1}}{\delta\tau_p^{k+1}} < (\delta_d)_{\max} \end{cases} \quad (3.21)$$



where  $\delta\tau_{(\cdot)}^{k+1} \equiv \tau_{(\cdot)}^{k+1} - \tau_{(\cdot)}^k$ ,  $\delta y_{(\cdot)}^{k+1} \equiv y_{(\cdot)}^{k+1} - y_{(\cdot)}^k$ , and  $\delta_{(\cdot)}$  is a bound of output changes in terms of the switching time changes.

If this is the case under certain conditions on  $(\delta_p)_{\max}$ ,  $(\delta_s)_{\max}$ ,  $(\delta_d)_{\max}$ ,  $(\delta_d)_{\min}$ , and  $(\delta_s)_{\min}$ , there will also exist some  $\gamma_p$ ,  $\gamma_s$ , and  $\gamma_d$  small enough to ensure that

$$\begin{aligned} |y_p^{k+1} - r| &< |y_p^k - r| \\ |y_s^{k+1} - y_p^{k+1}| &< |y_s^k - y_p^k| \\ |y_d^{k+1} - r| &< |y_d^k - r| \end{aligned} \quad (3.22)$$

for  $\tau_p^k \in \tau_p^*$ ,  $\tau_s^k \in \tau_s^*$ , and  $\tau_d^k \in \tau_d^*$ . Switching times within these ranges are then guaranteed to move the measured outputs closer to their targets in the next time step. To ensure convergence to the targets themselves, a closed subset of switching time ranges,  $\tau_p^{*c}$ ,  $\tau_s^{*c}$ , and  $\tau_d^{*c}$ , must be identified such that  $\tau_p^{k+1} \in \tau_p^{*c}$ ,  $\tau_s^{k+1} \in \tau_s^{*c}$ , and  $\tau_d^{k+1} \in \tau_d^{*c}$  if  $\tau_p^k \in \tau_p^{*c}$ ,  $\tau_s^k \in \tau_s^{*c}$  and  $\tau_d^k \in \tau_d^{*c}$ . In addition, for a given  $r$ ,  $y_p = r$ ,  $y_s = y_p$ , and  $y_d = r$  must be known to exist for some set of switching times among  $\tau_p^{*c}$ ,  $\tau_s^{*c}$ , and  $\tau_d^{*c}$ .

The convergence criteria above are ensuring that the object function in (3.19) is being reduced from step  $k$  to  $k+1$  due to (3.22) if  $\tau_p^k \in \tau_p^{*c}$ ,  $\tau_s^k \in \tau_s^{*c}$  and  $\tau_d^k \in \tau_d^{*c}$ , and that this must further be true in ensuing steps if both the switching time set is closed for a given set of adaptation gains and  $r$  may be reached for some set of switching times within the set. In other words, If there exists  $\boldsymbol{\varepsilon}^k = 0$  at the equilibrium point for (3.18) and a closed set,  $\mathbf{D} = [\tau_p^{*c} \ \tau_s^{*c} \ \tau_d^{*c}]$ , of switching times satisfying (3.21), which contains some set of switching times corresponding to  $\boldsymbol{\varepsilon}^k = 0$  in  $\mathbf{R}^N$ , and  $J: \mathbf{D} \rightarrow \mathbf{R}$  is a continuously differentiable function with respect to  $k$ , then we can select  $\gamma_p$ ,  $\gamma_s$ , and  $\gamma_d$  small enough that

$$\begin{aligned} J(0) &= 0 \text{ and } J(\boldsymbol{\varepsilon}^k) > 0 \text{ in } \mathbf{D} - \{0\} \\ J(\boldsymbol{\varepsilon}^{k+1}) - J(\boldsymbol{\varepsilon}^k) &< 0 \end{aligned} \quad (3.23)$$

is true throughout  $\mathbf{D}$ , with the second statement in (3.23) being true due to (3.22). Then, (3.19) can be a Lyapunov function and the convergence criteria (3.21) are ensuring

asymptotically stable convergence in a Lyapunov sense within the closed set of switching times.

### 3.3.2.2 Effects of Changes to Switching Times

In order to identify regions  $\tau_p^{*c}$ ,  $\tau_s^{*c}$ , and  $\tau_d^{*c}$  for various potential references,  $r$ , the known, nominal effects of incremental changes in switching times can be compared to uncertainties in these effects due to the unknown nonlinearities in the system model. To do this, the deviation in possible outputs from the nominal response of the system must first be found. Given the nominal system described by states  $\mathbf{x}$  and the real, but unknown system described by states  $\mathbf{x}_b$ , the error states,  $\mathbf{x}_e$ , has dynamics

$$\begin{aligned}\dot{\mathbf{x}}_e(t) &= \dot{\mathbf{x}}_b(t) - \dot{\mathbf{x}}(t) \\ &= \mathbf{A}\mathbf{x}_b(t) + \mathbf{f}_{\mathbf{x}_b}(\mathbf{x}_b(t)) + \mathbf{B}u(t) + \mathbf{f}_u(\mathbf{x}_b(t))u(t) - \mathbf{A}\mathbf{x}(t) - \mathbf{B}u(t) \\ &= \mathbf{A}\mathbf{x}_e(t) + \mathbf{f}_{\mathbf{x}_b}(\mathbf{x}_b(t)) + \mathbf{f}_u(\mathbf{x}_b(t))u(t)\end{aligned}\quad (3.24)$$

For time response of (3.24), because the precise error of states is unknown, the magnitude of error may merely be bounded, with the bound defined as a function of time by  $\Delta(t)$ ,

$$\mathbf{x}_e(t) = e^{\mathbf{A}(t-t_0)}\mathbf{x}_e(t_0) + \int_{t_0}^t e^{\mathbf{A}(t-s)} \left[ \mathbf{f}_{\mathbf{x}_b}(\mathbf{x}_b(s)) + \mathbf{f}_u(\mathbf{x}_b(s))u(s) \right] ds \quad (3.25a)$$

$$\begin{aligned}|\mathbf{x}_e(t)| &\leq \Delta(t) \\ &\equiv e^{\mathbf{A}(t-t_0)} |\Delta(t_0)| \\ &\quad + \int_{t_0}^t e^{\mathbf{A}(t-s)} \left[ \mathbf{C}_{\mathbf{x}_b}(|\mathbf{x}(s)| + \Delta(s)) + \mathbf{C}_u(|\mathbf{x}(s)| + \Delta(s))u(s) \right] ds\end{aligned}\quad (3.25b)$$

where  $t_0$  is an arbitrary starting point from which error  $\mathbf{x}_e(t)$  is to be calculated.

Given an upper bound on error at time  $t_0$ ,  $\Delta(t)$ , may be calculated numerically, as by iterating from a loose initial guess for  $|\mathbf{x}_e(t)|$ , such as  $2\mathbf{x}_{\max}$ . This typically results in a bound  $\Delta(t)$  reflecting a growing uncertainty in the true system response compared to the nominal system.

Using (3.25b), known nominal response, and known uncertain nonlinear bound (3.3) and (3.4), effect in real response of changes to switching times of input can be bounded as

$$\begin{aligned}
\Delta_{DT}^{k+1}(\tau_Q^{k+1}) &\leq \max_{(\tau_Q^k + \delta\tau_{Q-1}^{k+1}, \tau_Q^k)} \left[ \left| \mathbf{A} \left| \Delta^{k+1}(t) + \mathbf{C}_{x_b} \left( \left| \mathbf{x}^{k+1}(t) \right| + \Delta^{k+1}(t) \right) \right. \right. \right. \\
&\quad \left. \left. \left. + \mathbf{C}_u \left( \left| \mathbf{x}^{k+1}(t) \right| + \Delta^{k+1}(t) \right) u^{k+1}(t) \right| \right] \left| \delta\tau_Q^{k+1} - \delta\tau_{Q-1}^{k+1} \right| \\
\Delta_{IC}^{k+1}(\tau_Q^k) &\leq \left[ \sum_{q=1}^{Q-1} \left| e^{\mathbf{A}(\tau_Q^k - \tau_q^k)} \right| \left( \Delta_{DT}^{k+1}(\tau_q^{k+1}) + \Delta_{IC}^{k+1}(\tau_q^k) \right) \right] \\
&\quad + \int_{\tau_{Q-1}^k}^{\tau_Q^k} \left| e^{\mathbf{A}(t-s)} \right| \left[ \left| \mathbf{C}_{x_b} \left( \left| \mathbf{x}^{k+1}(s) - \mathbf{x}^k(s) \right| + \Delta_{IC}^{k+1}(s) \right) \right. \right. \\
&\quad \left. \left. + \mathbf{C}_u \left( \left| \mathbf{x}^{k+1}(s) - \mathbf{x}^k(s) \right| + \Delta_{IC}^{k+1}(s) \right) u(s) \right] ds
\end{aligned} \tag{3.26}$$

where  $\Delta_{DT}(t)$  denotes upper bounds on error in the estimated change in response due to changes in duration of the current ‘on’ or ‘off’ period at time  $t$ , and  $\Delta_{IC}(t)$  means effect of changes in initial conditions for the current ‘on’ or ‘off’ phase of motion, assuming the previous switching time were used during this phase. The detail procedure to achieve (3.26) is presented in Appendix B.

### 3.3.2.3 Application to Convergence Analysis

At a measurement point, which occurs at the same time in each iteration, the most recent switching time must be identified, denoted by index  $Q_n$ , in order to find uncertainty in the effects of the changes in switching times from iteration  $k$  to iteration  $k+1$ , becoming (3.27)

$$\begin{aligned}
Q_n &= \max(q | \tau_q < t_n) \\
\Delta_{DT}^{k+1}(t_n) &\leq \max_{(t_n + \delta\tau_{Q_n}^{k+1}, t_n)} \left[ \left| \mathbf{A} \Delta^{k+1}(t) + \mathbf{C}_{x_b} \left( |\mathbf{x}^{k+1}(t)| + \Delta^{k+1}(t) \right) \right. \right. \\
&\quad \left. \left. + \mathbf{C}_u \left( |\mathbf{x}^{k+1}(t)| + \Delta^{k+1}(t) \right) u^{k+1}(t) \right| \delta\tau_{Q_n}^{k+1} \right] \\
\Delta_{IC}^{k+1}(t_n) &\leq \left[ \sum_{q=1}^{Q_n} \left| e^{\mathbf{A}(t_n - \tau_q^k)} \left( \Delta_{DT}^{k+1}(\tau_q^{k+1}) + \Delta_{IC}^{k+1}(\tau_q^k) \right) \right| \right] \\
&\quad + \int_{\tau_{Q_n}^k}^{t_n} \left| e^{\mathbf{A}(t-s)} \right| \left[ \left| \mathbf{C}_{x_b} \left( |\mathbf{x}^{k+1}(s) - \mathbf{x}^k(s)| + \Delta_{IC}^{k+1}(s) \right) \right. \right. \\
&\quad \left. \left. + \mathbf{C}_u \left( |\mathbf{x}^{k+1}(s) - \mathbf{x}^k(s)| + \Delta_{IC}^{k+1}(s) \right) u(s) \right| \right] ds
\end{aligned} \tag{3.27}$$

which gives the uncertainty in the change in output at the measurement points from one iteration to the next, which in turn may be compared with the nominal change in output to determine whether  $y_p$ ,  $y_s$ , and  $y_d$  are certain to move in the desired directions.

In other words, combinations of  $\tau_p$ ,  $\tau_s$ ,  $\tau_d$ , are evaluated as to whether

$$\begin{aligned}
z_p^{k+1} > z_p^k &\ \& \ |z_p^{k+1} - z_p^k| > \mathbf{C} \Delta_{DT}^{k+1}(t_1) \\
z_s^{k+1} < z_s^k &\ \& \ |z_s^{k+1} - z_s^k| > \mathbf{C} \Delta_{DT}^{k+1}(t_2) + \mathbf{C} \Delta_{IC}^{k+1}(t_2) \\
z_d^{k+1} > z_d^k &\ \& \ |z_d^{k+1} - z_d^k| > \frac{1}{N+1} \sum_{n=2}^N \left( \mathbf{C} \Delta_{DT}^{k+1}(t_n) + \mathbf{C} \Delta_{IC}^{k+1}(t_n) \right)
\end{aligned} \tag{3.28}$$

for some  $\delta\tau_{p,max} > 0$ ,  $\delta\tau_{s,max} > 0$ ,  $\delta\tau_{d,max} > 0$ , where  $z_p$ ,  $z_s$ , and  $z_d$  are defined in the same manner as  $y_p$ ,  $y_s$ , and  $y_d$ , but for the nominal states,  $\mathbf{x}$ . If (3.36) is satisfied for some candidate switching times, then the behavior of the true response is will satisfy (3.21) for at least these switching times and shifts in switching times.

To create a closed set of  $\tau_p$ ,  $\tau_s$ , and  $\tau_d$  in which the measured outputs to move towards their targets, a second criterion must be applied, based on a specific reference  $r$  and set of adaptation gains, that requires

$$\begin{aligned}
& \tau_p^k + \gamma_p \left( r - z_p^k + \mathbf{C}\Delta^k(t_1) \right) \in \tau_p^{*c} \ \& \ \tau_p^k + \gamma_p \left( r - z_p^k - \mathbf{C}\Delta^k(t_1) \right) \in \tau_p^{*c} \\
& \tau_s^k + \gamma_s \left( z_s^k - z_p^k + \mathbf{C}\Delta^k(t_2) + \mathbf{C}\Delta^k(t_1) \right) \in \tau_s^{*c} \\
& \quad \& \ \tau_s^k + \gamma_s \left( z_s^k - z_p^k - \mathbf{C}\Delta^k(t_2) - \mathbf{C}\Delta^k(t_1) \right) \in \tau_s^{*c} \\
& \tau_d^k + \frac{\gamma_d}{f_d} \left( r - z_d^k + \frac{1}{N-1} \sum_{n=1}^N \mathbf{C}\Delta^k(t_n) \right) \in \tau_d^{*c} \\
& \quad \& \ \tau_d^k + \frac{\gamma_d}{f_d} \left( r - z_d^k - \frac{1}{N-1} \sum_{n=1}^N \mathbf{C}\Delta^k(t_n) \right) \in \tau_d^{*c}
\end{aligned} \tag{3.29}$$

Ranges of switching times  $\tau_p^{*c}$ ,  $\tau_s^{*c}$ , and  $\tau_d^{*c}$  whose content satisfy both (3.28) and (3.29) for a given reference,  $r$ , define a region in which the measured outputs will converge to their target values. One necessary condition (though not sufficient, alone) for a region satisfying (3.29) to exist is that within a continuous subset of  $\tau_p^*$ ,  $\tau_s^*$ , and  $\tau_d^*$  there exists a  $\tau_p$ ,  $\tau_s$ , and  $\tau_d$  resulting in  $z_p + \mathbf{C}\Delta(t_1) < r$ ,  $z_s + \mathbf{C}\Delta(t_2) < r$ , and  $z_d + 1/(N-1) \sum_{n=1}^N \mathbf{C}\Delta(t_n) < r$ , and some other  $\tau_p$ ,  $\tau_s$ , and  $\tau_d$  resulting in  $z_p - \mathbf{C}\Delta(t_1) > r$ ,  $z_s - \mathbf{C}\Delta(t_2) > r$ , and  $z_d - 1/(N-1) \sum_{n=1}^N \mathbf{C}\Delta(t_n) > r$ .

In other words, it is not possible to guarantee that switching times will remain within a closed region if it is not guaranteed for the closed region to contain switching time selections resulting in outputs below and above the final reference value. While this fact alone may not guarantee convergence, it can be useful for initial evaluation of reference values that may work, by choosing

$$\begin{aligned}
r < \max_{\tau_p, \tau_s, \tau_d \in \tau_p^*, \tau_s^*, \tau_d^*} \left[ \min \left( z_p - \mathbf{C}\Delta(t_1), z_s - \mathbf{C}\Delta(t_2), z_d - \frac{1}{N-1} \sum_{n=1}^N \mathbf{C}\Delta(t_n) \right) \right] \\
r > \min_{\tau_p, \tau_s, \tau_d \in \tau_p^*, \tau_s^*, \tau_d^*} \left[ \max \left( z_p + \mathbf{C}\Delta(t_1), z_s + \mathbf{C}\Delta(t_2), z_d + \frac{1}{N-1} \sum_{n=1}^N \mathbf{C}\Delta(t_n) \right) \right]
\end{aligned} \tag{3.30}$$

### 3.3.3 Convergence Analysis for 2<sup>nd</sup> Order Microactuator

To illustrate the use of the convergence analysis in Section 3.3.2, and to prove convergence to certain values of  $r$  for the experimental system used in system validation,

convergence analysis is performed for a 2<sup>nd</sup>-order piezoelectric microactuator. The nominal model for the actuator is

$$\begin{bmatrix} \dot{x}_{(1)}(t) \\ \dot{x}_{(2)}(t) \end{bmatrix} = \begin{bmatrix} 0 & 1 \\ -38590 & -12.1 \end{bmatrix} \begin{bmatrix} x_{(1)}(t) \\ x_{(2)}(t) \end{bmatrix} + \begin{bmatrix} 0 \\ 32300 \end{bmatrix} u(t) \quad (3.31)$$

and the nonlinear model has the form

$$\begin{bmatrix} \dot{x}_{b(1)}(t) \\ \dot{x}_{b(2)}(t) \end{bmatrix} = \begin{bmatrix} 0 & 1 \\ -38590 & -12.1 \end{bmatrix} \begin{bmatrix} x_{b(1)}(t) \\ x_{b(2)}(t) \end{bmatrix} + \begin{bmatrix} 0 \\ f_{x_b(1)}(x_{b(1)}(t)) + f_{x_b(2)}(x_{b(2)}(t)) \end{bmatrix} \\ + \begin{bmatrix} 0 \\ 32300 + f_{u(2)}(x_{b(2)}(t)) \end{bmatrix} u(t) \quad (3.32)$$

The unknown functions  $f_{x_b(1)}(x_{b(1)})$  and  $f_{u(2)}(x_{b(2)})$  are used to encompass nonlinearities due to piezoelectric hysteresis and nonlinear actuator gain as reflected in system gain and natural frequency behavior, and unknown function  $f_{x_b(2)}(x_{b(2)})$  accounts for uncertainty about the damping coefficient of the system. These nonlinear functions are estimated to have bounds of uncertainty matrices in (3.3) and (3.4) such as

$$\mathbf{C}_{x_b} = \begin{bmatrix} 0 & 0 \\ 1839 & 2.4 \end{bmatrix}, \mathbf{C}_u = \begin{bmatrix} 0 & 0 \\ 223 & 0 \end{bmatrix}, \mathbf{C}'_{x_b} = \begin{bmatrix} 0 & 0 \\ 7718 & 9.6 \end{bmatrix}, \mathbf{C}'_u = \begin{bmatrix} 0 & 0 \\ 446 & 0 \end{bmatrix} \quad (3.33)$$

based on prior experimentation with thin-film piezoelectric actuators. These bounds reflect approximately 5% uncertainty in spring stiffness and gain and 20% uncertainty in damping ratio.

These levels are actually much larger than uncertainty about the macro-scale piezoelectric actuator used for experimental testing [7] but consistent with model uncertainty for micro-scale piezoelectric actuators [74] for which the control algorithm is ultimately targeted (micro-scale actuators are not yet used for experimental testing as current prototypes lack integrated sensing, although such sensors have been demonstrated on vertical piezoelectric actuators created through the same microfabrication process).

The ‘on’ input for the system tested is taken to be  $u_{\max} = 15$  V, and samples are taken every 0.0083s.

Using the system model above,  $\mathbf{x}^K$  and  $\Delta^K$  are first calculated numerically for ranges of potential switching times,  $0 < \tau_p < 0.0083$ s,  $0.0083 < \tau_s < 0.0166$ s, and  $0 < \tau_d < 0.0083$ s. For an illustration of the uncertainty margins in comparison to the nominal response, Figure 3.3 shows a sample response when  $\tau_p = 0.001$ s,  $\tau_s = 0.009$ s, and  $\tau_d = 0.003$ s surrounded by the associated error bounds, with sensor updates to the estimated output at the sampling points. As can be seen, error bounds grow over time, such that there use to draw conclusions about the system is limited to transient responses, with typical duration on the order just a few times the period of an under-damped system such as that in this example.

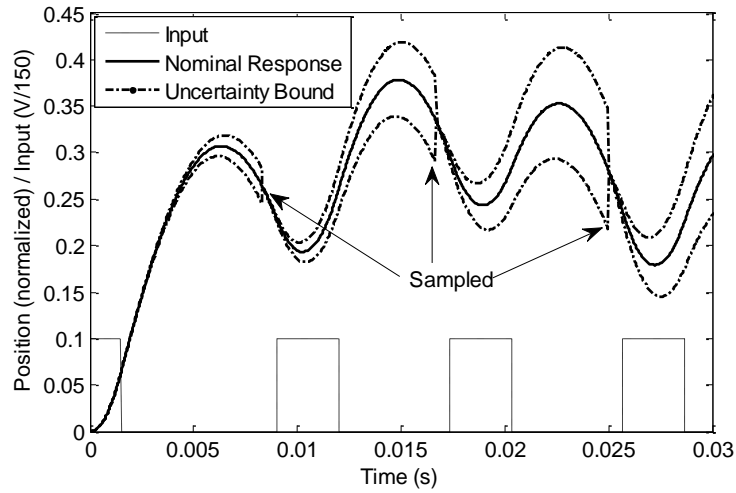


Figure 3.3 Sample nominal response to a switching input and bounds on uncertainty in output relative to response due to bounded, unknown nonlinearities

Next, the nominal response in the next iteration,  $\mathbf{x}^{k+1}$ , uncertainty in the full response,  $\Delta^{k+1}$ , and uncertainty in the change in response with respect to switching times,  $\Delta_{DT}^{k+1}$ , and initial conditions,  $\Delta_{IC}^{k+1}$ , are calculated numerically for hypothetical changes in switching times  $\delta\tau_p^{k+1}$ ,  $\delta\tau_s^{k+1}$ , and  $\delta\tau_d^{k+1}$ . As an illustration of the behavior observed, Figure 3.4 (a) shows the change in nominal response at the first measurement point,  $z_p^{k+1}$

$-z_p^k$  as a function of  $\tau_p^k$  and  $\delta\tau_p^{k+1}$ , while Figure 3.4 (b) shows the total uncertainty at time  $t_1$ ,  $\mathbf{C}\Delta_{DT}^{k+1}(t_1) + \mathbf{C}\Delta_{IC}^{k+1}(t_1)$ .

For this first output, we observe that the effect of a change in switching time  $\tau_p$  has a much larger effect on the output than uncertainty at time  $t_1$ , so that increasing  $\tau_p$  can be reliably expected to increase  $y_p$  for this system. The latter outputs,  $y_s$ , and  $y_d$ , face much greater uncertainty in the response, due to the growing error bounds, and more complicated dependence on switching times, with limits on  $\tau_s^k$  and  $\delta\tau_s^{k+1}$  being especially strict. Figure 3.5 shows the maximum change,  $\delta\tau_s^{k+1}$ , for various values of  $\tau_s^k$  and  $\tau_d^k$  that satisfies the desired properties for  $z_s$  and  $z_d$  from (3.29), for a sample value of  $\tau_p$ ,  $\tau_p = 0.003$ s.

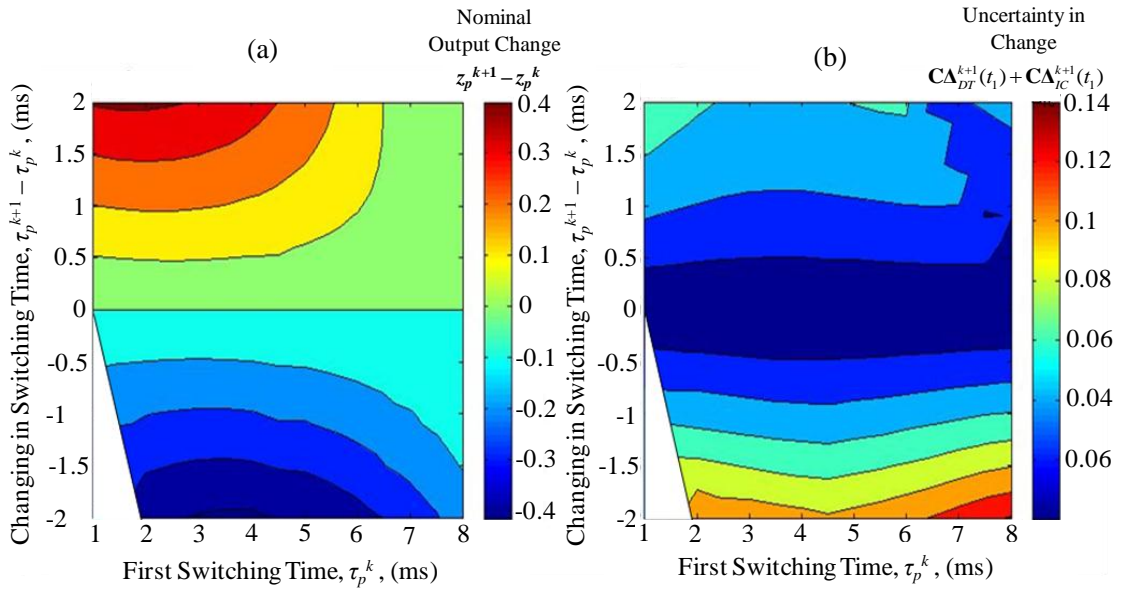


Figure 3.4 (a) Nominal change in output at first measurement point ( $x_p$ ) as a function of first switching time in current iteration ( $\tau_p$ ) and change in first switching time next iteration ( $\delta\tau_p$ ) (b) Magnitude of possible error in estimate of change in output at first measurement point ( $y_p^{k+1} - z_p^{k+1} - y_p^k - z_p^k$ )



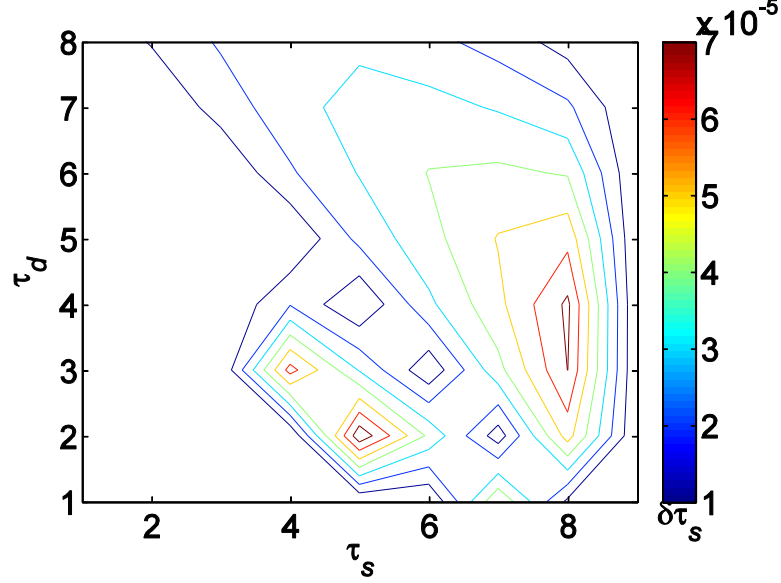


Figure 3.5 Maximum change in second switching time ( $\delta\tau_s$ ) satisfying convergence criteria as a function of switching times  $\tau_s$  and  $\tau_d$  for  $\tau_p = 0.003s$

Tabulating all  $\tau_p^k$ ,  $\tau_s^k$ , and  $\tau_d^k$  for which (3.21) is satisfied for  $\delta\tau_p^{k+1} < 100 \mu s$ ,  $\delta\tau_s^{k+1} < 10 \mu s$ , and  $\delta\tau_d^{k+1} < 100 \mu s$  produces ranges  $\tau_p^*$ ,  $\tau_s^*$ , and  $\tau_d^*$  as shown in Figure 3.5. To convert these bounds on changes in switching times to adaptation law gains, the maximum and minimum possible values for each output are calculated, to produce

$$\begin{aligned}
 \gamma_p &< \frac{\delta\tau_{p,\max}}{\max_{\substack{\tau_p, \tau_s, \tau_d \in \tau_p^*, \tau_s^*, \tau_d^* \\ \delta\tau_p < \delta\tau_{p,\max}}} \left( |z_p^{k+1} - z_p^k| + \mathbf{C}\mathbf{\Delta}^{k+1}(t_1) \right)} \\
 \gamma_s &< \frac{\delta\tau_{s,\max}}{\max_{\substack{\tau_p, \tau_s, \tau_d \in \tau_p^*, \tau_s^*, \tau_d^* \\ \delta\tau_s < \delta\tau_{s,\max}}} \left( |z_s^{k+1} - z_p^{k+1} - z_s^k - z_p^k| + \mathbf{C}\mathbf{\Delta}^{k+1}(t_2) + \mathbf{C}\mathbf{\Delta}^{k+1}(t_1) \right)} \\
 \gamma_d &< \frac{\delta\tau_{d,\max}}{\max_{\substack{\tau_p, \tau_s, \tau_d \in \tau_p^*, \tau_s^*, \tau_d^* \\ \delta\tau_d < \delta\tau_{d,\max}}} \left( |z_d^{k+1} - z_d^k| + \frac{1}{Q-1} \sum_{q=1}^Q \mathbf{C}\mathbf{\Delta}^{k+1}(t_q) \right)} f_d
 \end{aligned} \tag{3.34}$$

giving feasible  $\gamma_p < 0.011$ ,  $\gamma_s < 0.0091$ , and  $\gamma_d < 0.0085f_d$  for this specific system (note that  $k$  and  $k+1$  do not correspond to a specific time step above, but are retained in (3.34))

to signify the change in response for each candidate switching time and increment in switching time evaluated).

In addition, candidate reference values,  $r$ , for convergence analysis are selected using (3.30), with  $0.16 < r < 0.65$  guaranteed for some values of  $\tau_p^k$ ,  $\tau_s^k$ , and  $\tau_d^k$  in  $\tau_p^*$ ,  $\tau_s^*$ , and  $\tau_d^*$ . The closed set of switching times satisfying (3.29) as well as (3.21) for a sample target of  $r = 0.5$  and  $\delta\tau_p^{k+1} < 100 \mu\text{s}$ ,  $\delta\tau_s^{k+1} < 10 \mu\text{s}$ , and  $\delta\tau_d^{k+1} < 100\mu\text{s}$  is indicated by darker dots in Figure 3.6, with candidate switching times from the margins of the tested region and those that could, given uncertainty, respond to a perturbation in switching by pushing the response out of the set discarded. The outcome of the analysis, then, is that for various references,  $r$ , a set of  $\tau_p^{*c}$ ,  $\tau_s^{*c}$ , and  $\tau_d^{*c}$  may potentially be found that can be used to select an initial switching time guess, from which the adaptation algorithm will converge to the corresponding target values.

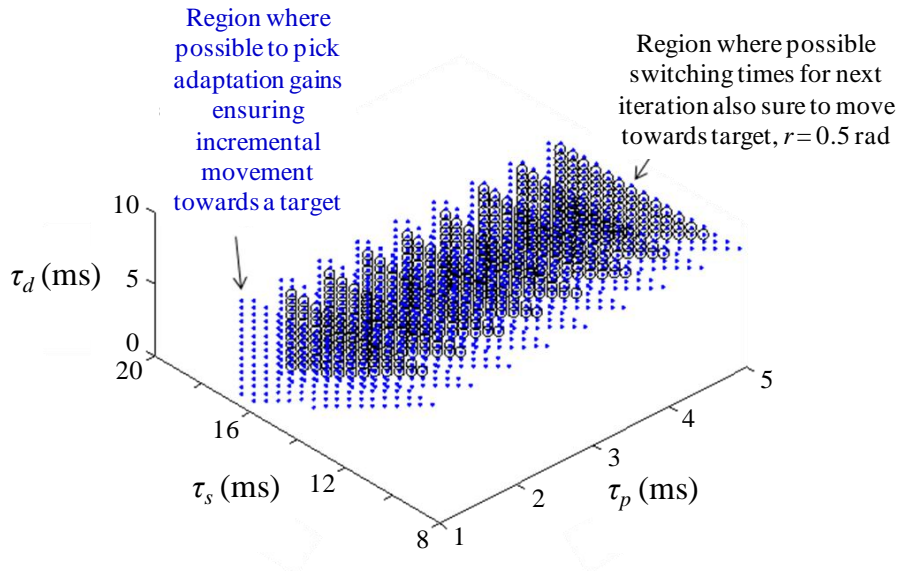


Figure 3.6 (Dotted points) Region of switching times for which some incremental change in switching time satisfies convergence criterion for at least one iteration (Circle points) Closed region of switching times satisfying convergence conditions when  $r = 0.5$

### 3.3.4 Validation by Simulation and Experiment

Controller performance was first tested in simulation on a variety of linear and nonlinear systems. A sample response is shown in Figure 3.7, for the nominal system (3.31) with uncertainties of 5% spring stiffness and gain and 20% of damping ratio.

Convergence was evaluated for a step duration of 0.05s as above, using  $\gamma_p = 0.009$ ,  $\gamma_s = 0.008$ , and  $\gamma_d = 0.008$  for the adaptation gains and  $u_{max} = 15$ . Generally fast adaptation of the simulated systems to which the controller is applied is observed, with convergence typically occurring in fewer than the 10<sup>th</sup> iteration. Experience with simulations indicated, as would be expected, that the convergence analysis is conservative, as systems are frequently observed to converge to target outputs when given initial switching time guesses or adaptation gains outside the guaranteed ranges for convergence. On the other hand, pure guessing of adaptation gain values rarely results in effective convergence, such that the convergence analysis was quite useful in controller testing on simulated systems.

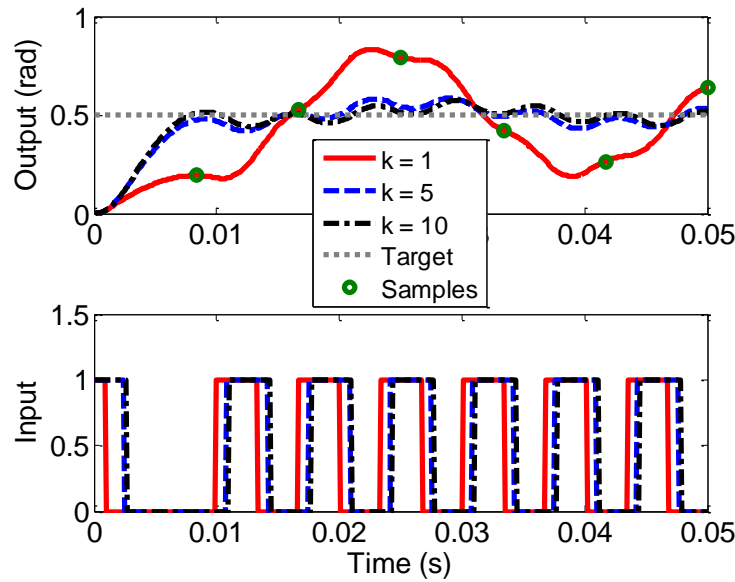


Figure 3.7 Simulation result of the nominal system (3.31) with model uncertainties

To evaluate the performance of the proposed iterative on-off controller experimentally, the controller is applied to a piezoelectric actuator test bed shown in

Figure 3.8. The actuator tested was a 40 mm long, 10 mm wide Ceratec bimorph actuator with a natural frequency of approximately 100 Hz. A strain gage was attached to the actuator to measure deflection, with output of the system being output voltage of the strain gage sensing circuit normalized to an output of 1 when the actuator is at its maximum steady-state displacement. Mass was added to the tip of the actuator to reduce the natural frequency of the experimental apparatus to 31.26 Hz and the damping ratio of the experimental system was 0.0307, to resemble the properties of a projected micro-robotic leg carrying a payload.

The control signal is generated on a TMS320F28335 digital signal processor, with an H-bridge circuit acting as the on-off interface between the low-voltage DSP and a 15 V supply for the actuator. For testing a converging case, the controller used  $\gamma_p = 0.009$ ,  $\gamma_s = 0.009$ ,  $\gamma_d = 0.0002$ ,  $f_d = 150$  Hz, and measurements taken every 0.0083s, or at a 120 Hz sampling rate. For testing a non-converging case, the controller used  $\gamma_p = 0.024$ ,  $\gamma_s = 0.009$ ,  $\gamma_d = 0.0002$ ,  $f_d = 150$  Hz, and  $T_s = 0.0083$  sec. As during the convergence analysis process of the simulated system (3.32), these control constants, driving frequency, and sample time are chosen to converge or to non-converge to a target reference level at a final adaptation cycle.

Sample responses for two scenarios are shown in Figure 3.9 (a) and (b). The experimental result with converging parameters show a successful convergence to the target reference level and has similar convergence trend to the simulation result. In the final adaptation cycle, system output rises successfully to the target reference level with minimal overshoot, and holds the system at the reference level using a limited number of on-off switching transitions. In addition, these results satisfy well the convergence criteria (3.21) and (3.22) as shown in Table 3.1. Once converged, the system maintains its behavior over many additional iterations, with up to several minutes repeated, with testing limited by data collection limits. However, there exists higher-order mode oscillation visible during the transient phase, possibly due weakness of the connection with the added mass. In contrast, the experimental result with predicted non-converging parameters does not show a successful convergence to the target reference level even if the adaptation cycle is increased.

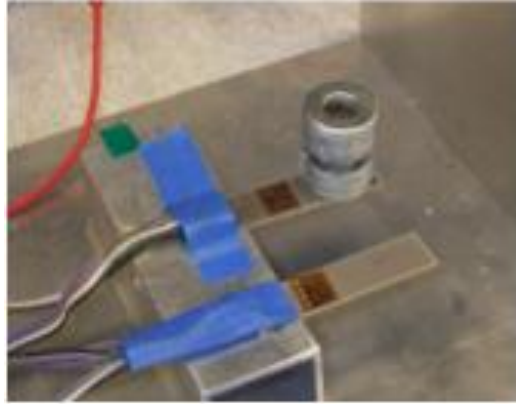


Figure 3.8 A piezoelectric actuator testbed

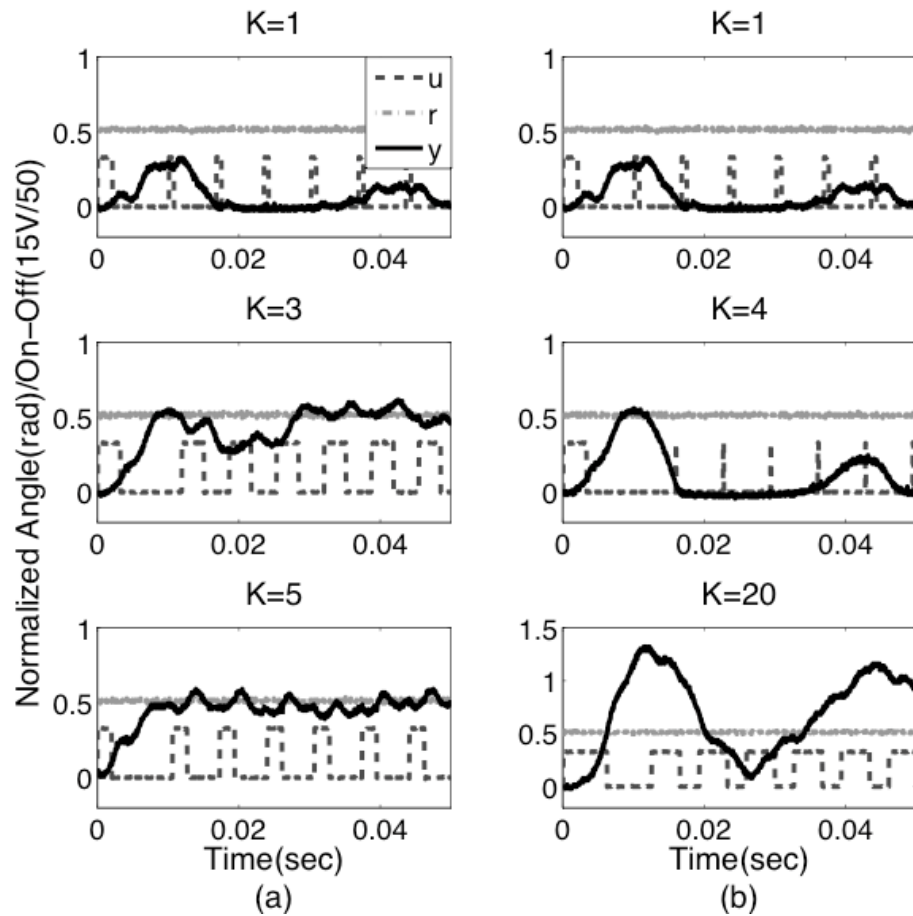


Figure 3.9 Sample experimental responses: (a) converging case and (b) non-converging case

Table 3.1 Measurement errors as  $k$  goes to infinity at Figure 3.9 (a)

	$ y_p^K - r $	$ y_s^K - y_p^K $	$ y_d^K - r $
$k = 1$	0.268	0.088	0.468
$k = 3$	0.052	0.064	0.012
$k = 5$	0.012	0.008	0.008

### 3.3.5 Summary of HA On-Off Controller

A model-free, iterative adaptive controller for on-off control of dynamic systems, has been proposed using a heuristic dynamic searching algorithm and associated behavior with respect to control of piezoelectric microactuators for autonomous micro-robots has been explored. The controller enables very low-power control of such actuators when many stepping motions are to be regulated. With careful selection of objectives by the designer, convergence can be obtained with relatively few output measurements, and on-off control lends itself to implementation with very little power and simple sensors and actuators. Simulation studies indicate a wide range of controller applicability for individual selections of controller parameters, particularly in the range needed for control of prototype micro-robot leg joints. In experimental testing on a macro-scale testbed, we have observed good convergence in the presence of modest nonlinearities and noise.

### 3.4 Stochastic Approximation Adaptive (SAA) On-Off Control

The second on-off adaptive controller, the SAA on-off controller presented in this section adjusts switching instances between “on” and “off” inputs to the actuator to minimize an objective function using simultaneous perturbation stochastic approximation (SPSA). This is an algorithm for gradient approximation of the object function using just a single sensor measurement in each iteration.

The strength of the proposed controller is that it relies on extremely simple sensing and input capabilities, which may allow it to perform control at very low power. The following section presents a detailed procedure to design the SAA on-off controller. Convergence conditions for the gradient approximation, then, are shown to apply when

the possibility for a range of possible switching times minimizing the objective function is accounted for, while a method is proposed for avoiding local minima for plants with bounded nonlinearities. Simulation and experimental verification is also shown.

### 3.4.1 Controller Design

#### 3.4.1.1 Problem Statements

The control objective of this second controller is to drive the true output of the system,  $z_b(t) = \mathbf{C}\mathbf{x}_b(t)$  of (3.5), at a specified final time to a desired target value,  $r$ , over several iterations of motion. Assuming that the control input in each iteration is a real, bounded function,  $h(\cdot)$ , of a parameter vector  $\boldsymbol{\theta}^k$ , the general control input case with continuous inputs,  $u^k \in \mathbf{R}$ , results in an iterative system input described by

$$u^k(t) = h(\boldsymbol{\theta}^k), \boldsymbol{\theta}^k = [\theta_1^k \quad \theta_2^k \quad \cdots \quad \theta_Q^k] \quad (3.35)$$

The control system goal becomes to find an optimized parameter vector set,  $\boldsymbol{\theta}^k$ , minimizing the error between the system output and desired target under fixed power consumption with a fixed on-off transitions rather than a full minimization of power output feedback, which is assumed to be made sufficiently low by using a small number of switching transitions and sensor measurements. The ideal minimization problem with respect to  $\boldsymbol{\theta}^k$  and output error can then be stated as follows:

$$\min_{\theta_i^k \geq 0, i=1, \dots, p} \left( J(\boldsymbol{\theta}^k) = \frac{1}{2} \int_0^{t_f} (\mathbf{C}\mathbf{x}_b(t) - r)^2 dt \right) \quad (3.36)$$

To solve problem (3.36), typically a gradient-based optimization method is used, as in

$$\begin{aligned} \boldsymbol{\theta}^{k+1} &= \boldsymbol{\theta}^k - \alpha^k \mathbf{g}(\boldsymbol{\theta}^k) \\ \mathbf{g}(\boldsymbol{\theta}^k) &= \left( \frac{\partial \mathbf{x}_b}{\partial \boldsymbol{\theta}^k} \right)^T \left( \frac{\partial J}{\partial \mathbf{x}_b} \right)^T \end{aligned} \quad (3.37)$$

where  $\alpha^k$  is the step size of the algorithm to be updated and  $\mathbf{g}(\boldsymbol{\theta}^k)$  is the  $Q$ -dimensional gradient vector for the cost function  $J(\cdot)$  with respect to  $\boldsymbol{\theta}^k$ . This approach is used by several model based controllers [41, 43, 44, 75]. In these controllers, the system dynamics function  $\boldsymbol{\psi}_{xb}(\cdot)$  in (3.9) is completely known and there is no consideration of minimal use of measurement outputs. However, the gradient in equation (3.37) for the cost function cannot be determined in this paper because it is assumed that equations (3.36) and (3.37) are based on an unknown functions,  $\boldsymbol{\psi}_{xb}(\cdot)$ . Additionally, reduction of measurements is not accounted for by the standard gradient approaches because the gradient is based on derivation of a complete function. Even though a tradition gradient approximation, Finite Difference Stochastic Approximation (FDSA), is not based on a complete function, FDSA should incorporate many measurements; SPSA uses  $Q$  times fewer gradient evaluations than FDSA [60].

Therefore, to reduce measurement frequency, the simultaneous perturbation stochastic approximation (SPSA) algorithm is used for gradient approximation in this paper. This approximation method was developed by previous researchers as a model-free approach for finding optimal control parameters [52, 76 – 78]. SPSA is based on relating random perturbations of controller parameters with their influence on a cost function, which is in turn a function of output measurements from an unknown system with random noise.

Thus, SPSA does not require full knowledge of the form of the system dynamics. Most importantly, since SPSA requires only one or two measurements to compute gradient approximations regardless of the dimension, such as the problem (3.37), it is very useful and effective for limited measured outputs. Previous controllers based on SPSA have utilized a fixed functional structure for a controller, such as a Neural Network or a polynomial, which generates analog inputs. In contrast, an on-off controller permits only two possible input states, and this behavior must be defined in a way that is compatible with the SPSA algorithm. As a drawback, at most one system state may be regulated at the measurement time using a single measurement in each iteration.



### 3.4.1.2 Adaptation Law using SPSA

For a single-measurement scenario, the control task is to steer the true output of the system at the final time,  $y_f^k = z^k(t_f)$ , to a desired target,  $r$ , by finite-time on-off control using  $Q$  switching instances and a single measurement output. Under finite-time on-off control, the input,  $u^k(t)$ , applied to the system (3.2) varies switching times while alternating between zero and one (a constant maximum value,  $u_{max}$ ).

Redefining the switching vector,  $\boldsymbol{\tau}^k$  in (3.13), as

$$\boldsymbol{\tau}^k = [\tau_1^k \quad \tau_2^k \quad \cdots \quad \tau_Q^k] \quad (3.38)$$

then the system output at the final time,  $t_f$ , can be rewritten as a function of  $\boldsymbol{\tau}^k$  with the input (3.35):

$$y_f^k = \mathbf{C}\boldsymbol{\Psi}_{x_b}(t_f, 0, h(\boldsymbol{\tau}^k)) \quad (3.39)$$

As shown in Figure 3.10, in this formulation, the time periods between switching instances,  $\boldsymbol{\tau}^k$ , serve as the parameter vector,  $\boldsymbol{\theta}^k$ , in (3.35), and so the relationship  $h(\cdot)$  between parameters and input  $u^k(t)$  may be described for  $q = 1, 2, \dots, (Q/2)$  by

$$u(t) = \begin{cases} 1, & \tau_{2q-1}^k \leq t < \tau_{2q}^k \\ 0, & \tau_{2q}^k \leq t < \tau_{2q-1}^k \\ 0, & \tau_Q^k \leq t < t_f \end{cases} \quad (3.40)$$

Since only one measurement output will be used,

$$\min_{\tau_1 \geq 0, \tau_i \leq \tau_{i+1}, \tau_Q \leq t_f} \left( J(\boldsymbol{\tau}^k) = \frac{1}{2} (y_f^k - r)^2 \right) \quad (3.41)$$

replaces the minimization problem (3.36). By the SPSA algorithm, the problem defined in (3.41) may be solved by updating the input parameter vector  $\boldsymbol{\tau}^k$  until the cost function

$J(\cdot)$  goes to zero as iterative index  $k$  goes to infinity.

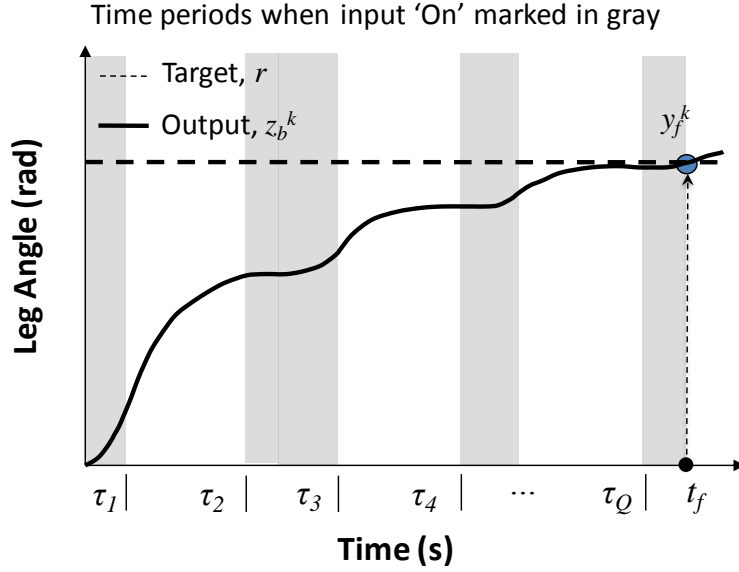


Figure 3.10 Illustration of input time parameter definitions for SAA on-off controller

The one-measurement form of the SPSA algorithm [12] for the control problem defined in (3.41) is applied to the switching control problem as follows:

Let  $\hat{\boldsymbol{\tau}}^k$  be the estimate of  $\boldsymbol{\tau}^k$  at the iteration  $k$ . SPSA has the standard iterative form

$$\begin{aligned}\hat{\boldsymbol{\tau}}^{k+1} &= \hat{\boldsymbol{\tau}}^k - a^k \hat{\mathbf{g}}^k(\hat{\boldsymbol{\tau}}^k) \\ a^k &= a / (k + A_g)^\alpha\end{aligned}\quad (3.42)$$

where  $a^k$  is a sequential gain coefficient and  $\hat{\mathbf{g}}^k(\cdot)$  is a simultaneously perturbed (SP) approximation to the unknown, real gradient vector,  $\mathbf{g}(\cdot)$ , for the cost function  $J(\cdot)$  with respect to  $\boldsymbol{\tau}^k$  at the  $k^{\text{th}}$  iteration. From the definition of (3.16), the adaptation law  $\mathbf{T}$  becomes  $a^k \hat{\mathbf{g}}^k(\hat{\boldsymbol{\tau}}^k)$ .

The one-measurement SPSA form of the  $\mathbf{g}(\cdot)$  estimation at iteration  $k$  is

$$\begin{aligned}\hat{\mathbf{g}}^k(\hat{\boldsymbol{\tau}}^k) &= \frac{\mathbf{Y}^{(+k)}}{c^k} \begin{bmatrix} 1/\sigma_1^k & 1/\sigma_2^k & \cdots & 1/\sigma_Q^k \end{bmatrix}^T \\ c^k &= c/k^\gamma\end{aligned}\quad (3.43)$$

where  $\{\boldsymbol{\sigma}^k \in \mathbf{R}^Q \mid \boldsymbol{\sigma}^k = [\sigma_1^k \ \sigma_2^k \ \dots \ \sigma_Q^k]^T\}$  is a vector of  $Q$  independent zero-mean random variables,  $c^k$  is a sequential gain, and  $Y^{(+k)}$  is the measured cost function value with the control parameter's random perturbation vector,  $\boldsymbol{\sigma}^k$ , and the noise isolated as  $d_v^k$ , i.e.

$$Y^{(+k)} = J(\hat{\boldsymbol{\tau}}^k + c^k \boldsymbol{\sigma}^k) + d_v^k \quad (3.44)$$

Note that only one measurement is required to form the gradient estimation at each iteration.

### 3.4.1.3 Implementation of Controller

The iterative on-off time-optimized control for the system (3.39) can be determined by using the method described in sections 3.4.1.2 with the following implementation procedure.

(Step 1) Pick initial guess for  $Q$ ,  $t_f$ ,  $\boldsymbol{\tau}^1$

(Step 2) Select coefficients,  $\alpha$ ,  $\gamma$ ,  $A_g$ ,  $c$ , and  $a$

Recommended values for  $\alpha$  and  $\gamma$  are 0.602 and 0.101 respectively, as established in [13]. An effective  $c$  can be equal or less to the estimated standard deviation of the measurement noise. The value of  $A_g$  is selected by a 10% (or less) value of the maximum number of expected/allowed iterations. Choose 'a' such that equation (3.52) holds:

$$\begin{aligned} & \frac{a}{(k + A_g)^\alpha} \times \max[\mathbf{g}^0(\hat{\boldsymbol{\tau}}^1)] \\ & = \textit{the smallest desired change} \\ & \quad \textit{magnitudes in } k = 1, \dots, K \end{aligned} \quad (3.45)$$

For detail of theoretical validation and practical effectiveness, see [62] and [79].

(Step 3) Generate the SP vector  $\sigma^k$

One of the candidates for the perturbation, and used in this paper, is a symmetric Bernoulli  $\pm 1$  distribution with a probability of  $1/2$  [80].

(Step 4) Generate  $u^k(t)$  in (3.40) by  $\hat{\tau}^{k+1} = \hat{\tau}^k + c^k \sigma^k$

(Step 5) Measure the system output at final time  $t_f$

(Step 6) Evaluate the cost function (3.41)

(Step 7) Approximate the gradient by equation (3.43)

(Step 8) Update  $\tau^k$  estimate (3.42) and check constraint (3.46): the ability to utilize constraints in the SPSA algorithm, having been shown in [81].

$$\text{Constraint: } \begin{aligned} \hat{\tau}^k &\in [0, \tau^1], \text{ for } y_f^1 > r \\ \hat{\tau}^k &\geq 0, \quad \text{for } y_f^1 \leq r \end{aligned} \quad (3.46)$$

(Step 9) go to (Step 3) or terminate algorithm if either  $\tau^k$  is smaller than a pre-specified bound or if a maximum allowable number of iterations has been reached, subject to available memory.

This implementation satisfies convergence conditions to reach a minimum of the objective function in (3.48) almost surely, as discussed in more detail below. The section 3.4.2 of this paper describes steps that may be taken in some cases to ensure  $y_f^k$  converges to the target,  $r$ , as  $k \rightarrow \infty$ , not just a local minima

### 3.4.2 Convergence Analysis

#### 3.4.2.1 Note for Convergence of the Proposed Algorithm

Certain specified properties of the dynamic system to be controlled and implementation of the adaptive on-off controller based on SPSA are necessary so that an approximated  $\hat{\tau}^k$  converges to a minimizing point  $\tau^*$ . These conditions are related to properties of gain sequence, boundedness in iteration domain, measurement noise,

smoothness of a cost function in its relation to system ODEs and statistical properties of the perturbations. Under them, the following Proposition 1 can be true.

*Proposition 1:*

If convergence conditions related to SPSA hold and there exists an optimal  $\tau^*$  for which  $\tau^1$  lies within the domain of attraction, then  $\hat{\tau}^k \rightarrow \tau^*$  as  $k \rightarrow \infty$  almost surely, or

$$P\left(\lim_{k \rightarrow \infty} \hat{\tau}^k \rightarrow \tau^*\right) = 1 \quad (3.47)$$

where  $\tau^*$  is a minimum of (3.41). For detailed properties of the conditions and theoretical proof of the proposition 1 for the general SPSA algorithm, see [59] and [61].

When applying the SPSA algorithm to on-off control, it is important to confirm that the properties of target plant subject to on-off control can satisfy convergence conditions of SPSA. First, for an on-off controller driving a system with continuous, differentiable dynamics, the finite duration,  $t_f$ , and finite input magnitude,  $u_{\max}$ , of the on-off controller ensure that the system output measurement,  $y_f$ , control parameters in  $\tau$ , and cost function,  $J(\cdot)$ , will be bounded. This ensures that properties of iterative boundedness are satisfied. Second, following (Step 2) and (Step 3) during implementation ensures that required properties of gain sequences and statistical properties of the perturbations are met. Third, since the source of noise in the system is taken to be white, Gaussian noise in sensor measurements independent of noise during prior steps and internal computations, properties of measurement noise can be satisfied. Finally, it was assumed that the system plant (3.2) satisfied Lipschitz continuity. This ensures that the cost function,  $J(\cdot)$ , is three times differentiable and that properties of smoothness can be satisfied.

In the nominal SPSA algorithm, proposition 1 implies almost sure convergence to the local minimum corresponding to an initial choice of  $\tau$  when convergence conditions are satisfied. For a specific minimizing solution to a cost function as in (3.41), the deterministic form and conceptual solution set of equation (3.42) can be related as an ODE as  $k$  goes to infinity [82, 83] as

$$\frac{d\boldsymbol{\tau}}{dt} = -\mathbf{g}(\boldsymbol{\tau}) \quad (3.48)$$

$$\mathbf{D}(\boldsymbol{\tau}^*) = \left\{ \boldsymbol{\tau}^l \mid \lim_{t \rightarrow \infty} \boldsymbol{\tau}(t \mid \boldsymbol{\tau}^l) = \boldsymbol{\tau}^* \right\} \quad (3.49)$$

where  $\mathbf{g}(\boldsymbol{\tau})$  is a continuous function on  $\mathbf{R}^Q$ ,  $\boldsymbol{\tau}^*$  is an asymptotically stable solution of (3.48),  $\mathbf{D}^*(\cdot)$  is a domain of convergence, and  $\boldsymbol{\tau}(t \mid \boldsymbol{\tau}^l)$  is the solution of (3.48) with initial condition  $\boldsymbol{\tau}^l$ .

For the proposed on-off control using the SPSA algorithm, minima may exist where  $\partial J^k / \partial \boldsymbol{\tau}^k = 0$ , which may occur if  $y_f^k = r$  (as desired) or  $\partial y_f^k / \partial \boldsymbol{\tau}^k = 0$  (a local minima), as seen in the derivative of the cost function,

$$\frac{\partial J^k}{\partial \boldsymbol{\tau}^k} = \left( \frac{\partial y_f^k}{\partial \boldsymbol{\tau}^k} \right)^T \left( \frac{\partial J^k}{\partial y_f^k} \right)^T = \left( \frac{\partial y_f^k}{\partial \boldsymbol{\tau}^k} \right)^T (y_f^k - r) \quad (3.50)$$

In the case of on-off control, and differing from prior control examples done using the SPSA algorithm, at the minima when  $y_f^k = r$ , there may exist several, continuous solutions  $\boldsymbol{\tau}^* \in \Theta^*$  which can drive system (3.39) to target  $r$ , where  $\Theta^*$  is a solution set of (3.39), such that an adjustment to standard SPSA convergence conditions is necessary.

To do so, define a new parameter vector such that  $\bar{\boldsymbol{\tau}}^k \equiv \|\boldsymbol{\tau}^k - \boldsymbol{\tau}^*\|$ , where  $\boldsymbol{\tau}^*$  is now the set of minima. Then the equation (3.48) and (3.49) can be restated as follows:

$$\frac{d\bar{\boldsymbol{\tau}}}{dt} = -\mathbf{g}(\bar{\boldsymbol{\tau}}) \quad (3.51)$$

$$\mathbf{D}(\bar{\boldsymbol{\tau}}^*) = \left\{ \bar{\boldsymbol{\tau}}^l \mid \lim_{t \rightarrow \infty} \bar{\boldsymbol{\tau}}(t \mid \bar{\boldsymbol{\tau}}^l) = \bar{\boldsymbol{\tau}}^* \right\} \quad (3.52)$$

Properties of iterate boundedness and smoothness of a cost function by  $\bar{\boldsymbol{\tau}}^k$  remain satisfied by properties of a system subject to on-off control as described by (3.51) and (3.52).

*Proposition 2:*

Suppose that standard convergence conditions of the SPSA hold, (3.51) and (3.52) hold, if the following assumptions A-1 and A-2 are satisfied, then from the extended Kushner-Clark theorem,

$$\bar{\boldsymbol{\tau}}^k \rightarrow \mathbf{0} \text{ as } k \rightarrow \infty$$

A-1:  $\|\mathbf{b}_g^k(\bar{\boldsymbol{\tau}}^k)\| \leq \infty$ , for a  $k$  and  $\mathbf{b}_g^k(\bar{\boldsymbol{\tau}}^k) \rightarrow 0$ , almost surely

A-2:  $\lim_{k \rightarrow \infty} P\left(\sup_{m \geq k} \left\| \sum_{i=k}^m a^i \mathbf{e}_g^i(\bar{\boldsymbol{\tau}}^k) \right\| \geq \rho\right) = 0$  for any  $\rho > 0$

where  $\mathbf{b}_g^k(\cdot)$  is the bias between a gradient estimator and the real gradient,  $\mathbf{b}_g^k(\bar{\boldsymbol{\tau}}^k) \equiv E\left[\hat{\mathbf{g}}^k(\bar{\boldsymbol{\tau}}^k) - \mathbf{g}(\bar{\boldsymbol{\tau}}^k) \mid \bar{\boldsymbol{\tau}}^k\right]$ ,  $\mathbf{e}_g^k(\cdot)$  is the error in the gradient estimate,  $\mathbf{e}_g^k(\bar{\boldsymbol{\tau}}^k) \equiv \hat{\mathbf{g}}^k(\bar{\boldsymbol{\tau}}^k) - E\left[\mathbf{g}(\bar{\boldsymbol{\tau}}^k) \mid \bar{\boldsymbol{\tau}}^k\right]$ , and  $a^k$  is the gain sequence from (3.42). For proof of Proposition 2 given A-1 and A-2, see [82], while A-1 and A-2 are used for derivation of the SPSA in [59] and [61].

By Proposition 1 and 2, it may be concluded that the proposed adaptive on-off controller will almost surely converge to a minima of the cost function associated with the initial control parameters provided to the system.

### 3.4.2.2 Local Minima for Bounded Uncertainty

The convergence analysis in Section 3.4.2.1 ensures almost certain (probability = 1) convergence of switching times to a solution minimizing (3.41), but does not yet distinguish between global minima and local minima or indicate how to select initial guesses  $\boldsymbol{\tau}^1$  to reach a specified  $y_f$ . For general nonlinear functions, there is not a known method for ensuring convergence to a global minimum. When dynamics are known, Kaya and Noakes suggest a method for selecting future initial guesses based on past results [41], while for unknown dynamics, some bounds on the nonlinear dynamics are required, as in [49].

For on-off control in the case of a short time duration with known bounds on the magnitude of nonlinearity it can be possible to identify values for  $\boldsymbol{\tau}$  that may result in local minima, and select the target output,  $r$ , and initial guess to avoid them. To do so, we note from (3.50) that a minima may exist where  $y_f = r$  (desired) or where  $\partial y_f / \partial \tau_q = 0$  for all  $q$  (undesired). For on-off control,  $y_f$  and partial derivatives of  $y_f$  with respect to switching times,  $\tau_q$ , may be written as

$$\begin{aligned}
\frac{\partial y_f}{\partial \tau_Q} &= \mathbf{C} \left[ -\mathbf{l}_0(\mathbf{x}_b(t_f)) + \frac{\partial \boldsymbol{\Psi}_0}{\partial \mathbf{x}_b(0)} \Big|_{t_f - \tau_Q} \mathbf{l}_1(\mathbf{x}_b(\tau_Q)) \right] \\
\frac{\partial y_f}{\partial \tau_{Q-1}} &= \mathbf{C} \frac{\partial \boldsymbol{\Psi}_0}{\partial \mathbf{x}_b(0)} \Big|_{t_f - \tau_Q} \left[ -\mathbf{l}_1(\mathbf{x}_b(\tau_Q)) + \frac{\partial \boldsymbol{\Psi}_1}{\partial \mathbf{x}_b(0)} \Big|_{\tau_Q - \tau_{Q-1}} \mathbf{l}_0(\mathbf{x}_b(\tau_{Q-1})) \right] \\
&\vdots \\
\frac{\partial y_f}{\partial \tau_1} &= \mathbf{C} \frac{\partial \boldsymbol{\Psi}_0}{\partial \mathbf{x}_b(0)} \Big|_{t_f - \tau_Q} \frac{\partial \boldsymbol{\Psi}_1}{\partial \mathbf{x}_b(0)} \Big|_{\tau_Q - \tau_{Q-1}} \dots \frac{\partial \boldsymbol{\Psi}_0}{\partial \mathbf{x}_b(0)} \Big|_{\tau_2 - \tau_1} [\mathbf{l}_1(\mathbf{x}_b(\tau_1))]
\end{aligned} \tag{3.53}$$

Due to

$$y_f = \mathbf{C} \boldsymbol{\Psi}_0(t_f - \tau_Q, \boldsymbol{\Psi}_1(\tau_Q - \tau_{Q-1}, \boldsymbol{\Psi}_0(\dots, \boldsymbol{\Psi}_1(\tau_1, \mathbf{0})))) \tag{3.54}$$

While the functions  $\mathbf{l}_0$ ,  $\mathbf{l}_1$ ,  $\boldsymbol{\Psi}_0$ , and  $\boldsymbol{\Psi}_1$  and their derivatives in (3.53) are unknown, if bounds are placed on the difference between the nonlinear system and a known dynamic system, the possible range of the partial derivative terms  $\partial y_f / \partial \tau_q$  may be obtained through use of Gronwall's theorem [84]. The error bounds between the known system's response and the actual, unknown system's response grow rapidly with time. However, for short time durations, as in the case of repeated stepping motions desired for the motivating example, it can be possible to identify ranges of values for switching time vector  $\boldsymbol{\tau}$  where  $\partial y_f / \partial \tau_q$  may be equal to zero for one or more  $q$ .

As an example, we consider a 2<sup>nd</sup>-order nonlinear system described by



$$\begin{aligned}
\begin{bmatrix} \dot{x}_{b(1)}(t) \\ \dot{x}_{b(2)}(t) \end{bmatrix} &= \begin{bmatrix} 0 & 1 \\ -a_1 & -a_2 \end{bmatrix} \begin{bmatrix} x_{b(1)}(t) \\ x_{b(2)}(t) \end{bmatrix} + \begin{bmatrix} 0 \\ f_{x_b(1)}(x_{b(1)}(t)) + f_{x_b(2)}(x_{b(2)}(t)) \end{bmatrix} \\
&+ \begin{bmatrix} 0 \\ f_{u(1)}(x_{b(1)}(t)) + b \end{bmatrix} u(t) \\
z_b(t) &= x_{b(1)}(t) + w
\end{aligned} \tag{3.55}$$

where nonlinear functions are estimated to have bounds of uncertainty matrices in (3.3) and (3.4) such as,

$$\mathbf{C}_{x_b} = \begin{bmatrix} 0 & 0 \\ \delta_1 & \delta_2 \end{bmatrix}, \mathbf{C}_u = \begin{bmatrix} 0 & 0 \\ \delta_u & 0 \end{bmatrix}, \mathbf{C}'_{x_b} = \begin{bmatrix} 0 & 0 \\ \delta'_1 & \delta'_2 \end{bmatrix}, \mathbf{C}'_u = \begin{bmatrix} 0 & 0 \\ \delta'_u & 0 \end{bmatrix} \tag{3.56}$$

Using (3.55), and (3.56), and Gronwall's theorem [84] for (3.53), ranges of possible  $\partial y_f / \partial \tau_Q$  values may finally be found, as for  $\tau_Q$ ,

$$\begin{aligned}
\frac{\partial y_f}{\partial \tau_Q} &= \begin{bmatrix} -x_{(2)}(t_f) - x_{e(2)}(t_f) \end{bmatrix} \\
&+ \begin{bmatrix} x_{sa(1)}(t_f - \tau_Q) + \left\{ \frac{\partial \psi_{0(1)}}{\partial x_{b(1)}(0)} - x_{sa(1)}(t_f - \tau_Q) \right\} \end{bmatrix} \begin{bmatrix} x_{(2)}(\tau_Q) + x_{e(2)}(\tau_Q) \end{bmatrix} \\
&+ \begin{bmatrix} x_{sb(1)}(t_f - \tau_Q) + \left\{ \frac{\partial \psi_{0(1)}}{\partial x_{b(2)}(0)} - x_{sb(1)}(t_f - \tau_Q) \right\} \end{bmatrix} \\
&\times \begin{bmatrix} -a_1 (x_{(1)}(\tau_Q) + x_{e(1)}(\tau_Q)) - a_2 (x_{(2)}(\tau_Q) + x_{e(2)}(\tau_Q)) \\
+ f_{x_b(1)}(x_{(1)}(\tau_Q) + x_{e(1)}(\tau_Q)) + f_{x_b(2)}(x_{(2)}(\tau_Q) + x_{e(2)}(\tau_Q)) \\
+ f_{u(1)}(x_{(1)}(\tau_Q) + x_{e(1)}(\tau_Q)) \end{bmatrix}
\end{aligned} \tag{3.57}$$

A detailed procedure to obtain (3.57) has been illustrated in Appendix C. In relationships such as (3.57), the  $\mathbf{x}$  terms may be known exactly, while the quantities in braces may be bounded, allowing evaluation of  $\partial y_f / \partial \tau_Q = 0$  feasibility. The evaluation of the remained  $\partial y_f / \partial \tau_q = 0$  for  $q = 1, \dots, Q-1$  can be performed with the same manner as (3.57).

Figure 3.11 shows the output of the nominal system in (3.54) as a function of switching times  $\tau_2$  and  $\tau_3$  when  $\tau_1 = 0.5\text{ms}$  and  $Q = 3$ . Nonlinearity bounds are given in Table 3.2, representing the experimental and simulational system in the following Section, where natural frequency (related to  $a_1$ ) and gain estimates (related to  $b$ ) are quite accurate, but there may be substantial error in damping estimates (related to  $a_2$ ). While  $\partial y_f / \partial \tau_2 = 0$  and  $\partial y_f / \partial \tau_3 = 0$  do not quite occur for the nominal system with this  $\tau_1$ , when uncertainty in the derivatives due to nonlinearities is accounted for, locations where  $\partial y_f / \partial \tau_2 = 0$  and  $\partial y_f / \partial \tau_3 = 0$  become possible and are outlined in white (with no distinction at present for local minima versus maxima). In addition, possible response variation is marked, indicating that the worst case system outputs for the points where  $\partial y_f / \partial \tau_2 = 0$  and  $\partial y_f / \partial \tau_3 = 0$  may be true are below 0.15 rad and above 0.42 rad. Taking into account  $\partial y_f / \partial \tau_1$  as well, we ultimately conclude that the range of outputs between 0.12 rad and 0.43 rad are free of local minima, and that selecting initial switching times according to  $0.1 < \tau_1 < 0.8$  ms,  $1 < \tau_2 < 1.4$  ms,  $1.6 < \tau_3 < 1.8$  ms should be sufficient to reach target outputs between 0.12 rad and 0.42 rad.

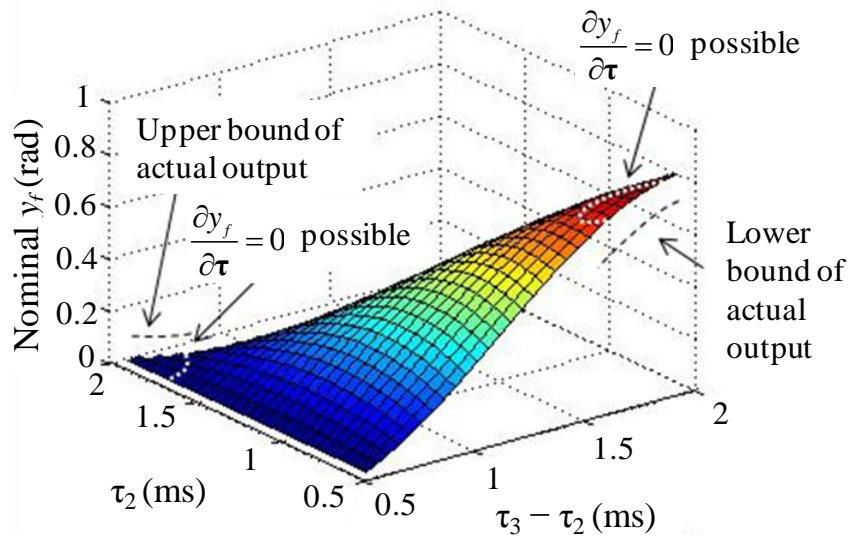


Figure 3.11 Nominal system output as a function of switching times  $\tau_2$  and  $\tau_3$  for  $p = 3$  and  $\tau_1 = 0.5\text{ms}$ , and marked regions of possible local minima/maxima when unknown, bounded nonlinearities present.

Table 3.2 Nominal system coefficients and bounds on corresponding nonlinearities deviating from these coefficients

	Value	Non-linearity	Bound $\delta$	Bound $\delta'$
$a_1$	$3.06 \cdot 10^6 \text{ s}^{-2}$	$f_{x_{b(1)}}(x_{b(1)})$	$6.1 \cdot 10^4 \text{ s}^{-2}/\text{rad}$	$2.5 \cdot 10^5 \text{ s}^{-2}/\text{rad}$
$a_2$	$51 \text{ s}^{-1}$	$f_{x_{b(2)}}(x_{b(2)})$	$10 \text{ s}^{-1}/(\text{rad}/\text{s})$	$40 \text{ s}^{-1}/(\text{rad}/\text{s})$
$b$	$6.9 \cdot 10^6 \text{ s}^{-2}/\text{V}$	$f_{u(1)}(x_{b(1)})$	$1.4 \cdot 10^3 \text{ s}^{-2}/\text{V}/\text{rad}$	$5.5 \cdot 10^3 \text{ s}^{-2}/\text{V}/\text{rad}$

### 3.4.3 Validation by Simulation and Experiment

A MEMS multi-actuator leg joint was used to verify behavior under the proposed controller. Figure 3.12 shows the leg joint tested. Several thin-film piezoelectric actuators compose this leg with a natural frequency of approximately 279 Hz and a nominal damping ratio 0.017.

The experimental system with the input range 0 to 20V, modeled as a 2<sup>nd</sup>-order linear system has a nominal linear model, as shown in Figure 3.13, of

$$\begin{bmatrix} \dot{x}_{(1)}(t) \\ \dot{x}_{(2)}(t) \end{bmatrix} = \begin{bmatrix} 0 & 1 \\ -3.06e^6 & -51 \end{bmatrix} \begin{bmatrix} x_{(1)}(t) \\ x_{(2)}(t) \end{bmatrix} + \begin{bmatrix} 0 \\ 6.9e^5 \end{bmatrix} u(t) \quad (3.58)$$

(3.58) with uncertainties of Table 3.2 was first examined in simulation as shown in Figure 3.14. In this case, the sample target angle was 0.3 rad, where a value of 0.45 rad corresponds to the maximum static actuator displacement as shown in Figure 3.13. Initial guesses for switching times were selected based on the convergence analysis as [0.7ms 1.1ms 1.7ms]. Selected gain coefficients values of  $a$ ,  $c$ ,  $A_g$ ,  $\alpha$ , and  $\gamma$  were 1.3E-5, 5E-5, 2000, 0.602, and 0.101, respectively based on rules of 3.4.1.3. Figure 3.14 shows effective convergence in fewer than 5<sup>th</sup> iteration, such that the convergence analysis was quite useful in controller testing on simulated system. The obtained optimal  $\tau$  was [0.5ms 0.89ms 1.27ms]<sup>T</sup>.

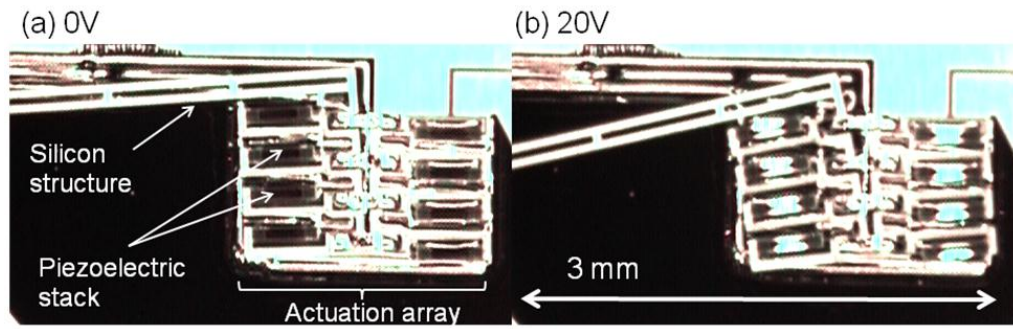


Figure 3.12 Sample image of the MEMS leg actuator

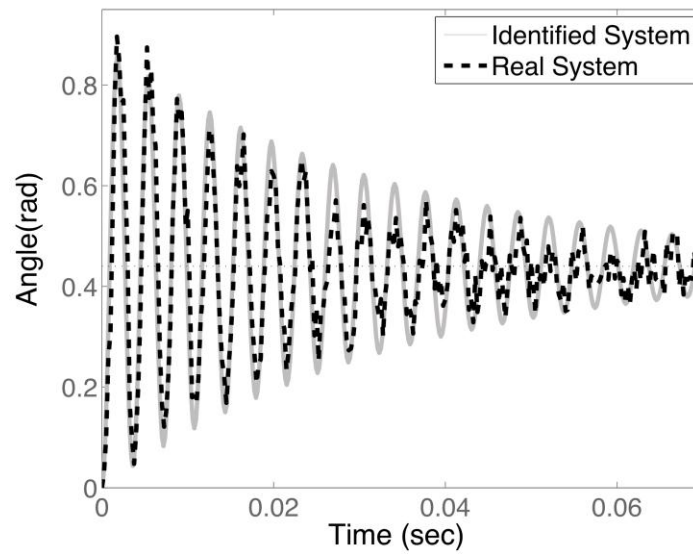


Figure 3.13 Step response and nominal linear dynamics of the experimental system

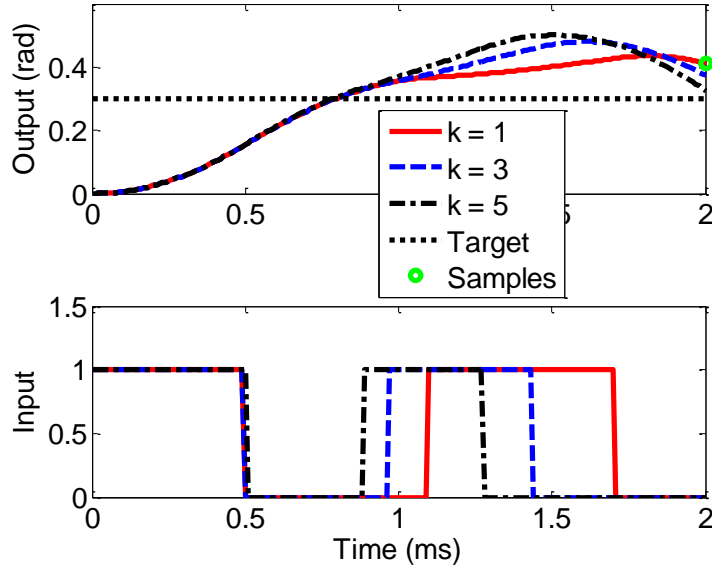


Figure 3.14 Simulation result of the nominal system (3.58) with model uncertainties

For the experimental test, leg motion was measured by filming the micro-scale leg through a stereoscope using a high-speed camera system. Images were collected at 4000 fps, and angle measurements in each frame were extracted using the Matlab Image Processing Toolbox; off-board sensing was used because, although integrated sensing has been implemented on other types of piezoelectric actuators on the test wafer, the current robotic leg prototypes are not yet instrumented with these sensors. Image measurement error was interpreted as noise, and estimated at  $\tilde{\varepsilon} = N(0, 0.01^2)$  as its influence on the cost function. The control signal is generated on a control circuitry, which was implemented with an off-board TMS320F28335 digital signal processor and a level shifter circuit based on CMOS inverter [7] acting as the on-off interface between the low-voltage DSP and a 20 V supply ( $u_{\max}$ ) for the actuator.

Various target motions were tested to verify controller performance. Two sample reference levels,  $r = 0.2$  rad and  $r = 0.3$  rad are shown in Figure 3.15. In both cases,  $p = 3$  for vector  $\tau$  and the final time,  $t_f$ , was 2 msec. Initial guesses for switching times were selected based on the convergence analysis as [0.7ms 1.1ms 1.7ms]. The CPU operation time was 0.05 msec. The experimental controller uses only one measured value at the

final time,  $t_f$ . Selected gain coefficients values of  $a$ ,  $c$ ,  $A$ ,  $\alpha$ , and  $\gamma$  were 0.0016,  $5e^{-5}$ , 2000, 0.602, and 0.101, respectively.

Figure 3.14 (a) and (b) shows sample experimental responses, with obtained optimal  $\tau$  of  $[0.7\text{ms } 1.1\text{ms } 1.2\text{ms}]^T$  and  $[0.6\text{msec } 1.1\text{ms } 1.21\text{ms}]^T$  for  $r = 0.3\text{rad}$  and  $r = 0.2\text{rad}$  respectively. The experimental results show a successful convergence to the target reference level as, and in just two to three iterations or two iterations. While a true gradient-based search is expected to be faster, if full model information were available [60], this is a rapid convergent rate when tens or hundreds of repeated motions are needed, as in a micro-robotic walking gait.

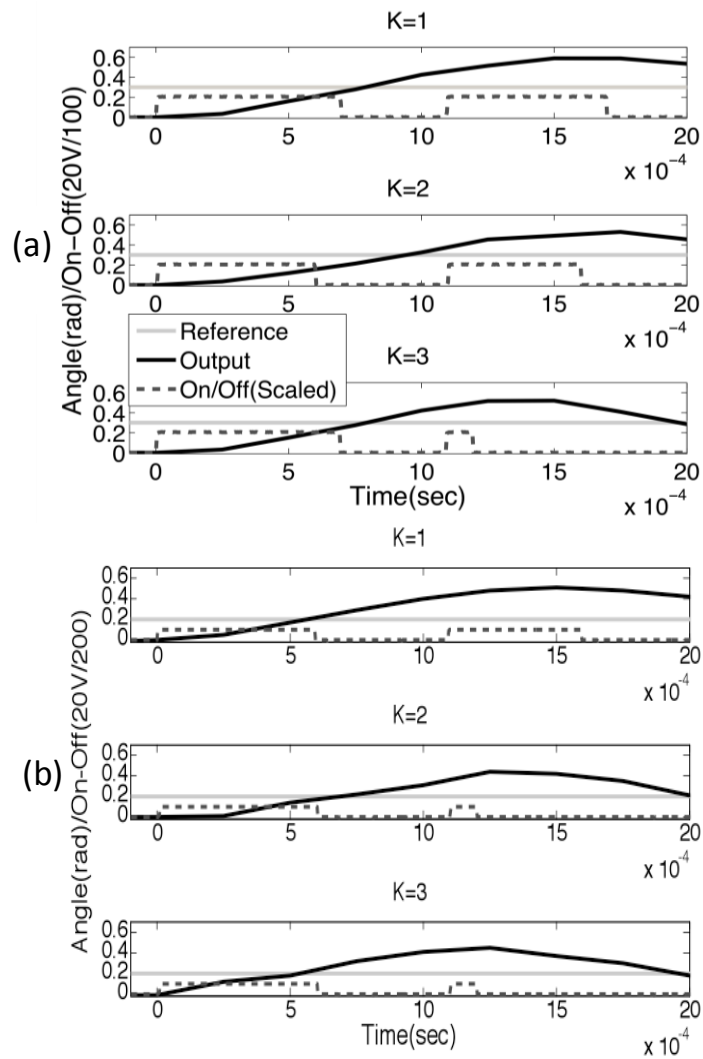


Figure 3.15 Experimental results for the system (3.58): (a) for target: 0.3 rad, (b) for target 0.2 rad

### 3.4.4 Summary of SAA On-Off Controller

This section has described a method for implementing model-free adaptive on-off control through the application of SPSA. The strength of the proposed controller for regulating micro-system motion is that it relies on extremely simple sensing and input capabilities, which allows it to perform control at very low power. Typically, good performance has been observed when using just a few more switching transitions than the order of the target system.

The use of a well-established gradient estimation algorithm allows the designer to be confident of convergence of the iterated response to a minimal value of the cost function presented, although greater effort is required to provide confidence in achieving a true global minimum. Increasing the number of switching times may reduce the likelihood of  $\partial y_j / \partial \tau_i = 0$  for all switching times, without a substantial reduction in convergence rate, but with an increase in power consumption by a capacitive load. No model of the system is required by the controller, reducing memory and modeling. However, at most one state of the system may be regulated at the desired final time of motion.

## **CHAPTER 4**

# **CONVERGENCE RATE ESTIMATION FOR THE ADAPTIVE ON-OFF CONTROLLERS AND PREDICTION OF POWER/ENERGY REQUIREMENT**

In the Chapter 3 and 4, eventual convergence of switching times to at least locally optimal values was guaranteed for some limited range of initial switching time selections and adaptation gains. However, the rate at which the switching time selections converge to optimal values could not be predicted. Thus, the controller can limit the energy expended during each iteration, but not make any predictions of total energy required to identify the optimal switching times.

A technique is presented in this chapter for estimating the convergence rate of the HA and SAA on-off controllers. The eventual application of a convergence estimator for an on-off iterative controller is to predict the number of iterations required to reach a desired level of output error. This is of primary use for ultra-low-power control of capacitive loads, where sensing costs and on-off transitions are expensive in terms of energy usage. Thus, being able to predict the cumulative number of sensing measurements to find an adequate input signal for a given number of on-off transitions per iteration can allow net system energy usage to be minimized.

### **4.1 Problem Statement**

The aim of this section is to estimate the rate of convergence of certain on-off iterative adaptive controllers, in this case the deterministic, HA on-off controller and the statistically designed SAA on-off controller based on gradient approximation, described prior sections. A variety of theoretical results for convergence rate related to well-known classes of iterative learning or adaptive controllers have been published [85, 90]. These



do not, unfortunately, include switching control systems at this time. For instance, Hillenbrand and Pandit could guarantee an exponential convergence rate for an iterative learning controller for an LTI discrete-time system [87]. This also allowed relatively slow sampling rates to be used, a feature of the authors' on-off controllers to be analyzed in this paper, but inputs were not constrained. Other analyses of convergence rates have introduced inequality constraints and/or nonlinearities on certain signals [86, 90].

However, it remains difficult to make predictions of convergence rates of iterative control for switched systems. This paper describes a limited method for doing so for certain simple switching controllers, namely the on-off controllers for micro-robotic leg joints described in previous works. The approach makes use of the binary nature of on-off inputs (0 or 1) and knowledge about adaptation behavior in the known regions of convergence. The resulting method for predicting error in each iteration is found to have reasonable agreement with simulated and experimental test cases.

## 4.2 Estimation of Convergence Rate

When an on-off adaptation rule discussed in previous section is given, it may be necessary to investigate how fast an objective function or output error reaches zero or desired range about zero in order to analyze energy usage of the given adaptation strategy. This investigation is generally known as analysis of convergence rate of output error, which can be obtained by convergence rate of input sequence with the given adaptation rule.

The objective of convergence analysis is to estimate the error in output measurements,  $\epsilon^k$ , in iteration  $k$  given a maximum initial error in iteration 1. The following estimation of convergence rate is derived using a maximum bound for error in each time step given error input timing and the magnitude of change in the input signal under certain adaptation criteria.

### 4.2.1 Requirement for Estimation of Convergence Rate

It is assumed that an adaptive controller (3.16) and an adaptation law (3.17) have the following properties:

#### *Property 1*

If a minimizing solution,  $\boldsymbol{\tau}^*$ , of the input parameter vector for the object function (3.15) is known, the adaptive algorithm is in a region of convergence such that

$$\lim_{k \rightarrow \infty} \|\boldsymbol{\tau}^k - \boldsymbol{\tau}^*\| = 0 \quad (4.1)$$

#### *Property 2*

The adaptation law of (3.8) can be designed to satisfy

$$|\tau_{i,j}^{k+1} - \tau_{i,j}^*| < |\tau_{i,j}^k - \tau_{i,j}^*| \quad \forall i, j \quad (4.2)$$

These properties imply an important behavior of an adaptive controller for ensuring convergence: that there exists a minimizing  $\boldsymbol{\tau}^*$  with a domain of attraction in terms of  $\boldsymbol{\tau}$ . If  $\tau_{n,q}^j$  for all  $n$  and  $q$  is then chosen to be within the domain of attraction, then a controller can be designed such that all input parameters in  $\boldsymbol{\tau}$  are steadily converging to their optimal value  $\boldsymbol{\tau}^*$ . Equations (4.1) and (4.2), it must be emphasized, are the restrictive assumptions on the current convergence analysis, and can be very difficult to verify for problems with large numbers of both measurements and switching instances. However, for the two controllers presented in Chapter 4, these conditions can be satisfied (either deterministically or in their expected value).

To derive the rate of convergence in the following section,  $L^1$ - and  $L^\infty$ -norms are used for a piecewise continuous function  $f(t)$  on an finite interval  $t \in [t_n, t_{n+1}]$  defined by

$$\begin{aligned} \|f\|_{1, [t_n, t_{n+1}]} &= \int_{t_n}^{t_{n+1}} |f(t)| dt < \infty \\ \|f\|_{\infty, [t_n, t_{n+1}]} &= \sup \{|f(t)| : t \in [t_n, t_{n+1}]\} \end{aligned} \quad (4.3)$$

and these norms hold the Holder's inequality [99] for given functions  $f(\cdot)$  and  $g(\cdot)$  such that

$$\|f(\cdot)g(\cdot)\|_1 \leq \|f(\cdot)\|_p \|g(\cdot)\|_q, 1/p + 1/q = 1 \text{ \& } 1 \leq p, q \leq \infty \quad (4.4)$$

#### 4.2.2 Evolution of Norm of Input Error

To convert the adaptive algorithm (3.16) to a time dependent input formulation, let  $u_n^k(t)$  be a piecewise continuous input function at  $k$ -th iteration with respect to (3.13) and (3.14) and  $u_n^*(t)$  be a redefined desired input function for the vector  $\tau^*$ , which are defined on a time interval  $t \in [t_{n-1}, t_n)$ . Here,  $\tau^*$  is the optimal switching time vector satisfying

$$\tau^* = \arg \min_{\tau} J(\tau) \quad (4.5)$$

Hence, a  $k$ -th and desired time domain input on the interval  $t \in [t_0, t_N)$  can be described as

$$\begin{aligned} u^k(t) &= \sum_{n=1}^N u_n^k(t) \\ u^*(t) &= \sum_{n=1}^N u_n^*(t) \end{aligned} \quad (4.6)$$

Now, we define input error from (4.6),

$$\eta_n^k(t) \equiv u_n^k(t) - u_n^*(t) \quad (4.7)$$

Applying  $L^1$ -norm to the input error (4.7) on an interval  $t \in [t_{n-1}, t_n)$  over the  $k$ -th and  $k+1$ -th iteration, the norm of  $n$ -th input error can be expressed, due to the binary nature of the inputs, as

$$\left\| \eta_n^{k+1} \right\|_{1, [t_{n-1}, t_n]} = \left\| \eta_n^k \right\|_{1, [t_{n-1}, t_n]} + \sum_{q=1}^{Q/2} \left( \mathbf{T}_{2q-1, n}^k - \mathbf{T}_{2q, n}^k \right) \quad (4.8)$$

Under the condition of (4.2), equation (4.8) is equivalent to

$$\left\| \eta_n^{k+1} \right\|_{1, [t_{n-1}, t_n]} = \left\| \eta_n^k \right\|_{1, [t_{n-1}, t_n]} - \sum_{q=1}^Q \left| \mathbf{T}_{q, n}^k \right| \quad (4.9)$$

which can be replaced by the bound

$$\left\| \eta_n^{k+1} \right\|_{1, [t_{n-1}, t_n]} \leq \left\| \eta_n^k \right\|_{1, [t_{n-1}, t_n]} - \sum_{q=1}^Q \sum_{i=1}^n \left| \frac{\partial \mathbf{T}_{q, n}^k}{\partial \varepsilon_i} \right|_{\min} \left| \varepsilon_i^k \right| \quad (4.10)$$

where  $\left| \frac{\partial \mathbf{T}_{q, n}}{\partial \varepsilon_i} \right|_{\min}$  is the minimum possible adaptation gain defined in (3.17) from measurement error  $i$  to switching time  $q$  in period  $n$ . Therefore, evolution in norm of input error can be formulated in matrix representation, as:

$$\begin{bmatrix} \left\| \eta_1^{k+1} \right\|_{1, [t_0, t_1]} \\ \left\| \eta_2^{k+1} \right\|_{1, [t_1, t_2]} \\ \vdots \\ \left\| \eta_N^{k+1} \right\|_{1, [t_{N-1}, t_N]} \end{bmatrix} - \begin{bmatrix} \left\| \eta_1^k \right\|_{1, [t_0, t_1]} \\ \left\| \eta_2^k \right\|_{1, [t_1, t_2]} \\ \vdots \\ \left\| \eta_N^k \right\|_{1, [t_{N-1}, t_N]} \end{bmatrix} \leq -\mathbf{\Gamma} \begin{bmatrix} \varepsilon_1^k \\ \varepsilon_2^k \\ \vdots \\ \varepsilon_N^k \end{bmatrix} \quad (4.11)$$

where entries  $\Gamma_{ij}$  in  $\mathbf{\Gamma} \in \mathbf{R}^{N \times N}$  are computed from (4.10).

### 4.2.3 Convergence Rate Estimation in Norm of Output Error

By using the evolution of the norm of input error, (4.11), estimation of the output error is next investigated. Output error can be bounded using the system dynamics and norm of input error: first, note that the output error of the system at measurement  $n$  over  $k$ -th iteration can be expressed as

$$\boldsymbol{\varepsilon}_n^k = \sum_{i=1}^n \int_{t_{i-1}}^{t_i} \mathbf{C}e^{\mathbf{A}(t_n-s)} \mathbf{B} \boldsymbol{\eta}_i^k(s) ds \quad (4.12)$$

since the input error  $\boldsymbol{\eta}_i^k(s)$  in time interval  $i$  using the definition (4.7) is zero for all  $t$  except  $t \in [t_{i-1}, t_i)$  such that

$$\begin{aligned} \boldsymbol{\varepsilon}_n^k &= \int_{t_0}^{t_1} \mathbf{C}e^{\mathbf{A}(t_n-s)} \mathbf{B} \boldsymbol{\eta}_1^k(s) ds + \int_{t_1}^{t_2} \mathbf{C}e^{\mathbf{A}(t_n-s)} \mathbf{B} \boldsymbol{\eta}_2^k(s) ds \\ &+ \dots + \int_{t_{n-1}}^{t_n} \mathbf{C}e^{\mathbf{A}(t_n-s)} \mathbf{B} \boldsymbol{\eta}_n^k(s) ds \end{aligned} \quad (4.13)$$

Applying  $L^{-1}$  norm to the output error (4.12) and then Holder's inequality (4.4), a bound for the  $n$ -th sampled output error over  $k$ -th iteration is obtained as,

$$\|\boldsymbol{\varepsilon}_n^k\|_{1,[t_0,t_n]} \leq t_n \sum_{i=1}^n \left\| \left( \mathbf{C}e^{\mathbf{A}(t_n-s)} \mathbf{B} \right) \right\|_{\infty,[t_{i-1},t_i]} \|\boldsymbol{\eta}_i^k\|_{1,[t_{i-1},t_i]} \quad (4.14)$$

To estimate convergence rate of the norm of output error, a matrix representation of equation (4.14) may be formulated as

$$\begin{bmatrix} \boldsymbol{\varepsilon}_1^k \\ \boldsymbol{\varepsilon}_2^k \\ \vdots \\ \boldsymbol{\varepsilon}_N^k \end{bmatrix} \leq \mathbf{F} \begin{bmatrix} \|\boldsymbol{\eta}_1^k\|_{1,[t_0,t_1]} \\ \|\boldsymbol{\eta}_2^k\|_{1,[t_1,t_2]} \\ \vdots \\ \|\boldsymbol{\eta}_N^k\|_{1,[t_{N-1},t_N]} \end{bmatrix} \equiv \mathbf{w}^k \quad (4.15)$$

where entries  $F_{i,j}$  in  $\mathbf{F} \in \mathbf{R}^{N \times N}$  are taken from (4.14) and  $\mathbf{w}^k$  is defined to be the error bound of actual error vector,  $\boldsymbol{\varepsilon}^k$ , in iteration  $k$ .

Therefore, the evolution of the output error can be bounded in an individual iteration step by combining (4.11) and (4.15):

$$\begin{aligned}
\mathbf{w}^{k+1} &= \mathbf{F} \begin{bmatrix} \|\eta_1^{k+1}\|_{1,[t_0,t_1]} \\ \|\eta_2^{k+1}\|_{1,[t_1,t_2]} \\ \vdots \\ \|\eta_N^{k+1}\|_{1,[t_{N-1},t_N]} \end{bmatrix} = \mathbf{F} \begin{bmatrix} \|\eta_1^k\|_{1,[t_0,t_1]} \\ \|\eta_2^k\|_{1,[t_1,t_2]} \\ \vdots \\ \|\eta_N^k\|_{1,[t_{N-1},t_N]} \end{bmatrix} + \mathbf{F} \left( \begin{bmatrix} \|\eta_1^{k+1}\|_{1,[t_0,t_1]} \\ \|\eta_2^{k+1}\|_{1,[t_1,t_2]} \\ \vdots \\ \|\eta_N^{k+1}\|_{1,[t_{N-1},t_N]} \end{bmatrix} - \begin{bmatrix} \|\eta_1^k\|_{1,[t_0,t_1]} \\ \|\eta_2^k\|_{1,[t_1,t_2]} \\ \vdots \\ \|\eta_N^k\|_{1,[t_{N-1},t_N]} \end{bmatrix} \right) \\
&\leq \mathbf{w}^k - \mathbf{F}\Gamma |\boldsymbol{\varepsilon}^k|
\end{aligned} \tag{4.16}$$

However, because only a bound on  $|\boldsymbol{\varepsilon}^k|$  is known in iteration  $k$ , to numerically calculate error estimates, a substitution of  $\mathbf{w}^k$  for  $|\boldsymbol{\varepsilon}^k|$  is finally done to complete the error estimator and predict convergence. Using the obtained inequalities (4.15), (4.16), and the assumed inequality,  $\mathbf{w}^{k+1} \leq \mathbf{w}^k$ , based on the property 2 (4.2), we can obtain three possibly bounded dynamics in terms of error estimation such that

$$\begin{cases} \mathbf{w}_a^{k+1} \leq \mathbf{w}_a^k - \mathbf{F}\Gamma \mathbf{w}_a^k \\ \mathbf{w}_b^{k+1} \leq \mathbf{w}_b^k - \mathbf{F}\Gamma \mathbf{w}_b^k + (\mathbf{F}\Gamma)^2 \mathbf{w}_b^k \\ \mathbf{w}_c^{k+1} = \mathbf{w}_c^k - \mathbf{F}\Gamma \mathbf{w}_c^k \end{cases} \tag{4.17}$$

Here, subscript  $a$ ,  $b$ , and  $c$  do not possess a special meaning but are simply provided to discriminate between scenarios.

Defining a maximum error bound in  $\mathbf{w}^k|_{\max}$  such that  $\mathbf{w}^k \leq \mathbf{w}^k|_{\max}$ , (4.17) may be transformed to

$$\begin{cases} \mathbf{w}_a^{k+1} \leq \mathbf{w}_a^k - \mathbf{F}\Gamma \mathbf{w}_a^k \leq \mathbf{w}_a^k|_{\max} - \mathbf{F}\Gamma \mathbf{w}_a^k|_{\max} \equiv \mathbf{w}_a^{k+1}|_{\max} \\ \mathbf{w}_b^{k+1} \leq \mathbf{w}_b^k - \mathbf{F}\Gamma \mathbf{w}_b^k + (\mathbf{F}\Gamma)^2 \mathbf{w}_b^k \\ \leq \mathbf{w}_b^k|_{\max} - \mathbf{F}\Gamma \mathbf{w}_b^k|_{\max} + (\mathbf{F}\Gamma)^2 \mathbf{w}_b^k|_{\max} \equiv \mathbf{w}_b^{k+1}|_{\max} \\ \mathbf{w}_c^{k+1} = \mathbf{w}_c^k - \mathbf{F}\Gamma \mathbf{w}_c^k \leq \mathbf{w}_c^k|_{\max} - \mathbf{F}\Gamma \mathbf{w}_c^k|_{\max} \equiv \mathbf{w}_c^{k+1}|_{\max} \end{cases} \tag{4.18}$$

The maximum error bound among the equations in (4.18) can be found from

$$\mathbf{w}^k|_{\max} = \max\left(\mathbf{w}_a^k|_{\max}, \mathbf{w}_b^k|_{\max}, \mathbf{w}_c^k|_{\max}\right) = \mathbf{w}_b^k|_{\max} \quad (4.19)$$

Therefore, we can get a convergence rate estimator for the maximum error bound can be taken as,

$$\mathbf{w}^{k+1}|_{\max} = \left\{I - \mathbf{F}\Gamma + (\mathbf{F}\Gamma)^2\right\} \mathbf{w}^k|_{\max} \quad (4.20)$$

### 4.3 Case Study I: HA On-Off Control

As the first test case, the HA on-off controller described in Chapter 3 is considered. This controller was designed to adapt the timing of three parameters describing an on-off input signal to produce a step-and-hold type response from the robot leg dynamics. These parameters are initial ‘on’ and ‘off’ periods, corresponding to transition times  $\tau_{1,1}$  and  $\tau_{1,1}$  as defined in (3.18), and a steady periodic input of duty cycle  $d$ , which may be translated into the remaining transition times  $\tau_{1,2}$  and  $\tau_{N,2}$  which are accompanied by  $N$  measurements. Using these parameters, the convergence rate of the HA on-off controller is explored.

#### 4.3.1 Test System Description

The adaptation laws identified in the Section 3.3 can be written according to,

$$\begin{cases} \mathbf{T}_{1,1}^k = -\gamma_p e_1^k \\ \mathbf{T}_{2,1}^k = \mathbf{T}_{2,n}^k = -\gamma_s e_2^k, n = 2, \dots, N \\ \mathbf{T}_{1,n}^k = -\gamma_s e_2^k - \gamma_d e_d^k / f_d, n = 2, \dots, N \end{cases} \quad (4.21)$$

where  $e_d^k$  is an average of  $e_3^k$  to  $e_5^k$  and  $f_d$  is a sample and driving frequency.

Note that, for the HA on-off controllers previously described in the Section 3.3, regions of convergence to a local minimum are identified by finding regions where the

derivatives of output errors with respect to transition times are monotonically increasing or decreasing, given bounded but unknown variations of the real system matrix  $\mathbf{A}$  from some set of nominal values. In those regions, for at least some selections of adaptation gains, switching times may all approach their optimal values simultaneously (although for fixed gains this is not guaranteed to remain true as error becomes small). These selections can satisfy property 2 in (4.2) so that the estimator of convergence rate can be applied for this practical application. The nominal system dynamics for the robot leg in (3.31) were taken to be studied.

Convergence estimation is performed to identify how quickly errors in output measurements, as reflected in the cost function from (3.19), would be reduced from various initial input signals when applied to the nominal system in (3.31). As noted earlier, in the Section 3.3, a region of convergence was identified in which the output error is reduced in each time step, but the rate of convergence could only be measured empirically from full system simulation, in a non-comprehensive way.

### 4.3.2 Simulation Results

To analyze the above on-off controller, by applying the adaptation gains from (4.10) to create matrix  $\Gamma$  in (4.11), and evaluating matrix  $\mathbf{F}$  from (4.15) using the system dynamics in (3.31), an approximate error vector  $\mathbf{w}^k$  may be quickly generated. This could in turn be related to the objective function as  $J(\tau^k) \approx \text{mean}(\mathbf{w}^k)$ .

Figure 4.1 illustrates the speed with which the adaptive laws (4.21) produced convergence to near zero error while the estimated error maintains similar values. In this example, values used for  $\gamma_p$ ,  $\gamma_s$ ,  $\gamma_d$ , and  $f_d$  are 0.005, 0.008, 0.3, and 100 Hz respectively. Figure 4.2 shows the convergence rate for several mean initial error of output.



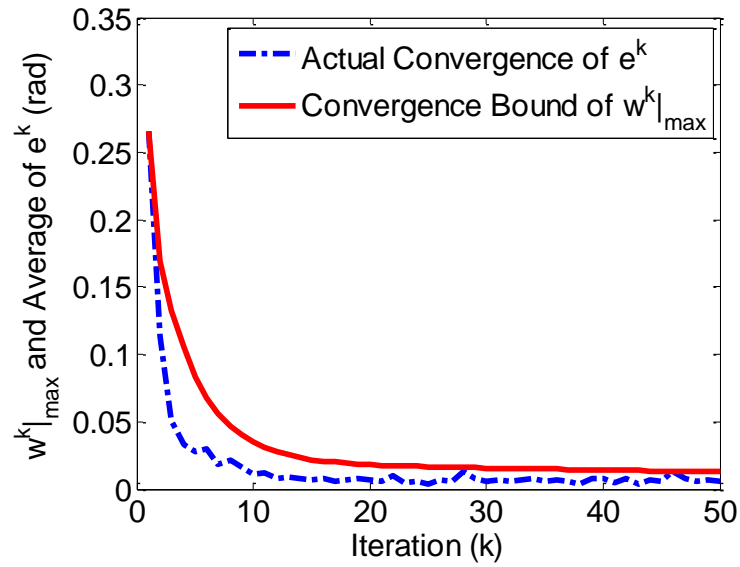


Figure 4.1 Actual Vs. estimated convergence rate for HA on-off controller with 100 Hz sample and driving frequency

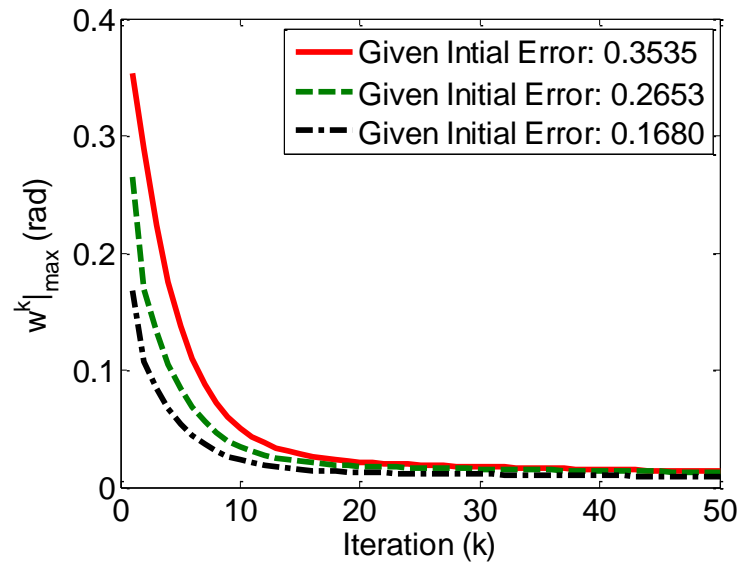


Figure 4.2 Estimated convergence rate with respect to several initial values for the HA on-off controller

### 4.3.3 Experimental Results

Adaptive controller performance has also been verified experimentally, and experimental convergence rates are also available. Since the current robotic leg

prototypes are not yet instrumented with sensors, a macro scale piezoelectric cantilever testbed with a strain gauge was used to test the proposed estimation instead of a microscale actuator, as was discussed in Chapter 3. The testbed actuator has a natural frequency of approximately 31.26 Hz and a nominal damping ratio 0.0307.

A sample result is shown in Figure 4.3. This result demonstrates a successful estimation of convergence rate with the maximum bounded error. In this results, the estimated error are converged to zero from 5 iterations with  $N = 6$  measurements and  $Q = 2$  transitions per measurement. The used time domain and desired position were  $t \in [t_0 = 0, t_s = 0.05 \text{sec}]$  and  $r_1 = r_2 = \dots = r_7 = r = 0.5$  rad. The controller used  $\gamma_p = 0.009$ ,  $\gamma_s = 0.009$ ,  $\gamma_d = 0.0002$ , and  $f_d = 150$  Hz based on the previous convergence analysis and these coefficient were used to analyze a convergence rate for this control approach. Initial guesses for switching times were selected under the convergence analysis as  $[\tau_{1,1}^1 \ \tau_{2,1}^1 \ \tau_{1,n}^1 \ \tau_{2,n}^1] = [2 \text{msec} \ 10 \text{msec} \ \tau_{2,n}^1 + 1 \text{msec} \ \tau_{2,n}^1 + 6 \text{msec}]$  and the corresponding initial output error with mean value was 0.41 rad.

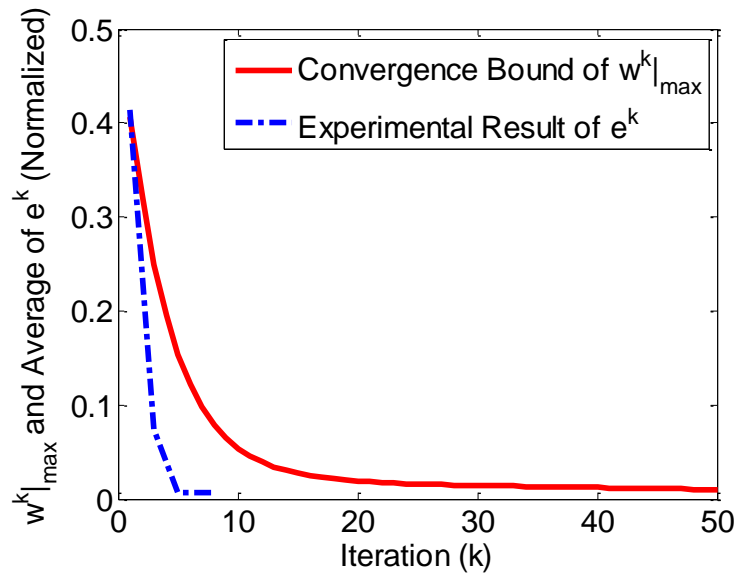


Figure 4.3 Experimental Vs. estimated convergence for HA on-off control

#### 4.3.4 Estimation of Power/Energy Consumption

Once predictions of controller convergence behavior can be made for various selections of adaptation gains, numbers of switching instances, and sampling times, it becomes possible to identify strategies for reducing total control system energy usage. For instance, Figure 4.4 shows the estimated convergence rate for HA on-off controller applied to the test system with various sampling frequencies, and 2 switching transitions between each measurement. As can be seen for a given final error target, sampling at higher frequencies tends to result in adaptation to the desired error level over a smaller number of iterations. However, increasing sampling rate increases power consumption, and thus there exists a sampling rate such that convergence speed is not significantly improved.

One approach to very low-power control is to utilize sensing only until an effective input sequence is found, if a system is making multiple motions in a comparatively consistent environment. If convergence is fast, sensing circuitry need only be operated for a small number of robotic leg stepping motions. However, energy savings from reducing the duration of the sensor usage must be compared to increased power consumption during each iteration due to the higher sampling frequency. For a given sensing circuit architecture, then, the convergence estimates in Figure 4.4 can be compared to power/energy consumption versus sampling frequency of the sensing circuit to select a preferred sampling frequency for robotic leg control. In this analysis, one can estimate the number of iteration required to reach an error level for a specific application. For instance, the error level 0.03 rad (7% of maximum angle) is used to predict the number of iterations in this work since this error level is similar in resolution to the oscillation remaining after on-off control.

Based on the results in Figure 4.4, power and energy dissipation to reach the target error versus sample rate are obtained as shown in Figure 4.5 and 4.6, respectively. In addition the energy evolution after convergence is examined as shown in Figure 4.7. In this evolution, the sensing operation is turned off when the response is converged to the target error level, and control is performed in open-loop for some period of time. The total and sensing energy use decreases from lower sample rates to 150Hz sample rate but then increases with faster sample rates, while slightly more driving energy is required

throughout the sampling rate increase. Thus, convergence rate knowledge can be used to estimate optimal sampling rates. For the example system, for instance, a 150Hz sample rate may be suggested as the proper sampling rate.

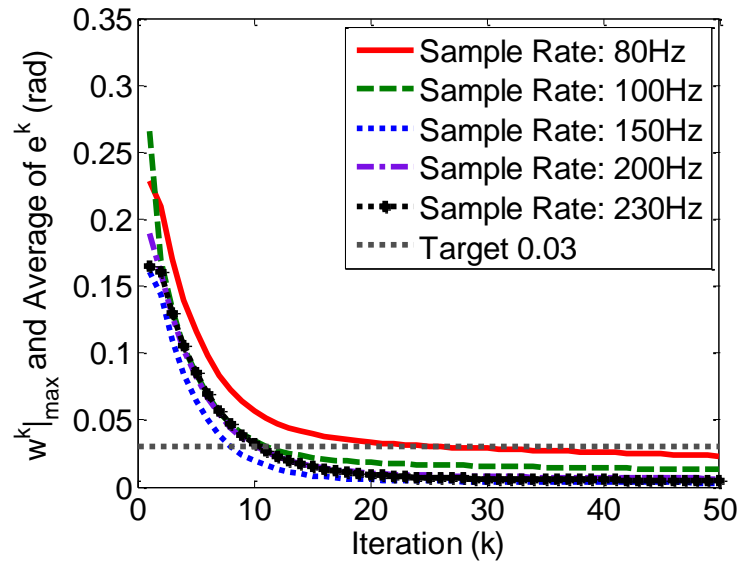


Figure 4.4 Estimated convergence rate with respect to several sample rates for HA on-off controller

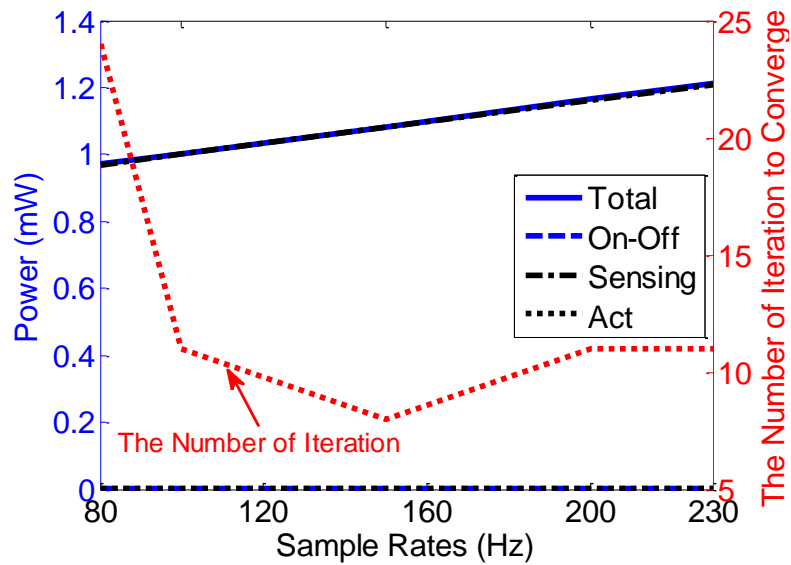


Figure 4.5 Power consumption to reach the target error with respect to sample rates for HA on-off controller

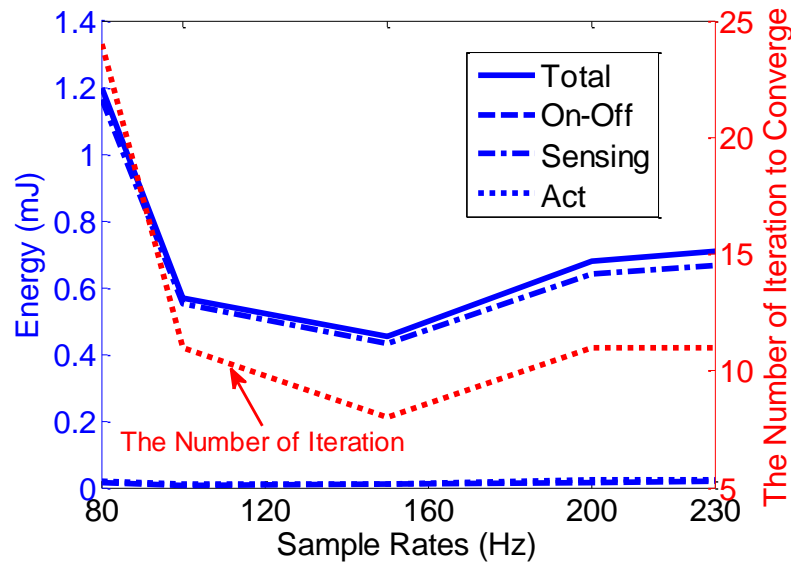


Figure 4.6 Energy Dissipation to reach the target error with respect to sample rates for HA on-off controller

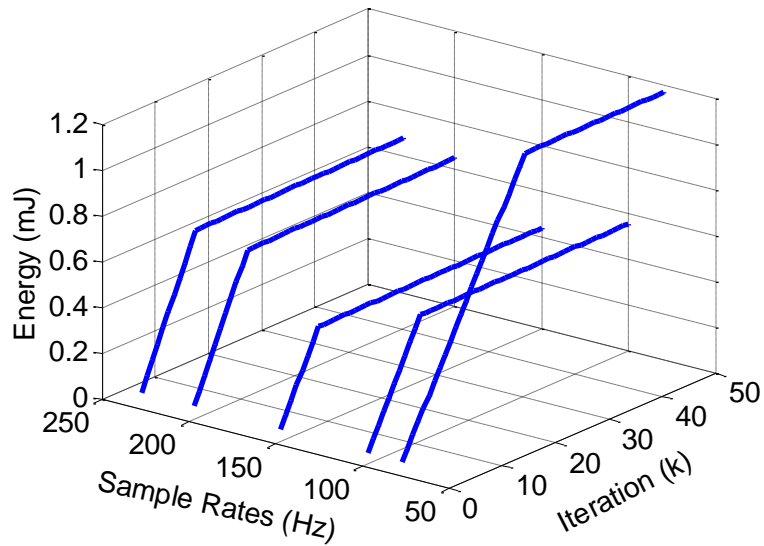


Figure 4.7 Energy evolution of HAA on-off control with further iterations after converging with respect to Sample rates

## 4.4 Case Study II: SAA on-off control

The second test case considers the SAA on-off controller discussed in Chapter 3. In this controller, switching instances are adjusted using SPSA. The nominal dynamics in (3.58) were taken to be tested. This controller searches for a pre-determined number of switching instances (4 in the nominal case,  $\tau_{1,1}$  to  $\tau_{4,1}$ ) as defined in Figure 3.1 with  $N = 1$  measurement at the final time and a single target output for displacement only at that time.

### 4.4.1 Test System Description

The adaptation laws for this controller can be written as

$$\Gamma_{q,1}^k = -\frac{a^k}{c^k \sigma_{q,1}^k} J(\boldsymbol{\tau}^k), q = 1, \dots, 4 \quad (4.22)$$

Where  $a^k$  and  $c^k$  are sequential gain coefficients in (3.42) and (3.43) and  $J(\cdot)$  is a object function in (3.44).

It is noted, in this case study, that the restrictive property 2 (4.2) is only satisfied statistically since the utilized controller does not assure “pointwise” convergence but “almost surely” convergence. Thus, (4.2) may only be replaced with

$$E\left[\|\tau_{i,j}^{k+1} - \tau_{i,j}^*\|_1\right] < E\left[\|\tau_{i,j}^k - \tau_{i,j}^*\|_1\right] \quad \forall i, j \quad (4.23)$$

Under the specific properties of the dynamic system to be controlled, (4.23) can be true using SPSA [98] so that the expected monotonic condition can be satisfied to apply the proposed convergence rate estimation. These conditions are related to properties of measurement noise, smoothness and boundedness of cost function, statistical properties of perturbed variables, and asymptotic normality. The detailed conditions of properties and theoretical proof of (4.23) are described in [98]. In addition, in section 3.4.2, it was described how these conditions can be satisfied for on-off control

of a micro-actuator, with appropriate noise conditions and reasonable description of the micro-robotic leg test case.

Using the statistical condition in (4.23), the deterministically identified equations, such as evolution of input error, (4.11), a bound of output error, (4.15), and estimation of the maximum error bound sequence, (4.20), can be written statistically as:

$$E\left[\left\|\eta_n^{k+1}\right\|_{1,[t_{n-1},t_n]}\right] \leq E\left[\left\|\eta_n^k\right\|_{1,[t_{n-1},t_n]}\right] - E[\Gamma_n] E\left[\sum_{i=1}^n |\mathcal{E}_i^k|\right] \quad (4.24)$$

$$E\left[\left\|\boldsymbol{\varepsilon}^k\right\|\right] \leq \mathbf{F} E\left[\left\|\boldsymbol{\eta}^k\right\|_1\right] \equiv \mathbf{w}^k \quad (4.25)$$

$$\mathbf{w}^{k+1}\Big|_{\max} = \left\{I - \mathbf{F} E[\Gamma] + (\mathbf{F} E[\Gamma])^2\right\} \mathbf{w}^k\Big|_{\max} \quad (4.26)$$

#### 4.4.2 Simulation Results

In this example, this algorithm deals with only one measurement to search optimal switching instances  $\boldsymbol{\tau}$  with respect to time domain,  $t \in [t_0 = 0, t_1 = 0.002]$ , and a desired position,  $r_I = 0.3$  rad so that  $\mathbf{F}$  and  $E[\Gamma]$  in (4.26) have only one element. These  $\mathbf{F}$  and  $E[\Gamma]$  are obtained by the nominal dynamics (3.58) and the adaptation laws (4.22). The evaluation of (4.26) could be then related to the cost function

$$J(\boldsymbol{\tau}^k) \approx \frac{1}{2} \left(w_1^k\Big|_{\max}\right)^2 \quad (4.27)$$

The expected error bound (4.26) for the test case is shown in Figure 4.8 with same simulation condition tested in Section 3.4.3.2. As can be seen, as the controller is iterated average error of output from 40 test cases decrease and actual error is bounded by the estimated error.

Due to the stochastic nature of the controller, on a case by case basis violations of the error bound may occur. This is shown in Figure 4.9 where several individual simulation runs are displayed. It is noted that, as mentioned earlier, this phenomena

shows that this controller cannot guarantee pointwise convergence due to the stochastic nature (4.23) of SPSA. However, even though violations exist, the estimator still predicts quite well the general convergence behavior, and thus is still effective for evaluating trends in convergence rate by the proposed SPSA approach.

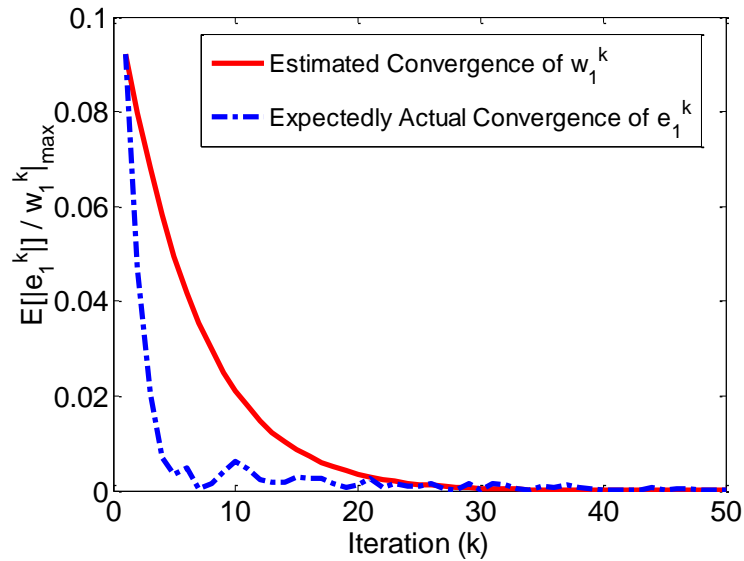


Figure 4.8 Actual Vs. estimated convergence rate for SAA on-off controller

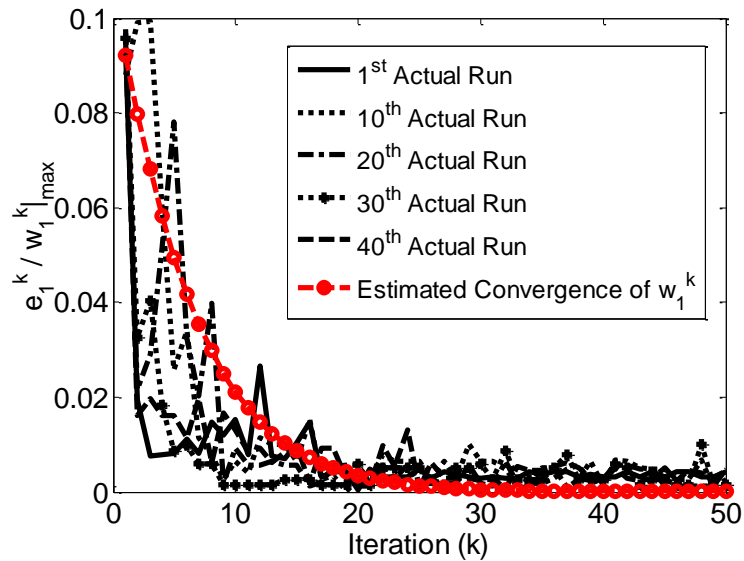


Figure 4.9 Several single runs of actual convergence rate for SAA on-off controller



### 4.4.3 Experimental Results

Performance of convergence rate estimation for the SAA controller was also verified experimentally. Experimental setup and conditions are taken to be same as the Section 3.4.3. Initial guesses for switching times were selected under the convergence analysis as  $[\tau_{1,1}^1 \ \tau_{2,1}^1 \ \tau_{3,1}^1 \ \tau_{4,1}^1] = [0.7\text{msec} \ 1.1\text{msec} \ 1.7\text{msec} \ 2\text{msec}]$  and the corresponding initial output error was 0.2349 rad.

Figure 4.10 shows a sample experimental and estimated convergence rate. The estimated bound of convergence rate shows a similar trend to the experimental result although experimental convergence for the test system was much faster. This is most likely simply the consequence of being a stochastic event, though other potential sources of error include unmodeled image measurement error contribution to noise, which is estimated at  $N(0, 0.01^2)$ , or model uncertainties due to nonlinearity, which are not included in convergence analysis.

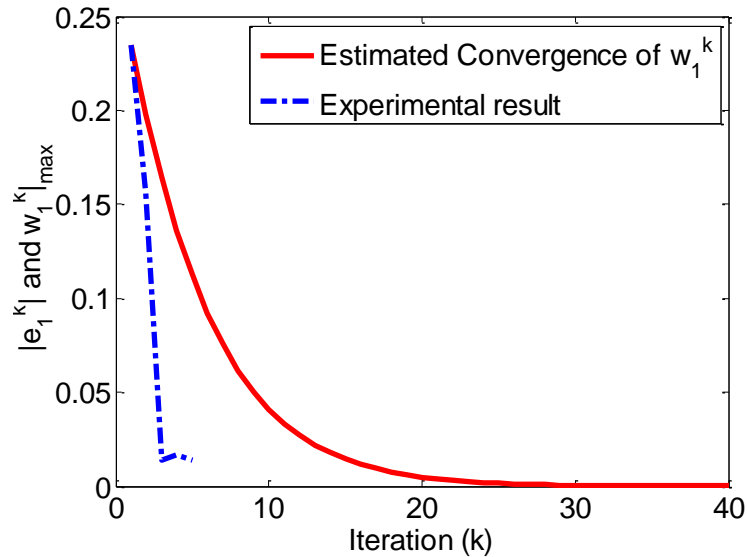


Figure 4.10 Experimental Vs. estimated convergence rate for SAA on-off controller

Unfortunately, only a single test is available due to a choice in the original controller implementation to test effectiveness of the SPSA approach using a pre-determined sequence of random  $\sigma$  to mimic limitations of on-board processing

capabilities in autonomous micro-robots. As a result, the earlier simulation study is regarded as a more accurate indication of convergence rate estimation effectiveness.

#### **4.4.4 Estimation of Power/Energy Consumption**

In this control architecture, the primary trade-off between convergence performance and energy dissipation arises from the number of switching instance to adapt during each iteration, since only a single sensor measurement is taken in all cases.

Figure 4.11 shows the estimated convergence rate for the on-off controller applied to the test system with various switching transitions and one measurement. As can be seen, more switching instances produces convergence to reach a desired error level over fewer iterations. However, improvement in convergence becomes insignificant beyond a certain number of iterations (approximately 10 in this case).

To identify a desired number of switching instances to use with respect to power/energy usage, power and energy of sensing and driving schemes must be compared as shown in Figure 4.12, Figure 4.13, and 4.14. The target error level 0.01rad (2% of maximum angle) is used to predict the number of iteration in this work. This error level is related to the oscillation by on-off control.

Sensor energy increases with the number of iterations needed, and thus decreases until approximately 10-12 switching instances are used, and convergence improvement is minimal. Power and energy used to drive the actuators increases proportionally with switching instances. However, the more number of switching is used, the more energy is consumed after converging procedure due to turning off measurements as shown in Figure 4.15. Again in this evolution, the sensing operation is turned off when the response is converged to the target error level. According to these results, 2 switching instances may be appropriate for low-power-control system tested in this case study.

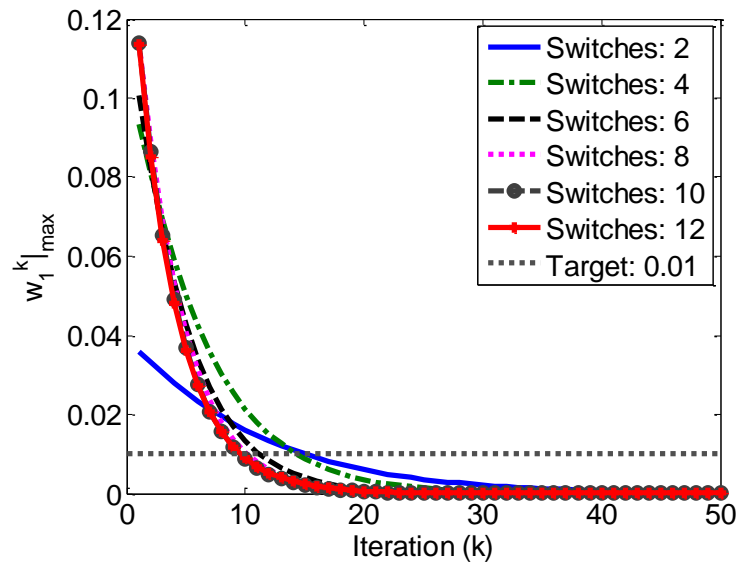


Figure 4.11 Estimated convergence rate with respect to the number of switching for the adaptive controller with SPSA

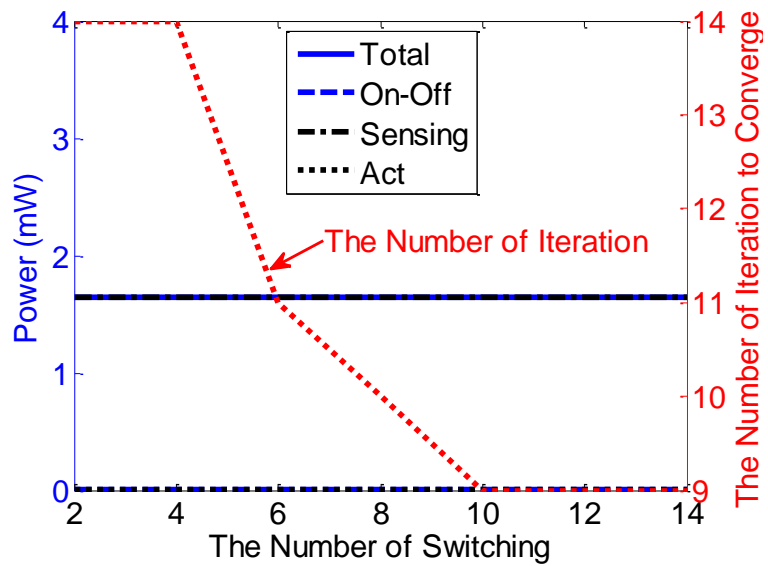


Figure 4.12 Power consumption to reach the target error with respect to the number of switching for SAA on-off control

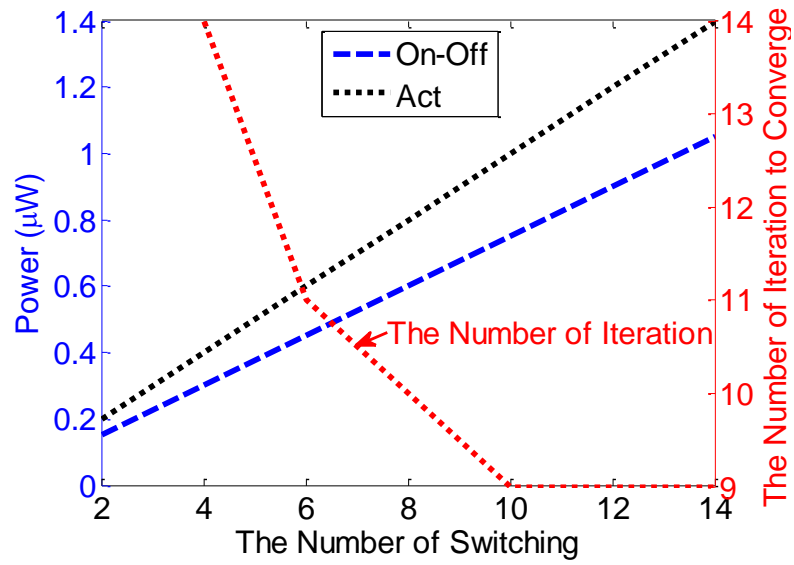


Figure 4.13 Detail of Figure 4.12.

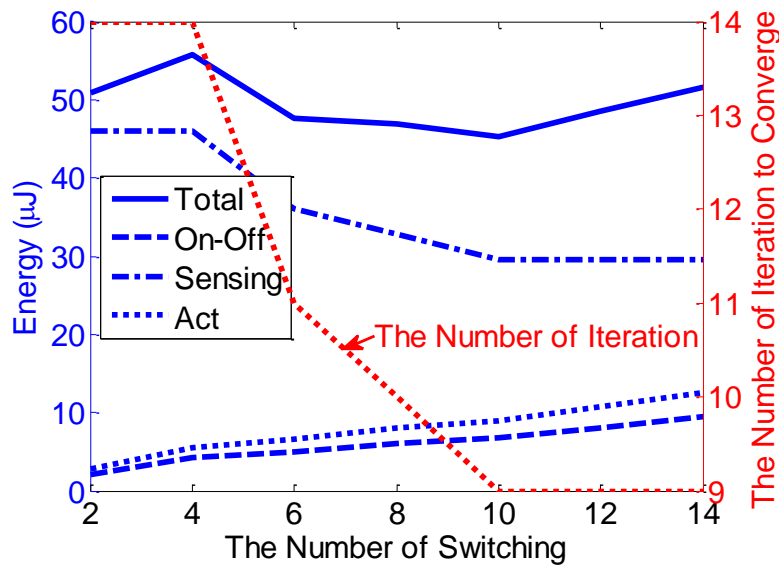


Figure 4.14 Energy consumption to reach the target error with respect to the number of switching for SAA on-off control

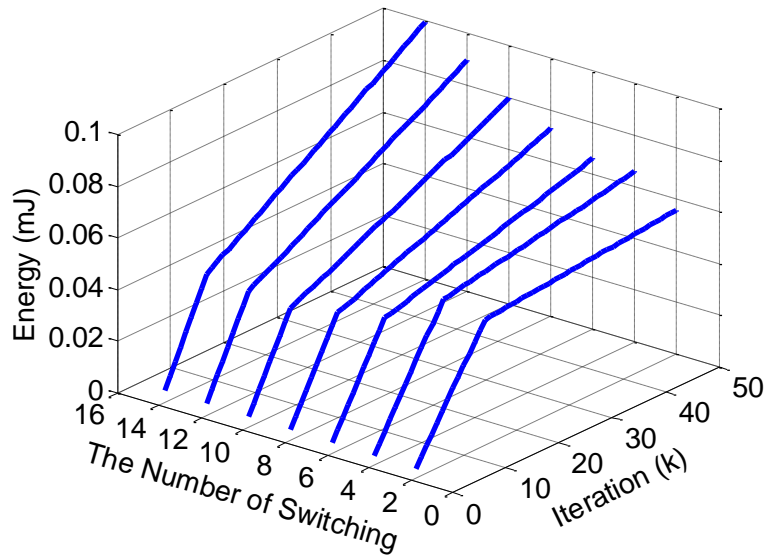


Figure 4.15 Energy evolution of SAA on-off control with further iterations with respect to the number of switching

#### 4.5 Summary

An approach to predicting convergence rate of certain types of iterative adaptive on-off controller has been presented. Once predictions of controller convergence behavior for various selections of adaptation gains, numbers of switching instances, and sampling times can be made, it becomes possible to identify strategies for reducing total control system energy usage when identifying optimal input sequences for repeated actuator motions. For example, in test cases with two different on-off controllers, it is found that taking larger numbers of sensor samples and allowing the controller to switch more frequently reduce the number of iterations for convergence. However, since each of these changes increase energy consumption within individual iterations, optimal sampling rates or switching quantities, respectively, can be estimated. In addition, there exist saturated values of sampling rates and switching instances beyond which convergence rate is not further improved.

The convergence analysis provided here should provide a useful tool for energy management when controlling micro-actuators operating in uncertain but only slowly

varying environments. Over a finite number of iterations, suitable switching instances of an on-off controller may be obtained, and then used for many additional repeated motions before re-starting sensor measurements and input adaptation. The author views this approach as especially desirable for autonomous micro-robots making hundreds or thousands of stepping motions with very limited power availability. Furthermore, it is observed by the author that both convergence and accurate prediction of convergence rate are often seen outside the ranges of guaranteed convergence obtained using the methods described, even though successful adaptation over these larger ranges of initial errors in switch timing cannot currently be predicted analytically.

## CHAPTER 5

### COMPARISON OF PERFORMANCE, POWER, AND ENERGY UNDER VARIOUS CONTROL SCHEMES

In this chapter, the proposed controllers discussed in Chapter 3 are compared to conventional LQG and PWM control in terms of performance, power, and energy to verify effectiveness and power consumption of the proposed control strategies for microactuators. Power and noise estimates of servo components follow the analysis of Chapter 2.

#### 5.1 Description of LQG and PWM Controller

LQG control with a Kalman filter is used to design a conventional analog controller, since an LQG controller has an advantage of good responses with weighting for input effort and robustness against model uncertainties or external disturbances. For a nominal SISO system, with white process noise  $\mathbf{d}_p$  and white measurement noise  $d_v$ , such as

$$\begin{aligned}\dot{\mathbf{x}}(t) &= \mathbf{A}\mathbf{x}(t) + \mathbf{B}u(t) + \mathbf{G}\mathbf{d}_p \\ z(t) &= \mathbf{C}\mathbf{x}(t) + d_v(t)\end{aligned}\tag{5.1}$$

If noise properties satisfy  $E(\mathbf{d}_p) = E(d_v) = 0$ ,  $E(\mathbf{d}_p\mathbf{d}_p^T) = \mathbf{Q}_K$ , and  $E(d_v^2) = R_K$ , the Kalman state estimate that minimizes the steady state error covariance is well known as

$$\begin{aligned}\dot{\hat{\mathbf{x}}}(t) &= (\mathbf{A} - \mathbf{L}\mathbf{C})\hat{\mathbf{x}}(t) + \mathbf{B}u(t) + \mathbf{L}z(t) \\ \hat{z}(t) &= \mathbf{C}\hat{\mathbf{x}}(t)\end{aligned}\tag{5.2}$$

where,  $\hat{\mathbf{x}}$  is state estimate of  $\mathbf{x}$ ,  $\mathbf{L}$  is a estimate gain matrix obtained by solving an

algebraic Riccati equation in terms of the steady state error covariance and noise covariance  $\mathbf{Q}_K$  and  $R_K$ .

Then, the state feedback law with a Gain matrix  $\mathbf{K}_u$  is achieved as

$$u(t) = -\mathbf{K}_u (\hat{\mathbf{x}}(t) - \mathbf{x}(t)) \equiv -\mathbf{K}_u \hat{\mathbf{e}}(t) \quad (5.3)$$

to minimize the quadratic cost function,

$$J(u) = \int_0^{\infty} (\hat{\mathbf{e}}^T \mathbf{Q}_x \hat{\mathbf{e}} + R_u u^2) dt \quad (5.4)$$

subject to (5.1) and (5.2). In (5.3), the feedback gain  $\mathbf{K}_u$  can be obtained from an associated Riccati equation in terms of  $\mathbf{Q}_x$  and  $R_u$ . The detail procedure selecting the weight coefficient will be presented in each case study section.

The PWM controller uses the LQG controller above to determine a desired voltage input commands. These commands are then modulated to define the duty cycle of a high frequency square wave applied by a switching drive circuit. The duty cycle of the PWM commands are determined by comparison between carrier signal of saw tooth wave and a desired signal as shown in Figure 5.1. In general, the modulating frequency has to be at least twice as fast as the fastest frequency of a desired voltage input commands obtained from LQG controller.

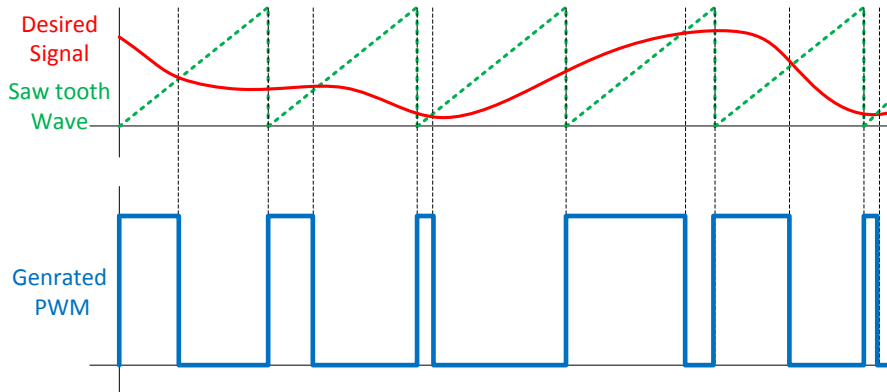


Figure 5.1 PWM generation with a saw tooth carrier wave and a desired signal



To perform power and energy comparison over many iterations of stepping motions of a simulated robot, it is assumed that sensing circuitry is turned off when the final position of the actuator is converged to a target angle and error bound. This takes place after the first iteration when using the LQG and PWM controller or when the adaptive on-off controllers meet are projected to meet target error levels as shown in Fig. 4.4 or 4.11.

## 5.2 Comparison to HA On-Off Control

For the first test case, LQG and PWM controller is designed to illustrate analogous performance with the HA on-off controller for the system in (3.31). Controller gain and sample rates are adjusted to obtain the performance. The resulting performance and power/energy consumption of these controllers are compared to the results of the HA on-off controller.

### 5.2.1 Controller Design and Results of LQG and PWM Control for the System in (3.31)

The estimator gain  $\mathbf{L}$  and state feedback gain  $\mathbf{K}_u$  described above were obtained using the Matlab toolbox for LQR and Kalman estimators with the nominal dynamics (3.31) used in analysis of HA on-off control. Noise properties used for the toolbox were estimated at  $Q_k = 0.0001$  and  $R_k = 0.0001$ , which are obtained from noise analysis from the sensing circuit. Weight coefficients,  $\mathbf{Q}_x$  and  $R_u$  of (4.4), were tuned manually to produce a system response with less than 5% steady state error and a peak time of less than 0.5msec. This response is an analogous response to the converged response of HA on-off controller. The resulting coefficients are [200 0 : 0 400] for  $\mathbf{Q}_x$  and 0.2 for  $R_u$ . The target angle of the actuator was 0.4 rad.

To obtain state estimates (5.2), measurements were taken with sample rate of 1msec which is the close to the Nyquist sample rate of the nominal system (3.31). Simulation results with slower sample rates than 1msec showed deterioration or

instability of the output response, as would be expected. It is noted that the simulation was performed with model uncertainties of 10% spring stiffness and output gain and 20% of damping ratio.

The resulting step response and input voltage  $u(t)$  are shown in Figure 5.2, which has the error accuracy of 0.015rad (4% of maximum angle). Using this input voltage  $u(t)$ , PWM duties are determined with 5 kHz carrier frequency. This frequency is the minimum frequency required to implement LQG input voltage without deterioration of the output response. The maximum operating frequency of the LQG input voltage was 2.5 kHz.

Figure 5.3 shows the obtained step response by PWM control and PWM input corresponding to LQG input. Due to the memory limitation with fast computation time, only transient and steady state response could be simulated. Note that minus switching of PWM needs another interfaces but this is not considered in this work. The resulting accuracy is 0.016rad (3.6% of maximum angle).

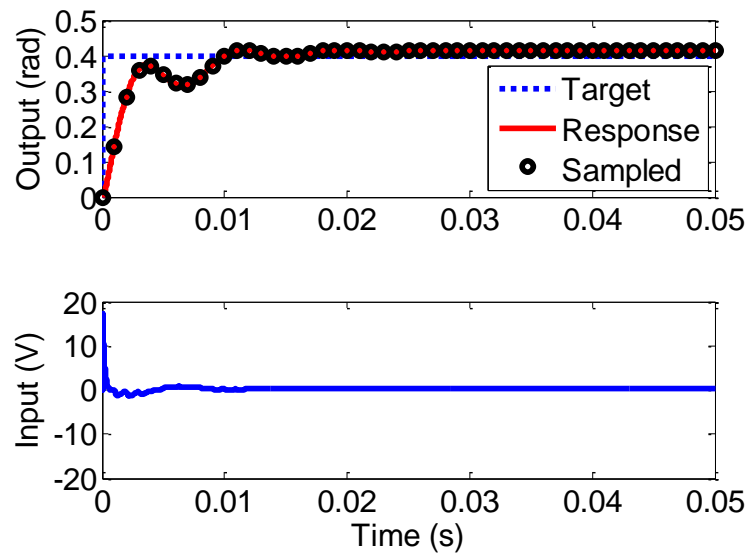


Figure 5.2 LQG controller step response with 1ms measurement sample rate for the system (3.31) with model uncertainties

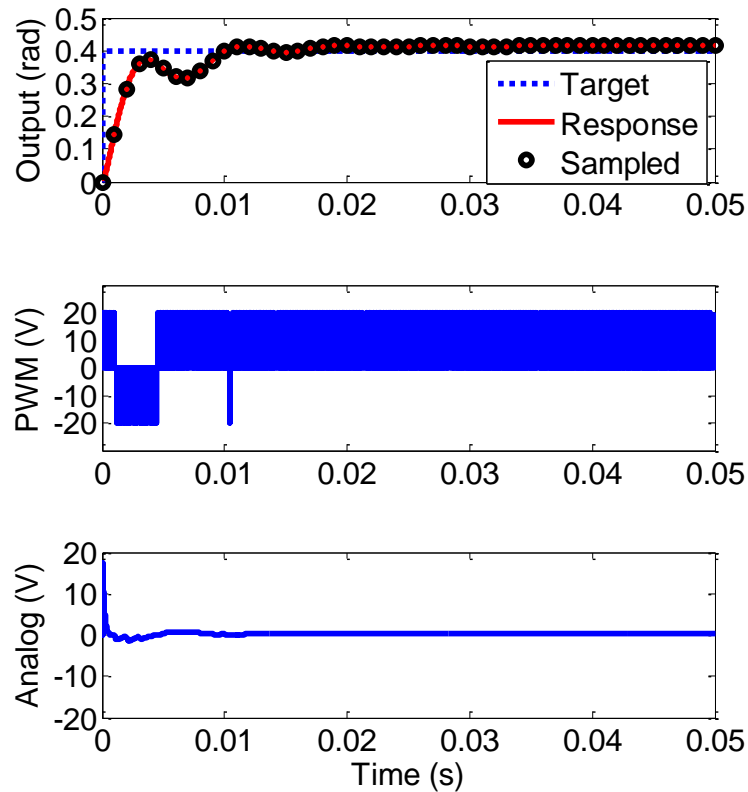


Figure 5.3 PWM controller step response with 1ms measurement samples for the system (3.31) with model uncertainties

### 5.2.2 Comparison of Performance, Power, and Energy

Figure 5.4 shows the resulting accuracy of the system under LQG, PWM, and HA on-off control. While the performance of HA on-off controller is worse than LQG or PWM controller through the first 10 stepping motion of the actuator, relative error in later iteration becomes analogous to LQG or PWM controllers. It is noted that the error estimator of HA on-off controller cannot predict oscillation by on-off actuation due to limitations of estimator.

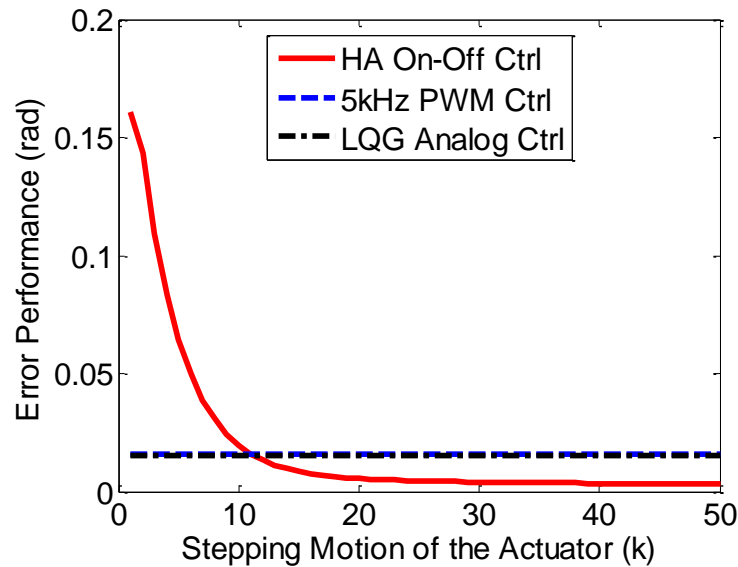


Figure 5.4 Control accuracy under various control schemes for the system (3.31) with model uncertainties over several stepping motions

Despite accuracy loss of the HA on-off controller through the initial stepping motions, this scheme dissipates less power and energy than LQG or PWM control as shown in Figure 5.5 and 5.6. Although the analog driving circuit is assumed to be designed by the currently announced low power amplifier with very low quiescent current, power dissipation with LQG control is larger than PWM control or HA on-off control. In addition, due to many measurements being required, sensing power usage by LQG or PWM control is about twice as large as HA on-off control. It should be noted that the HA on-off controller consumes less energy than LQG or PWM controller even though the HA on-off controller needs many stepping motion to converge a desired angle, which may require a larger number of accumulated measurements.

Using the results of Figure 5.4, 5.5, and 5.6, it is summarized in Table 5.1 how much power and energy are consumed under the discussed control schemes with the specific number of switching and sample rates, to achieve estimated performance.

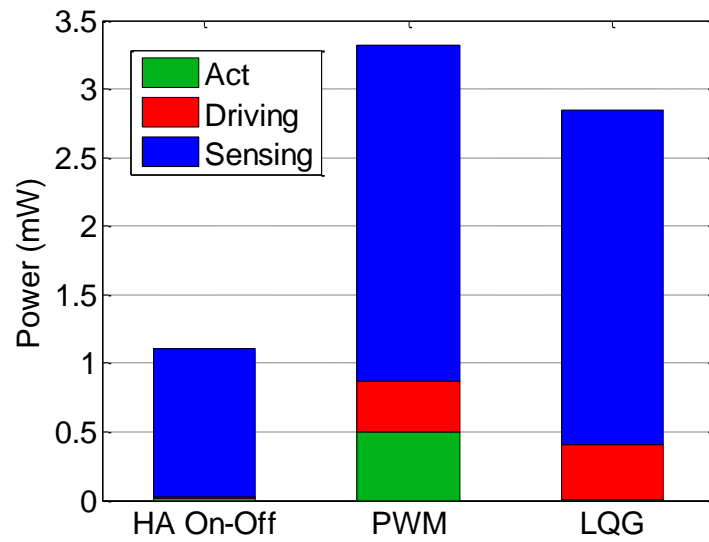


Figure 5.5 Average power consumption of servo system components under various control schemes for the system (3.31) with model uncertainties

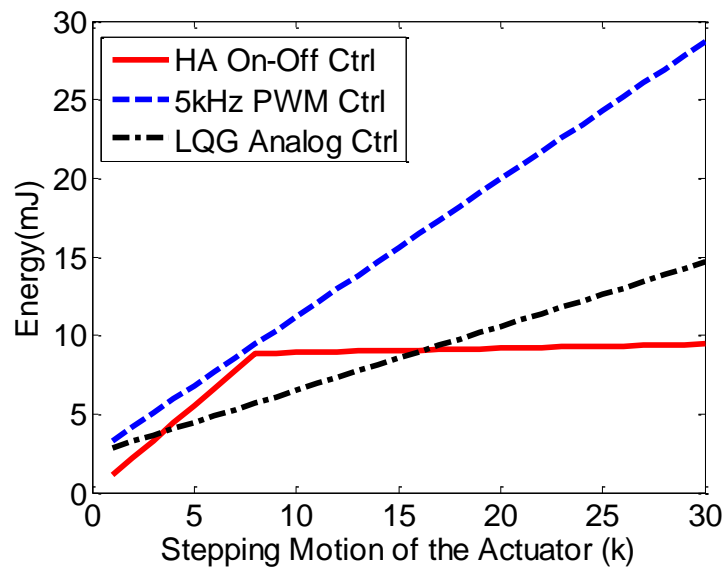


Figure 5.6 Energy dissipation under various control schemes for the system (3.31) with model uncertainties over several stepping motions

Table 5.1 The summary of estimated power and energy required to achieve a desired performance under various control schemes with typical switching instances and sample rate to control the system (3.31) with model uncertainties

The System (Heuristic)		LQG	PWM	HA on-off
Sampling Period (msec) per Iteration		1	1	6.7
No. of Switches per Iteration		0	500	15
Position Error (rad)		0.015 (4%)	0.016 (3.6%)	< 0.015 (4%)
Power Consumption( $\mu$ W)	Sensing	2400	2400	1100
	Driving	400	375	11.3
	Actuator	6.9	500	15
	Total	2807	3275	1126
Energy Consumption ( $\mu$ J) through 20 <sup>th</sup> Iteration		1100	2000	917

### 5.3 Comparison to SAA On-Off Control

For the second comparison, LQG and PWM controller are designed to control the system in equation (3.58), which was used to perform the SAA on-off control. Those two conventional controllers may result in similar dynamic responses to the SAA on-off controller. The resulting performance and power/energy usage are compared again to the case of the SAA controllers.

#### 5.3.1 Controller Design and Results of LQG and PWM Control for the System in (3.58)

The nominal dynamics (3.58) was again utilized to achieve the estimator gain  $\mathbf{L}$  and state feedback gain  $\mathbf{K}_u$  of LQG controller, which is same dynamics of the system used in SAA on-off controller. Noise properties were estimated at  $Q_k = 0$  and  $R_k = 1E-4$ . Weight coefficient  $\mathbf{Q}_x$  and  $R_u$  of (5.4) were tuned manually to produce analogous response with the converged response of SAA on-off controller without overshoot. The resulting coefficients are  $[0 \ 0 \ 0 \ 1]$  of  $\mathbf{Q}_x$  and  $1E-4$  of  $R_u$ . The target angle of the actuator was 0.3 rad.

Although aim of this application is to make a final output angle reach a target angle at a fixed finite time, a measurement was taken at every 1msec. Simulation results with fewer measurements showed deterioration of the output response. Model uncertainties were accounted such as 10% spring stiffness and output gain and 20% of damping ratio under simulation.

Figure 5.7 shows the resulting step response and input voltage  $u(t)$ . Obtained error accuracy is 0.003rad (0.7% of maximum angle). Based on the analog input voltage  $u(t)$ , PWM input is determined with 37 kHz modulating frequency. This frequency is the minimum frequency required to implement the LQG input voltage without deterioration of the output response. The obtained step response by the PWM control and PWM input related to LQG input is shown in Figure 5.8. The resulting accuracy is 0.0025rad (0.5% of maximum angle).

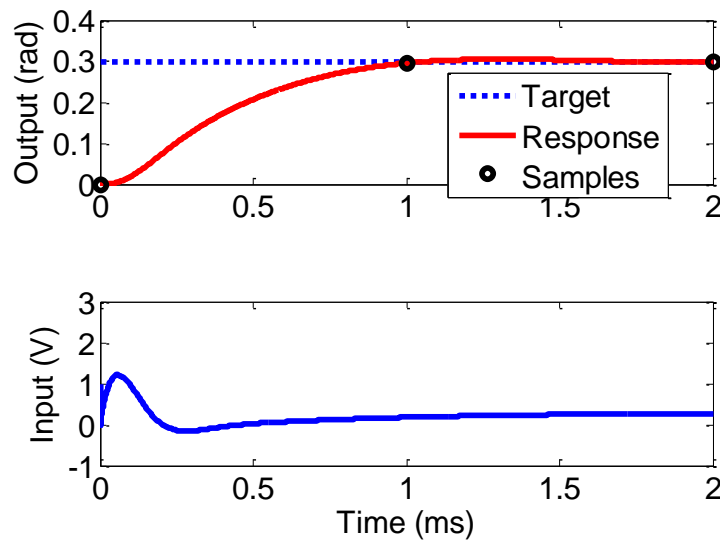


Figure 5.7 LQG controller step response with single measurement for the system (3.58) with model uncertainties

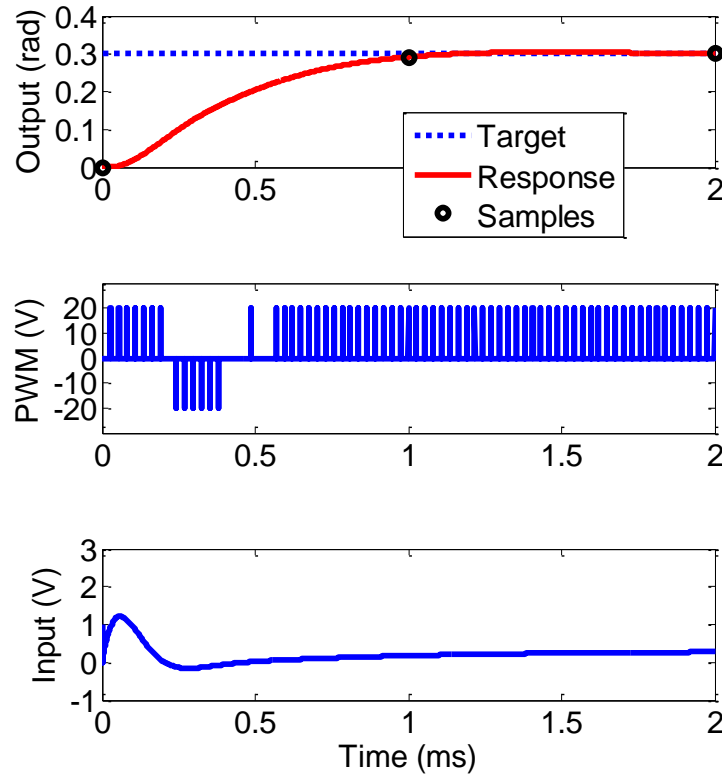


Figure 5.8 PWM controller step response with single measurement for the system (3.58) with model uncertainties

### 5.3.2 Comparison of Performance, Power, and Energy

The resulting accuracy of LQG, PWM, and SAA on-off control for the second sample system is shown in Figure 5.9. The accuracy trend obtained is same as HA on-off controller such that initial accuracy of SAA on-off control through the first 10-13 iteration is worse than the other control schemes but relative error in later iteration becomes equal or better than that of LQG or PWM controllers.

Based on the designed parameters of controllers above and SAA on-off controller in Chapter 3, power and energy dissipation are compared as shown in Figure 5.10 and 5.11. Despite the very fast PWM switching frequency, less power and energy is wasted by switching drive circuit in PWM control. However, if operating at the maximum speed permitted by system dynamics, all control schemes consume larger amounts of power



than for the previous set of controllers. As was the case of the previous section, the analog driving circuit is assumed to be designed by low power amplifier with very low quiescent current, but still a larger amount of power and energy are needed for an LQR controller to control the actuator. In addition, it is also noted that SAA on-off controller consumes less energy than LQR or PWM controller although SAA on-off controller needs more stepping motion to converge a desired angle.

Table 5.2 shows how much power and energy are consumed to achieve a desired performance under the discussed control schemes with the specific number of switching and sample rates.

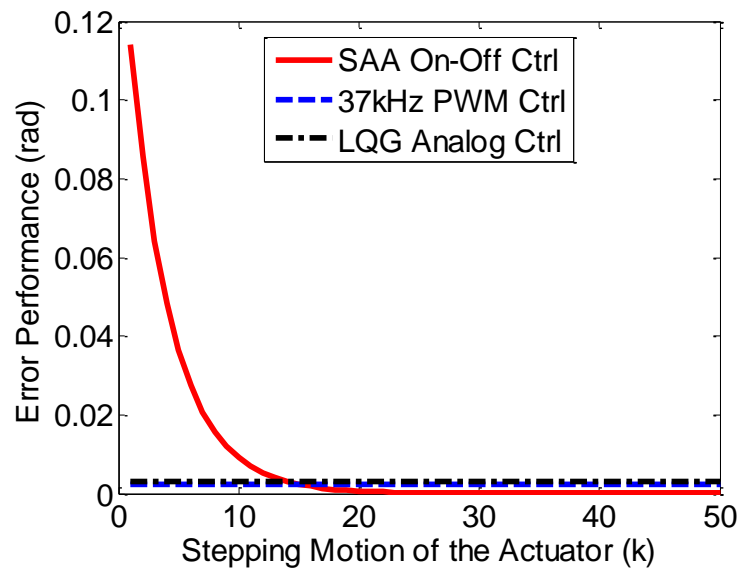


Figure 5.9 Control accuracy under various control schemes for the system (3.69) with model uncertainties over several stepping motions

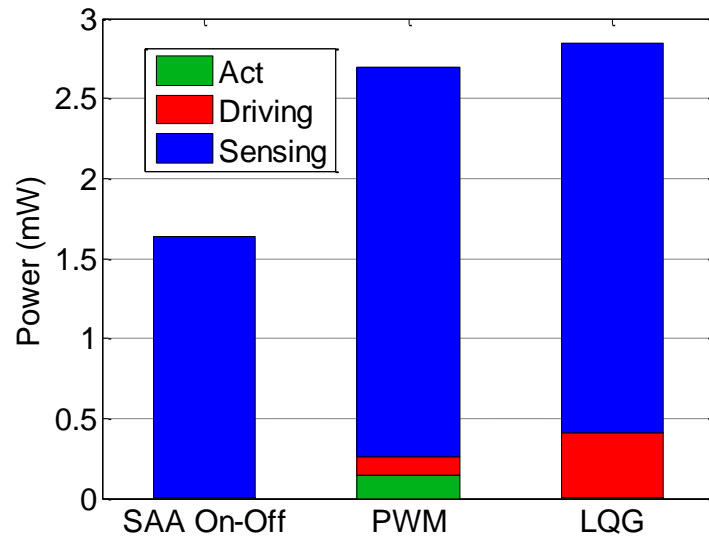


Figure 5.10 Average power consumption under various control schemes for the system (3.58) with model uncertainties

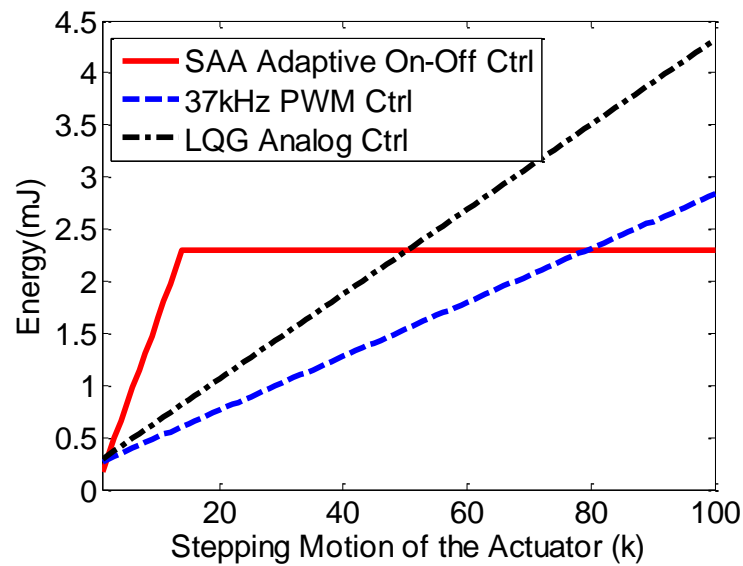


Figure 5.11 Energy dissipation under various control schemes for the system (3.58) with model uncertainties over several stepping motions

Table 5.2 The summary of estimated power and energy required to achieve a desired performance under various control schemes with typical switching instances and sample rate to control the system (3.58) with model uncertainties

The System (SPSA)		LQG	PWM	SAA on-off
Sampling Period (msec) per Iteration		1	1	2
No. of Switches per Iteration		0	148	6
Performance Error (rad)		0.003 (0.7%)	0.0025 (0.5%)	< 0.003 (0.7%)
Power Consumption( $\mu$ W)	Sensing	2400	2400	1600
	Driving	400	111	0.003
	Actuator	6.9	148	0.2
	Total	2806.9	2659	1600.2
Energy Consumption (mJ) through 100 <sup>th</sup> stepping motion		4.3	2.8	2.3

## 5.4 Summary

As shown in Table 5.1 and 5.2, the primary benefit for implementing a servo controller in the proposed manners such as HA and SAA on-off control is that it requires much less power than traditional PWM or analog driving controllers implemented on capacitive microactuators.

To summarize, typical power consumption using HA on-off controller was 1.1mW and energy usages was 917 $\mu$ J of energy up over 20 stepping motions to achieve performance. For the case of SAA on-off controller, average power consumption was 1.6mW of power and 2.3mJ of energy over 100 stepping motions. Both results are competitively less than LQG and PWM controllers. These results hence showed that the proposed control schemes will be extremely useful for autonomous micro-robots based on capacitive actuators under strict power budgets.

## **CHAPTER 6**

### **DISCUSSION AND CONCLUSIONS**

In this dissertation, two model-free iterative adaptive on-off controllers have been proposed. Associated behavior of piezoelectric microactuators using these controllers was explored with respect to power consumption, convergence guarantees, and convergence rate estimation. Performance, power and energy efficiency of the proposed controllers was verified by simulation and experiments. These results were compared to conventional controllers and showed that the proposed controllers can be more effective for very low-power control applications than the conventional controllers.

#### **6.1 Discussion**

##### **6.1.1 Power and Energy Consumption**

The primary benefit for implementing a servo controller in the proposed manner is that it requires much less power and energy than traditional PWM or analog controllers implemented on small, capacitively-loaded actuators. As illustrated in Chapter 5, the heuristic adaptive (HA) approach to on-off controller needed 1.1mW average power during adaptation and consumed 405 $\mu$ J of energy up over 10 stepping motions to achieve performance comparable to a higher power LQR controller. A stochastic approximation adaptive (SAA) on-off controller, operating at a significantly higher iteration frequency, consumed 1.6mW of power and 53 $\mu$ J of energy over 20 stepping motions. In both cases, the power and energy usage satisfy the power/energy budget projected for thin-film piezoelectric micro-robots. This, hence, will be extremely useful for autonomous micro-robots based on thin-film piezoelectric microactuators, examined for example systems.

However, even though power consumption was reduced dramatically in driving schemes, the servo system is still power hungry using the sensing circuit with very low

power amplifiers and strictly limited number of measurements used in this dissertation. This may be caused by existing electronic components to configure the sensing circuit.

It should also be noted that the proposed controllers have accounted only for electrical energy consumption, so mechanical energy may be used more than necessary. For instance, the responses in Figure 3.14 and 3.15 by SAA on-off controller show motions with relatively large amount of overshoot. In this case, because the actuators move extra distance to reach a target, more mechanical energy may be in use compared to non-overshoot motion. This overshoot in the actuators may also cause unwanted robot motion such as back and forth movement during walking toward a target position of the robot. Hence, non-overshoot motion in the actuators may be ideal and important to reduce the mechanical energy and unwanted robot walking. However, this phenomena does not mean that this controller consumes more electrical energy since electrical energy in the proposed control architecture is not dictated by the amount of time spent in the ‘on’ state of electrical input but by the rate of on-off transition of electrical input. Therefore, although longer time in the ‘on’ state of input makes it possible to result in bigger overshoot of response, the electrical energy usage can be same in the case of using the fixed number of switches which was optimized for minimum energy in the dissertation.

To improve servo system performance in the future, it is likely that more advanced, a state-of-the art sensing circuitry under developing in research-level will be required, although the steps taken to limit sensing and driving frequency in this work will still be beneficial. Recent low-power capacitive sensing circuits reported in the literature [15, 36] show an approximate exponential relationship between power and sample rates, in  $\mu\text{W}$ , of  $1.6(1/T_s)^{0.65}$ . This relationship is derived by compiling power consumption data in [15] and [36]. Note that again there is a significant increase in power consumption as sampling period decreases, though baseline power and the rate of increase are dramatically reduce.

Given this capability, it is possible to compare sensing power consumption between a common capacitive sensing circuit analyzed in this dissertation and state-art-of-the circuit, as shown in Figure 6.1. As can be seen, the power consumption by the sensing circuit is much less than the conventional circuit with very low power amplifier. Based on this data, total power consumption of the proposed controller can be projected

as shown in Figure 6.2 and 6.3 for the case of HA on-off control and SAA on-off control, respectively. In both cases, total power can be reduced dramatically with state-of-the-art, research-grade circuits.

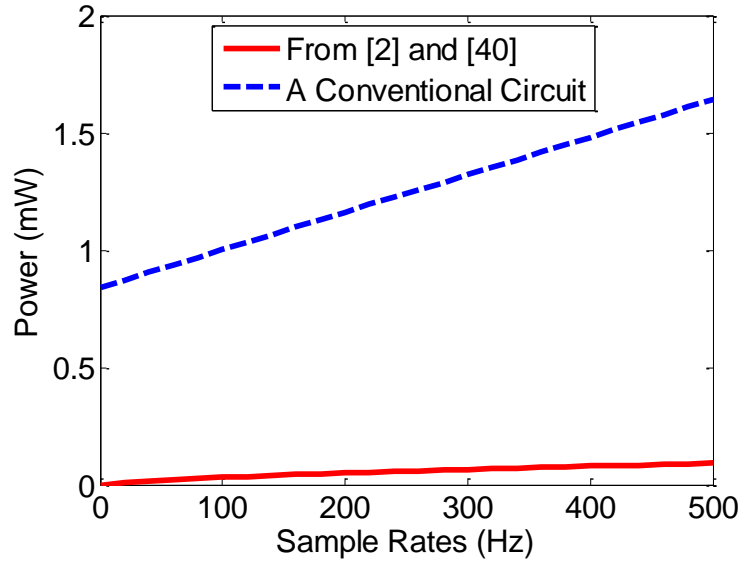


Figure 6.1 Comparison of sensing power consumption between the state-of -the art circuit and the conventional configuration

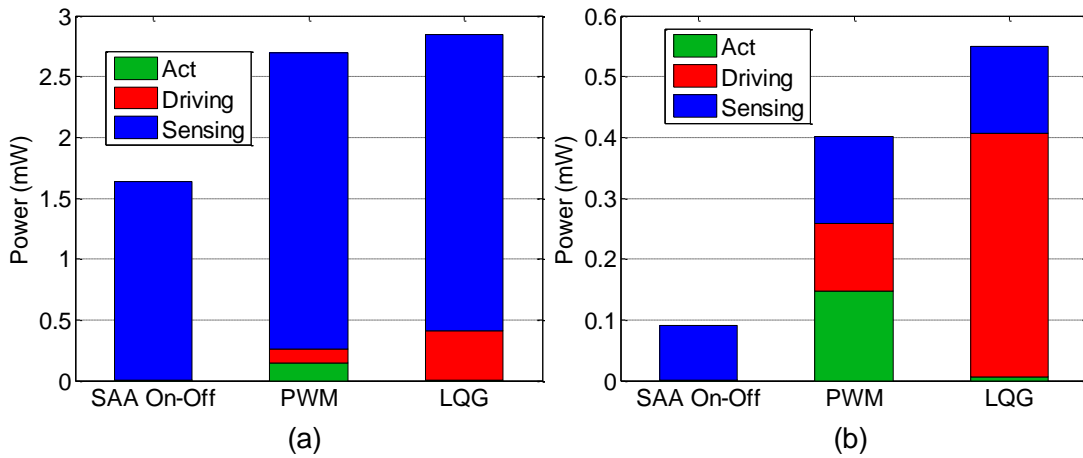


Figure 6.2 Comparison of power consumption using (a) conventional circuit to (b) state-of-the-art one for HA on-off control case

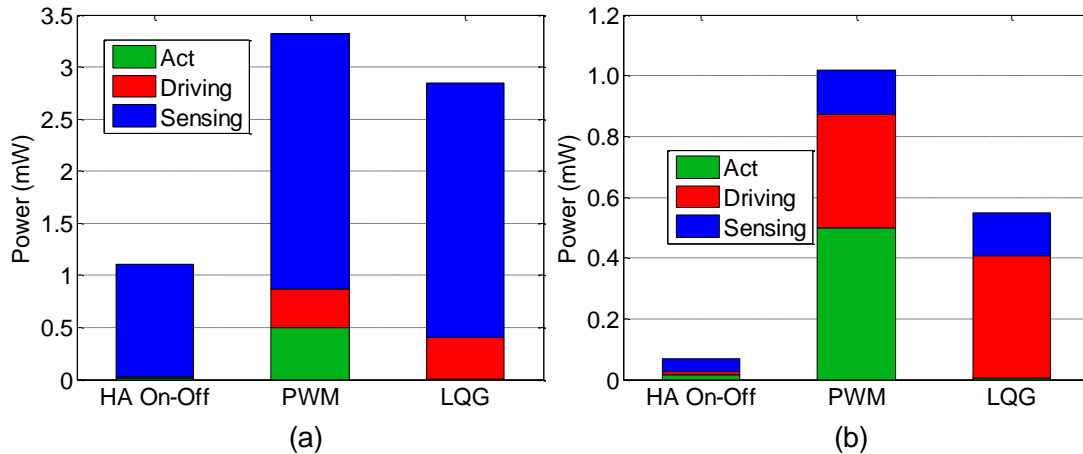


Figure 6.3 Comparison of power consumption using (a) conventional circuit to (b) state-of-the-art one for SAA on-off control case

### 6.1.2 Limitations of the Proposed Controllers and Convergence Rate Estimation

It is important to note that the proposed controllers face significant limitations due to their specialization for simple implementation and power savings. From practical standpoints, the HA on-off controller has been specifically intended to adapt a step-and-hold motion during a finite time. In addition, this controller has required the controller designer to choose an appropriate driving frequency for the steady-state response that balances power usage and oscillation between switching instants. Thus, the HA on-off control scheme may not work for long time durations of motion and cannot avoid some oscillation of the response. Meanwhile, the SAA on-off controller only assesses motion at one point of the final time at each iteration. This assessment cannot be used to hold the system output at its target beyond the final time; its usefulness to microrobotics, for instance, is tied to the ability to switch motion to another leg when one actuator is finished moving, and may be limited further by the inability to regulate leg velocity at these times. Furthermore, response time of the system using these controllers is constrained by the system dynamics on open-loop properties and cannot be significantly reduced, as this could be done for a system without input saturation.

While convergence analysis can be applied to an arbitrary system, it is complicated, and the numerical integrations require significant calculation time. The corresponding benefit of the approach is that convergence analysis may be performed entirely off-line, providing guarantees on convergence when only running the very simple adaptation algorithm within an autonomous system, but it still may be cumbersome to prepare and analyze many potential controller parameter options for convergence. In all cases, some bounds on nonlinearities of the system must be known, and convergence analysis will not generally work for long time durations of motion, due to growing uncertainty about the response.

Furthermore, convergence guarantees are only local and are conservative, with a definite region of convergence obtained but unlikely to show all initial conditions and target motions that in reality would converge. And, fundamentally, the control approach is only applicable to systems where the same motion is to be repeated many times to converge to the desired step motion in simulation and experimental testing.

In the case of convergence rate estimation, the most restrictive limitation is that a true bound on error is only available when the adaptation law can be designed so that all switching times are converging. While this is possible in the regions of convergence of the two controllers presented, it can be difficult to confirm for other controllers with many switching instants. On the implementation side of the estimation for the HA on-off controller, use of fixed adaptation gains causes some oscillation in error to be frequently observed at small error levels, as the monotonic assumption is often no longer maintained in practice. Meanwhile, when the SAA controller is analyzed, as in the second case, the error bound may be violated within individual iteration runs, although on average the error estimates provide good predictions of controller behavior.

## **6.2 Conclusions and Future Works**

Despite some limitations of the proposed methods, this dissertation has contributed on;



- (1) Providing insight of primary factors and mutual correlation between microscale servo components and control strategies in terms of power/energy losses and noise levels [10, 12, 91].
- (2) Determining a unique perspective on reducing energy losses and to dealing with model uncertainties in feedback control of capacitively-loaded microactuators using the proposed model-free iterative adaptive on-off controllers [92 – 93].
- (3) Predicting convergence behavior in terms of adaptation gains, the number of switching instances, and sampling times and, thus identifying strategies for reducing total energy usage of control system using the proposed convergence analysis [94, 95].

To conclude, these control techniques of HA and SAA on-off controller can be very useful in control of repeated motions by systems with extremely limited power budgets, where power consumption at sensor measurements and in analog drive circuitry is to be avoided. The controllers presented can be implemented with just a single or relatively few sensor measurements per iteration and have been showed to result in rapid convergence to a desired output. The convergence analysis provided here should provide a useful tool for energy management when controlling micro-actuators operating in uncertain but only slowly varying environments. Over a finite number of iterations, suitable switching instances and sampling rates of an on-off controller may be obtained, and then used for many additional repeated motions before re-starting sensor measurements and input adaptation.

Furthermore, for autonomous micro-robotics these controllers have the potential to be a powerful tool in regulation of walking. Changing environments and terrains can cause significant changes in dynamics, yet model-based identification is comparatively power and computation intensive. On the other hand, the small size of micro-robots would typically correspond to hundreds or thousands of repeated stepping motions in any given condition, while the proposed algorithm utilizes relatively simple calculations and low sampling within the robot processor to bring about efficient motion.

Meanwhile, to improve strength and usefulness of the proposed methods in the future, some issues are still remained to be further studied for;

(1) Further reducing sensing power

As discussed in the section 6.1.1, the sensing circuits can consume a large amount of power and this can be further reduced by using a very efficiently designed sensing circuit. Unfortunately, these techniques are still at the research stage so that may be obstacles to implement on real applications.

(2) Extending the duration of transient or finite time motions

Although the currently controlled motions may be potentially useful for gait-walking of micro-robots, a method for extending the duration of the motions needs to be accommodated in the controllers. This extending will be able to provide control flexibility and accuracy for the locomotion.

(3) Integrating convergence region and rate analysis in terms of various controller parameters

As discussed in the section of limitations, convergence rate estimation is possible only when the region of convergence is known. This method, hence, is only available for specific switching controllers such as two proposed controllers in this dissertation. Integration of two analysis methods may be useful to identify controller settings minimizing total energy use as a function of various control parameters. In addition, this integration makes it possible to further explore with analyses of other candidate sensor and driving circuit's power consumption.

(4) Finally, an efficient method for jointly optimizing both adaptation laws as well as sampling and driving schemes would provide greater flexibility in control design.

### 6.3 List of Publications

#### Journals

- (1) **B. Hahn** and K. Oldham, "Convergence rate estimation for iterative adaptive on-off control of a piezoelectric microactuator," *IEEE Trans. Control System Tech.*, Submitted on June 2012.
- (2) **B. Hahn** and K. Oldham, "On-off iterative adaptive controller for low-power micro-robotic step regulation," *Asian Journal of Control*, published online, DOI: 10.1002/asjc.410, 2011.
- (3) **B. Hahn** and K. Oldham, "A model-free on-off iterative adaptive controller based on stochastic approximation," *IEEE Trans. Control System Tech.*, vol. 20, no. 1, pp. 196-204. 2012.
- (4) B. Edamana, **B. Hahn**, J. Pulskamp, R. Polcawich, and K. Oldham, "Modeling and optimal low-power on-off control of thin-film piezoelectric rotational actuators," *IEEE/ASME Trans. Mechatronics*, vol. 16, no. 5, pp. 884-896, 2011.

#### Conferences

- (5) **B. Hahn** and K. Oldham, "Convergence rate estimation for iterative adaptive on-off control of a micro-robotic leg joint," accepted on *Proc. 2012 ASME Dynamics Systems and Control Conference*, Ft. Lauderdale, FL, USA, 2012.
- (6) **B. Hahn** and K. Oldham, "Sensing parameter selection for ultra-low-power system identification," accepted on *Proceedings of 2012 the American Control Conference*, Montreal, Canada, 2012.
- (7) K. Oldham, B. Edamana, and **B. Hahn**, "Coordinated voltage conversion and low-power micro-actuator switching," *Proc. 2011 ASME Dynamics Systems and Control Conference*, Arlington, VA, USA, 2011.
- (8) **B. Hahn** and K. Oldham, "A Model-Free On-Off Iterative Adaptive Controller Based on Stochastic Approximation," *Proc. 2010 American Control Conference*, pp. 1665 -16670, Baltimore, MD, USA, 2010.

- (9) **B. Hahn**, and K. Oldham, "Model-free Adaptive On-Off Step Controller For Piezoelectric Micro-Robotics," *Proc. 2009 ASME Dynamic Systems and Control Conference*, pp. 137 -134 (Vol.2), Hollywood, CA, USA, 2009.
- (10) K. Oldham, B. Edamana, and **B. Hahn**, "Low-power control strategies for thin-film piezoelectric micro-robotic actuators," *Proceedings of the ASME 2009 Conference on Smart Materials, Adaptive Structures and Intelligent Systems*, Oxnard, CA, USA, 2009.
- (11) K. Oldham, **B. Hahn**, B. Edamana, J. Pulskamp, R. Polcawich, "Low-power switching control schemes for piezoelectric micro-robotic actuators," *Proc. 2008 ASME Conf. on Smart Mat., Adaptive Struct., and Intelligent Syst.*, pp. 823 – 830 (Vol.2), Ellicot, MD, USA, 2008.
- (12) K. Oldham, **B. Hahn**, and P. Park, "On-off control for low-power servo control in piezoelectric microrobotics," *Proc. 2008 ASME Dynamics Systems and Control Conference*, Ann Arbor, MI, USA, 2008.

## APPENDICES

### APPENDIX A. VOLTAGE OUTPUT AT EACH FUNCTIONAL COMPONENT IN FIGURE 2.9

$$v_{s1}(t) = \frac{C_r}{C_r + C_0 + C_x} v_{sm}(t) \quad (\text{A.1})$$

$$v_{s2}(t) = \frac{C_r}{C_r + C_0 + C_x} v_{sm}(t) \quad (\text{A.2})$$

$$v_D(t) = \frac{2C_x C_r}{(C_r + C_0 - C_x)(C_r + C_0 + C_x)} v_{sm}(t) \quad (\text{A.3})$$

$$v_H(s) = -\frac{\gamma_H C_H R_H s}{1 + C_H R_H s} v_D(s) \quad (\text{A.4a})$$

$$v_H(t) \approx -\gamma_H v_D(t), \quad \because f_{sm} \gg f_H \quad (\text{A.5b})$$

$$v_M(s) = \gamma_M v_H(s) v_{sm}(s) \quad (\text{A.6a})$$

$$v_M(t) \approx -\gamma_M \gamma_H v_D(t) v_{sm}(t), \quad \because f_{sm} \gg f_H \quad (\text{A.7b})$$

$$v_O(s) = -\frac{\gamma_{LF} s}{1 + \gamma_{LF} C_{LF} R_{LF} s} v_M(s) \quad (\text{2.24a})$$

$$v_O(t) \approx \gamma_{LF} \gamma_M \gamma_H \frac{2C_x C_r}{(C_r + C_0 - C_x)(C_r + C_0 + C_x)}, \quad \because f_{sm} \gg f_H \text{ and } f_L \gg f_a \quad (\text{2.24b})$$

### APPENDIX B. EFFECTS OF CHANGES TO SWITCHING TIMES IN THE HA ON-OFF CONTROL

$\tau_p$ ,  $\tau_s$ , and  $\tau_d$  in Figure 3.2 can be converted from  $\tau_{1,1}$ ,  $\tau_{1,2}$ ,  $(\tau_{1,3} + \tau_{1,N})/(N-2)$  in Figure 3.1. To examine the change in system outputs from one iteration to the next, the procedure is illustrate by first considering the change in system response at the 2<sup>nd</sup>

switching time,  $\tau_2$ , which concludes an ‘off’ period. First, using (3.9), we may separate the change in response as

$$\begin{aligned}
\mathbf{x}_b^{k+1}(\tau_2^{k+1}) - \mathbf{x}_b^k(\tau_2^k) &= \Psi_0(\tau_2^{k+1} - \tau_1^{k+1}, \mathbf{x}_b^{k+1}(\tau_2^{k+1})) - \Psi_0(\tau_2^k - \tau_1^k, \mathbf{x}_b^k(\tau_2^k)) \\
&= \int_{\tau_2^k - \tau_1^k}^{\tau_2^{k+1} - \tau_1^{k+1}} \dot{\Psi}_0(t, \mathbf{x}_b^{k+1}(\tau_1^{k+1})) dt \\
&\quad + \Psi_0(\tau_2^k - \tau_1^k, \mathbf{x}_b^{k+1}(\tau_1^{k+1})) - \Psi_0(\tau_2^k - \tau_1^k, \mathbf{x}_b^k(\tau_1^k)) \\
&= \int_{\tau_2^k + \tau_1^{k+1} - \tau_1^k}^{\tau_2^{k+1}} \dot{\Psi}_0(t - \tau_1^{k+1}, \mathbf{x}_b^{k+1}(\tau_1^{k+1})) dt \\
&\quad + \Psi_0(\tau_2^k - \tau_1^k, \mathbf{x}_b^{k+1}(\tau_1^{k+1})) - \Psi_0(\tau_2^k - \tau_1^k, \mathbf{x}_b^k(\tau_1^k)) \\
&= \int_{\tau_2^k + \delta\tau_1^{k+1}}^{\tau_2^{k+1}} \dot{\Psi}_{\mathbf{x}_b}(t - \tau_1^{k+1}, \mathbf{x}_b^{k+1}(\tau_1^{k+1}), u^{k+1}(t)) dt \\
&\quad + \Psi_0(\tau_2^k - \tau_1^k, \mathbf{x}_b^{k+1}(\tau_1^{k+1})) - \Psi_0(\tau_2^k - \tau_1^k, \mathbf{x}_b^k(\tau_1^k)) \\
&= \int_{\tau_2^k + \delta\tau_1^{k+1}}^{\tau_2^{k+1}} \dot{\Psi}_{\mathbf{x}_b}(t - \tau_1^{k+1}, \mathbf{x}_b^{k+1}(\tau_1^{k+1}), u^{k+1}(t)) dt \\
&\quad + \Psi_0(\tau_2^k - \tau_1^k, \mathbf{x}_b^{k+1}(\tau_1^{k+1})) - \Psi_0(\tau_2^k - \tau_1^k, \mathbf{x}_b^k(\tau_1^k))
\end{aligned} \tag{B.1}$$

where the component under the integral reflects the change in the response due to the change in the duration of the ‘off’ period, and the remaining terms reflect the influence of the change in initial conditions for the ‘off’ period due to changes in previous time steps (in this case,  $\tau_1$ ).

Inserting dynamics from (3.2) into the integral portion of (B.1) and separating it into nominal states and unknown states components using (3.1) and (3.2) gives

$$\begin{aligned}
\mathbf{x}_b^{k+1}(\tau_2^{k+1}) - \mathbf{x}_b^k(\tau_2^k) &= \int_{\tau_2^k + \delta\tau_1^{k+1}}^{\tau_2^{k+1}} \dot{\mathbf{x}}^{k+1}(t) \Big|_{t_0=\tau_1^{k+1}} dt \\
&\quad + \int_{\tau_2^k + \delta\tau_1^{k+1}}^{\tau_2^{k+1}} \left[ \mathbf{A}(\mathbf{x}_b^{k+1}(t) - \mathbf{x}^{k+1}(t)) + \mathbf{f}_{\mathbf{x}_b}(\mathbf{x}_b^{k+1}(t)) \right. \\
&\quad \left. + \mathbf{f}_u(\mathbf{x}_b^{k+1}(t)) u^{k+1}(t) \right] \Big|_{t_0=\tau_1^{k+1}} dt \\
&\quad + \Psi_0(\tau_2^k - \tau_1^k, \mathbf{x}_b^{k+1}(\tau_1^{k+1})) - \Psi_0(\tau_2^k - \tau_1^k, \mathbf{x}_b^k(\tau_1^k))
\end{aligned} \tag{B.2}$$

Nominal dynamics under the integral in (B.2) may be used to create nominal error components for the remainder of the expression,

$$\begin{aligned}
\mathbf{x}_b^{k+1}(\tau_2^{k+1}) - \mathbf{x}_b^k(\tau_2^k) &= \mathbf{x}^{k+1}(\tau_2^{k+1}) \Big|_{t_0=\tau_1^{k+1}} - \mathbf{x}^{k+1}(\tau_2^{k+1} + \delta\tau_1^{k+1}) \Big|_{t_0=\tau_1^{k+1}} \\
&\quad + \int_{\tau_2^k + \delta\tau_1^{k+1}}^{\tau_2^{k+1}} \left[ \mathbf{A}(\mathbf{x}_b^{k+1}(t) - \mathbf{x}^{k+1}(t)) + \mathbf{f}_{\mathbf{x}_b}(\mathbf{x}_b^{k+1}(t)) \right. \\
&\quad \quad \left. + \mathbf{f}_u(\mathbf{x}_b^{k+1}(t))u^{k+1}(t) \right] \Big|_{t_0=\tau_1^{k+1}} dt \\
&\quad + \Psi_0(\tau_2^k - \tau_1^k, \mathbf{x}_b^{k+1}(\tau_1^{k+1})) - \Psi_0(\tau_2^k - \tau_1^k, \mathbf{x}_b^k(\tau_1^k)) \\
&= \Phi(\tau_2^{k+1} - \tau_1^{k+1})\mathbf{x}^{k+1}(\tau_1^{k+1}) - \Phi(\tau_2^k - \tau_1^k)\mathbf{x}^k(\tau_1^k) \\
&\quad + \int_{\tau_2^k + \delta\tau_1^{k+1}}^{\tau_2^{k+1}} \left[ \mathbf{A}(\mathbf{x}_b^{k+1}(t) - \mathbf{x}^{k+1}(t)) + \mathbf{f}_{\mathbf{x}_b}(\mathbf{x}_b^{k+1}(t)) \right. \\
&\quad \quad \left. + \mathbf{f}_u(\mathbf{x}_b^{k+1}(t))u^{k+1}(t) \right] \Big|_{t_0=\tau_1^{k+1}} dt \tag{B.3} \\
&\quad + \Psi_0(\tau_2^k - \tau_1^k, \mathbf{x}_b^{k+1}(\tau_1^{k+1})) - \Phi(\tau_2^k - \tau_1^k)\mathbf{x}^{k+1}(\tau_1^{k+1}) \\
&\quad - \Psi_0(\tau_2^k - \tau_1^k, \mathbf{x}_b^k(\tau_1^k)) + \Phi(\tau_2^k - \tau_1^k)\mathbf{x}^k(\tau_1^k) \\
&= \mathbf{x}^{k+1}(\tau_2^{k+1}) - \mathbf{x}^k(\tau_2^k) \\
&\quad + \int_{\tau_2^k + \delta\tau_1^{k+1}}^{\tau_2^{k+1}} \left[ \mathbf{A}(\mathbf{x}_b^{k+1}(t) - \mathbf{x}^{k+1}(t)) + \mathbf{f}_{\mathbf{x}_b}(\mathbf{x}_b^{k+1}(t)) \right. \\
&\quad \quad \left. + \mathbf{f}_u(\mathbf{x}_b^{k+1}(t))u^{k+1}(t) \right] \Big|_{t_0=\tau_1^{k+1}} dt \\
&\quad + \Psi_0(\tau_2^k - \tau_1^k, \mathbf{x}_b^{k+1}(\tau_1^{k+1})) - \Phi(\tau_2^k - \tau_1^k)\mathbf{x}^{k+1}(\tau_1^{k+1}) \\
&\quad - \Psi_0(\tau_2^k - \tau_1^k, \mathbf{x}_b^k(\tau_1^k)) + \Phi(\tau_2^k - \tau_1^k)\mathbf{x}^k(\tau_1^k)
\end{aligned}$$

In the above equation, the change in nominal response,  $\mathbf{x}^{k+1}(\tau_2^{k+1}) - \mathbf{x}^k(\tau_2^k)$  is easily calculated, while the remaining terms may be bounded. First,

$$\begin{aligned}
&\int_{\tau_2^k + \delta\tau_1^{k+1}}^{\tau_2^{k+1}} \left[ \mathbf{A}(\mathbf{x}_b^{k+1}(t) - \mathbf{x}^{k+1}(t)) + \mathbf{f}_{\mathbf{x}_b}(\mathbf{x}_b^{k+1}(t)) + \mathbf{f}_u(\mathbf{x}_b^{k+1}(t))u^{k+1}(t) \right] \Big|_{t_0=\tau_1^{k+1}} dt \\
&\leq \max_{(\tau_2^k + \delta\tau_1^{k+1}, \tau_2^{k+1})} \left\{ \left[ \left| \mathbf{A} \right| \Delta^{k+1}(t) + \mathbf{C}_{\mathbf{x}_b} \left( \left| \mathbf{x}^{k+1}(t) \right| + \Delta^{k+1}(t) \right) + \mathbf{C}_u \left( \left| \mathbf{x}^{k+1}(t) \right| + \Delta^{k+1}(t) \right) u^{k+1}(t) \right] \right. \\
&\quad \quad \left. \times \left| \delta\tau_2^{k+1} - \delta\tau_1^{k+1} \right| \right\} \tag{B.4} \\
&\equiv \Delta_{DT}^{k+1}(\tau_2^{k+1})
\end{aligned}$$

with the right-side portion of (B.4) in brackets acting as an upper bound on the rate of change of error between the nominal and true response over the change in ‘off’ duration, and the quantity  $\Delta_{DT}(t)$  denoting an upper bound on error in the estimated change in response due to change in duration of the current ‘on’ or ‘off’ period at time  $t$ .

The influence of changing initial conditions for the ‘off’ period is more complicated to bound, following a procedure similar to that for bounding  $\mathbf{x}_e(t)$ . A second set of error states,  $\mathbf{x}_{eIC}$ , is defined

$$\mathbf{x}_{eIC}^{k+1} \equiv \boldsymbol{\Psi}_i(t-t_0, \mathbf{x}_b^{k+1}(t_0)) - \boldsymbol{\Phi}(t-t_0)\mathbf{x}^{k+1}(t_0) - \boldsymbol{\Psi}_i(t-t_0, \mathbf{x}_b^k(t_0)) + \boldsymbol{\Phi}(t-t_0)\mathbf{x}^k(t_0) \quad (\text{B.5})$$

to evaluate the difference in two responses beginning from different initial conditions, with  $i = 0$  or  $1$  depending on whether the system is in the ‘on’ or ‘off’ case over the current time period. This error evolves according to dynamics (3.24)

$$\begin{aligned} \dot{\mathbf{x}}_{eIC}^{k+1}(t) &= \mathbf{A}\boldsymbol{\Psi}_j(t-t_0, \mathbf{x}_b^{k+1}(t_0)) + \mathbf{f}_{\mathbf{x}_b}(\boldsymbol{\Psi}_j(t-t_0, \mathbf{x}_b^{k+1}(t_0))) \\ &\quad + \left[ \mathbf{B} + \mathbf{f}_u(\boldsymbol{\Psi}_j(t-t_0, \mathbf{x}_b^{k+1}(t_0))) \right] u^{k+1}(t) \\ &\quad - \mathbf{A}\boldsymbol{\Phi}(t-t_0)\mathbf{x}^{k+1}(t_0) - \mathbf{B}u^{k+1}(t) \\ &\quad - \mathbf{A}\boldsymbol{\Psi}_j(t-t_0, \mathbf{x}_b^k(t_0)) - \mathbf{f}_{\mathbf{x}_b}(\boldsymbol{\Psi}_j(t-t_0, \mathbf{x}_b^k(t_0))) \\ &\quad - \left[ \mathbf{B} + \mathbf{f}_u(\boldsymbol{\Psi}_j(t-t_0, \mathbf{x}_b^k(t_0))) \right] u^k(t) \\ &\quad - \mathbf{A}\boldsymbol{\Phi}_j(t-t_0)\mathbf{x}^k(t_0) - \mathbf{B}u^k(t) \\ &= \mathbf{A}\mathbf{x}_{eIC}^{k+1}(t) + \mathbf{f}_{\mathbf{x}_b}(\boldsymbol{\Psi}_j(t-t_0, \mathbf{x}_b^{k+1}(t_0))) - \mathbf{f}_{\mathbf{x}_b}(\boldsymbol{\Psi}_j(t-t_0, \mathbf{x}_b^k(t_0))) \\ &\quad + \mathbf{f}_u(\boldsymbol{\Psi}_j(t-t_0, \mathbf{x}_b^{k+1}(t_0)))u^{k+1}(t) - \mathbf{f}_u(\boldsymbol{\Psi}_j(t-t_0, \mathbf{x}_b^k(t_0)))u^k(t) \end{aligned} \quad (\text{B.6})$$

and it may be noted that within a given ‘on’ or ‘off’ period in the sequence of inputs,  $u^k(t)$  and  $u^{k+1}(t)$  will have the same constant 0 or 1 value. An upper bound on error due to a change in initial conditions for the current ‘on’ or ‘off’ period,  $\Delta_{IC}(t)$ , may be applied that is obtained numerically from

$$\begin{aligned} \left| \mathbf{x}_{eIC}^{k+1}(t) \right| &\leq \Delta_{IC}^{k+1}(t) \\ &\equiv \left| e^{\mathbf{A}(t-t_0)} \right| \Delta_{IC}^{k+1}(t_0) + \int_{t_0}^t \left| e^{\mathbf{A}(t-s)} \right| \left[ \mathbf{C}_{\mathbf{x}_b} \left( \left| \mathbf{x}^{k+1}(s) - \mathbf{x}^k(s) \right| + \Delta_{IC}^{k+1}(s) \right) \right. \\ &\quad \left. + \mathbf{C}_u \left( \left| \mathbf{x}^{k+1}(s) - \mathbf{x}^k(s) \right| + \Delta_{IC}^{k+1}(s) \right) u(s) \right] ds \end{aligned} \quad (\text{B.7})$$

Applying (B.5 - B.7) to remaining term of (B.3), the other bound is obtained as,



$$\begin{aligned}
& \left| \Psi_0(\tau_2^k - \tau_1^k, \mathbf{x}_b^{k+1}(\tau_1^{k+1})) - \Phi(\tau_2^k - \tau_1^k) \mathbf{x}^{k+1}(\tau_1^{k+1}) \right. \\
& \quad \left. - \Psi_0(\tau_2^k - \tau_1^k, \mathbf{x}_b^k(\tau_1^k)) + \Phi(\tau_2^k - \tau_1^k) \mathbf{x}^k(\tau_1^k) \right| \\
& \leq \left| e^{\mathbf{A}(\tau_2^k - \tau_1^k)} \right| \Delta_{IC}^{k+1}(\tau_1^{k+1}) \\
& \quad + \int_{\tau_1^k}^{\tau_2^k} \left| e^{\mathbf{A}(t-s)} \right| \left[ \mathbf{C}_{\mathbf{x}_b} \left( \left| \mathbf{x}^{k+1}(s) - \mathbf{x}^k(s) \right| + \Delta_{IC}^{k+1}(s) \right) \right. \\
& \quad \quad \left. + \mathbf{C}_u \left( \left| \mathbf{x}^{k+1}(s) - \mathbf{x}^k(s) \right| + \Delta_{IC}^{k+1}(s) \right) u(s) \right] ds \\
& \equiv \Delta_{IC}^{k+1}(\tau_2^k)
\end{aligned} \tag{B.8}$$

where the initial error for this period,  $\Delta_{IC}^{k+1}(\tau_1^{k+1})$ , is any error due to change in the previous switching times, which in this case is only the effect of the change in ‘on’ time,  $\tau_1^{k+1}$  versus  $\tau_1^k$ . The bound here,  $\Delta_{IC}^{k+1}(\tau_2^k)$  is the maximum effect of changes in initial conditions for the current ‘on’ or ‘off’ phase of motion, assuming the previous switching time were used during this phase (while effects of the change in duration of this ‘on’ or ‘off’ phase on overall behavior is captured in (B.4)).

Therefore, using same procedure of (B.2 – B.4) and assumption (3.8), we can obtain a relation,

$$\begin{aligned}
\Delta_{IC}^{K+1}(\tau_1^{k+1}) &= \left| \mathbf{x}_b^{k+1}(\tau_1^{k+1}) - \mathbf{x}_b^k(\tau_1^k) \right|_{\max} \\
&= \left| \begin{aligned} &\mathbf{x}^{k+1}(\tau_1^{k+1}) - \mathbf{x}^k(\tau_1^k) + \\ &\int_{\tau_1^k + \delta\tau_0^{k+1}}^{\tau_1^{k+1}} \left[ \mathbf{A}(\mathbf{x}_b^{k+1}(t) - \mathbf{x}^{k+1}(t)) + \mathbf{f}_{\mathbf{x}_b}(\mathbf{x}_b^{k+1}(t)) \right. \\ &\quad \left. + \mathbf{f}_u(\mathbf{x}_b^{k+1}(t))u^{k+1}(t) \right] \Big|_{t_0=0} dt \\ &+ \Psi_1(\tau_1^k - 0, \mathbf{x}_b^{k+1}(\tau_0^{k+1})) - \Phi(\tau_1^k - 0)\mathbf{x}^{k+1}(\tau_0^{k+1}) \\ &- \Psi_1(\tau_1^k - 0, \mathbf{x}_b^k(\tau_0^k)) + \Phi(\tau_1^k - 0)\mathbf{x}^k(\tau_0^k) \end{aligned} \right|_{\max} \\
&= \left| \begin{aligned} &\mathbf{x}^{k+1}(\tau_1^{k+1}) - \mathbf{x}^k(\tau_1^k) + \\ &\int_{\tau_1^k}^{\tau_1^{k+1}} \left[ \mathbf{A}(\mathbf{x}_b^{k+1}(t) - \mathbf{x}^{k+1}(t)) + \mathbf{f}_{\mathbf{x}_b}(\mathbf{x}_b^{k+1}(t)) \right. \\ &\quad \left. + \mathbf{f}_u(\mathbf{x}_b^{k+1}(t))u^{k+1}(t) \right] \Big|_{t_0=0} dt \\ &+ \Psi_1(\tau_1^k, \mathbf{x}_b^{k+1}(0)) - \Phi(\tau_1^k)\mathbf{x}^{k+1}(0) \\ &- \Psi_1(\tau_1^k, \mathbf{x}_b^k(0)) + \Phi(\tau_1^k)\mathbf{x}^k(0) \end{aligned} \right|_{\max} \\
&= \left| \int_{\tau_1^k}^{\tau_1^{k+1}} \left[ \mathbf{A}(\mathbf{x}_b^{k+1}(t) - \mathbf{x}^{k+1}(t)) + \mathbf{f}_{\mathbf{x}_b}(\mathbf{x}_b^{k+1}(t)) \right. \right. \\ &\quad \left. \left. + \mathbf{f}_u(\mathbf{x}_b^{k+1}(t))u^{k+1}(t) \right] \Big|_{t_0=0} dt \right|_{\max} \\
&= \max_{(\tau_1^k, \tau_1^{k+1})} \left[ \left| \mathbf{A} \Delta^{k+1}(t) + \mathbf{C}_{\mathbf{x}_b} \left( \left| \mathbf{x}^{k+1}(t) \right| + \Delta^{k+1}(t) \right) \right. \right. \\ &\quad \left. \left. + \mathbf{C}_u \left( \left| \mathbf{x}^{k+1}(t) \right| + \Delta^{k+1}(t) \right) u^{k+1}(t) \right] \delta\tau_1^{k+1} \\
&\equiv \Delta_{DT}^{k+1}(\tau_1^{k+1})
\end{aligned} \tag{B.9}$$

that reflects the fact that the initial conditions for the first ‘on’ step are constant, but in later time steps becomes the cumulative effect of switching time changes at previous transitions, or in other words, for the  $Q$ -th switching time,

$$\begin{aligned}
\Delta_{DT}^{k+1}(\tau_Q^{k+1}) &\leq \max_{(\tau_Q^k + \delta\tau_{Q-1}^{k+1}, \tau_Q^k)} \left[ \left| \mathbf{A} \Delta^{k+1}(t) + \mathbf{C}_{\mathbf{x}_b} \left( \left| \mathbf{x}^{k+1}(t) \right| + \Delta^{k+1}(t) \right) \right. \right. \\
&\quad \left. \left. + \mathbf{C}_u \left( \left| \mathbf{x}^{k+1}(t) \right| + \Delta^{k+1}(t) \right) u^{k+1}(t) \right] \left| \delta\tau_Q^{k+1} - \delta\tau_{Q-1}^{k+1} \right| \\
\Delta_{IC}^{k+1}(\tau_Q^k) &\leq \left[ \sum_{q=1}^{J-1} \left| e^{\mathbf{A}(\tau_Q^k - \tau_q^k)} \right| \left( \Delta_{DT}^{k+1}(\tau_q^{k+1}) + \Delta_{IC}^{k+1}(\tau_q^k) \right) \right] \\
&\quad + \int_{\tau_{Q-1}^k}^{\tau_Q^k} \left| e^{\mathbf{A}(t-s)} \right| \left[ \left| \mathbf{C}_{\mathbf{x}_b} \left( \left| \mathbf{x}^{k+1}(s) - \mathbf{x}^k(s) \right| + \Delta_{IC}^{k+1}(s) \right) \right. \right. \\
&\quad \left. \left. + \mathbf{C}_u \left( \left| \mathbf{x}^{k+1}(s) - \mathbf{x}^k(s) \right| + \Delta_{IC}^{k+1}(s) \right) u(s) \right] ds
\end{aligned} \tag{B.10}$$

### APPENDIX C. RANGES OF POSSIBLE $\partial y_f / \partial \tau_Q$ DURING SAA ON-OFF CONTROL FOR A 2ND-ORDER NONLINEAR SYSTEM

As an example, the system in (3.55) and known uncertainty bounds (3.56) is utilized to obtain possible ranges of  $\partial y_f / \partial \tau_Q$ . Because the response  $\mathbf{x}(t)$  may be easily solved for a given  $u(t)$ , the individual terms are known, and bounds on the difference  $\mathbf{x}_e$  between  $\mathbf{x}_b$  and  $\mathbf{x}$  may be obtained from:

$$\begin{aligned}
\frac{d}{dt} \begin{bmatrix} |x_{e(1)}(t)| \\ |x_{e(2)}(t)| \end{bmatrix} &\leq \begin{bmatrix} |x_{e(2)}(t)| \\ \left( |a_1| + \delta_1' + \delta_u' u(t) \right) |x_{e(1)}(t)| + \left( |a_2| + \delta_2' \right) |x_{e(2)}(t)| \end{bmatrix} \\
&\quad + \begin{bmatrix} 0 \\ \left( \delta_1 + \delta_u u(t) \right) |x_{(1)}(t)| + \delta_2 |x_{(2)}(t)| \end{bmatrix}
\end{aligned} \tag{C.1}$$

Derivatives of  $\boldsymbol{\psi}$  with respect to initial conditions may likewise be bounded. By [84], these derivatives are known to be solutions to the set of differential equations

$$\begin{aligned}
\frac{d}{dt} \left( \frac{\partial \psi_{i(1)}(t)}{\partial x_{b(1)}(0)} \right) &= \frac{\partial \psi_{i(2)}(t)}{\partial x_{b(1)}(0)} \\
\frac{d}{dt} \left( \frac{\partial \psi_{i(1)}(t)}{\partial x_{b(2)}(0)} \right) &= \frac{\partial \psi_{i(2)}(t)}{\partial x_{b(2)}(0)} \\
\frac{d}{dt} \left( \frac{\partial \psi_{i(2)}(t)}{\partial x_{b(1)}(0)} \right) &= \left( -a_1 + \frac{df_{x_b(1)}(x_{b(1)}(t))}{dx_{b(1)}} + \frac{df_{u(1)}(x_{b(1)}(t))}{dx_{b(1)}} u_{\max} \cdot i \right) \left( \frac{\partial \psi_{i(1)}(t)}{\partial x_{b(1)}(0)} \right) \\
&\quad + \left( -a_2 + \frac{df_{x_b(2)}(x_{b(2)}(t))}{dx_{b(2)}} \right) \left( \frac{\partial \psi_{i(2)}(t)}{\partial x_{b(1)}(0)} \right) \\
\frac{d}{dt} \left( \frac{\partial \psi_{i(2)}(t)}{\partial x_{b(2)}(0)} \right) &= \left( -a_1 + \frac{df_{x_b(1)}(x_{b(1)}(t))}{dx_{b(1)}} + \frac{df_{u(1)}(x_{b(1)}(t))}{dx_{b(1)}} u_{\max} \cdot i \right) \left( \frac{\partial \psi_{i(1)}(t)}{\partial x_{b(2)}(0)} \right) \\
&\quad + \left( -a_2 + \frac{df_{x_b(2)}(x_{b(2)}(t))}{dx_{b(2)}} \right) \left( \frac{\partial \psi_{i(2)}(t)}{\partial x_{b(2)}(0)} \right)
\end{aligned} \tag{C.2}$$

with initial conditions

$$\frac{\partial \psi_{i(1)}}{\partial x_{b(1)}(0)} = 1, \frac{\partial \psi_{i(2)}}{\partial x_{b(2)}(0)} = 0, \frac{\partial \psi_{i(2)}}{\partial x_{b(1)}(0)} = 0, \frac{\partial \psi_{i(2)}}{\partial x_{b(2)}(0)} = 1 \tag{C.3}$$

In (C.2) and (C.3),  $i = (0,1)$  corresponding to ‘on’ and ‘off’ responses.

The equations in (C.2) thus become a pair of 2<sup>nd</sup>-order differential equations that may be bounded as in (C.1),

$$\begin{aligned}
& \frac{d}{dt} \begin{bmatrix} \left| \frac{\partial \psi_{i(1)}(t)}{\partial x_{b(1)}(0)} - x_{sa(1)}(t) \right| \\ \left| \frac{\partial \psi_{i(1)}(t)}{\partial x_{b(2)}(0)} - x_{sb(1)}(t) \right| \\ \left| \frac{\partial \psi_{i(2)}(t)}{\partial x_{b(1)}(0)} - x_{sa(2)}(t) \right| \\ \left| \frac{\partial \psi_{i(2)}(t)}{\partial x_{b(2)}(0)} - x_{sb(2)}(t) \right| \end{bmatrix} \\
& \leq \begin{bmatrix} \left| \frac{\partial \psi_{i(2)}(t)}{\partial x_{b(1)}(0)} - x_{sa(2)}(t) \right| \\ \left| \frac{\partial \psi_{i(2)}(t)}{\partial x_{b(2)}(0)} - x_{sb(2)}(t) \right| \\ \left( |a_1| + \delta_1' \right) \left| \frac{\partial \psi_{i(1)}(t)}{\partial x_{b(1)}(0)} - x_{sa(1)}(t) \right| + \left( |a_2| + \delta_2' \right) \left| \frac{\partial \psi_{i(2)}(t)}{\partial x_{b(1)}(0)} - x_{sa(2)}(t) \right| \\ \left( |a_1| + \delta_1' \right) \left| \frac{\partial \psi_{i(1)}(t)}{\partial x_{b(2)}(0)} - x_{sb(1)}(t) \right| + \left( |a_2| + \delta_2' \right) \left| \frac{\partial \psi_{i(2)}(t)}{\partial x_{b(2)}(0)} - x_{sb(2)}(t) \right| \end{bmatrix} \tag{C.4} \\
& + \begin{bmatrix} 0 \\ 0 \\ \left( \delta_1' + \delta_u' u_{\max} \cdot i \right) |x_{sa(1)}(t)| + \delta_2' |x_{sa(2)}(t)| \\ \left( \delta_1' + \delta_u' u_{\max} \cdot i \right) |x_{sb(1)}(t)| + \delta_2' |x_{sb(2)}(t)| \end{bmatrix}
\end{aligned}$$

where  $\mathbf{x}_{sa} = [x_{sa(1)}(t) \ x_{sa(2)}(t)]^T$  and  $\mathbf{x}_{sb} = [x_{sb(1)}(t) \ x_{sb(2)}(t)]^T$  are solutions to linear portions of (3.55) with initial conditions [1 0] and [0 1] in (C.3).

By finding nominal responses  $\mathbf{x}$ ,  $\mathbf{x}_{sa}$ , and  $\mathbf{x}_{sb}$ , and solving for bounds between them and true system responses as a function of time using (C.1) and (C.4), ranges of possible  $\partial y / \partial \tau_Q$  values may finally be found, as for  $\tau_Q$ ,

$$\begin{aligned}
\frac{\partial y_f}{\partial \tau_Q} = & \left[ -x_{(2)}(t_f) - x_{e(2)}(t_f) \right] \\
& + \left[ x_{sa(1)}(t_f - \tau_Q) + \left\{ \frac{\partial \psi_{0(1)}}{\partial x_{b(1)}(0)} - x_{sa(1)}(t_f - \tau_Q) \right\} \right] \left[ x_{(2)}(\tau_Q) + x_{e(2)}(\tau_Q) \right] \\
& + \left[ x_{sb(1)}(t_f - \tau_Q) + \left\{ \frac{\partial \psi_{0(1)}}{\partial x_{b(2)}(0)} - x_{sb(1)}(t_f - \tau_Q) \right\} \right] \\
& \times \left[ -a_1 \left( x_{(1)}(\tau_Q) + x_{e(1)}(\tau_Q) \right) - a_2 \left( x_{(2)}(\tau_Q) + x_{e(2)}(\tau_Q) \right) \right. \\
& \quad + f_{x_b(1)} \left( x_{(1)}(\tau_Q) + x_{e(1)}(\tau_Q) \right) + f_{x_b(2)} \left( x_{(2)}(\tau_Q) + x_{e(2)}(\tau_Q) \right) \\
& \quad \left. + f_{u(1)} \left( x_{(1)}(\tau_Q) + x_{e(1)}(\tau_Q) \right) \right]
\end{aligned} \tag{C.5}$$

## BIBLIOGRAPHY

- [1] E. Gaura and R. Newman, *Smart MEMS and Sensor Systems*, Imerial Collage Press. 2006.
- [2] N. C. Tien, A. Ongkodjojo, R. C. Roberts, and D. Li, "The furture of MEMS in energy technologies," *Proceedings of the 9th International Conference on Solid-State and Integrated-Circuit Tech.*, Beijing, China, pp. 2452–2455, 2008.
- [3] K. A. Cook-Chennault, N. Thambi, and A. M. Sastry, "Powering MEMS protable devices - a review of non-regenerative and regenerative power supply systems with special emphasis on piezoelectric energy harvesting systems," *Smart Materials and Structures*, vol. 17, no. 4, pp.1-33, 2008.
- [4] R. Amirtharajah and A. P. Chandrakasan, "A micropower programmable DSP using approximate signal processing based on distributed arithmetic," *IEEE Journal of Solid-State Circuits*, vol 39, no. 2, pp. 337-347. 2004.
- [5] W. Bracke and R. Puers, *Ultra Low Power Capacitive Sensor Interfaces*, Springer, 2007
- [6] A. P. Chandrakasan, N. Verma, and D. C. Daly, "Ultralow-power electronics for biomedical applications," *Annual Review of Biomedical Engineering*, vol. 10, pp. 247-274, 2008.
- [7] B. Edamana, B. Hahn, J. Pulskamp, R. Polcawich, and K. Oldham, "Modeling and optimal low-power on-off control of thin-film piezoelectric rotational actuators," *IEEE/ASME Trans. Mechatronics*, vol. 16, no. 5, pp. 884-896, 2011.
- [8] E. Sarajlic, E. Berenschot, N. Tas, H. Fujita, G. Krijnen, and M. Elwenspoek, "Fabrication and characterization of an electrostatic contraction beams micromotor," *Proceedings of the 19th IEEE International Conference on Micro Electro Mechanical Systems (MEMS)*, Istanbul, Turkey, pp. 814–817, 2006.
- [9] K. Oldham, J. S. Pulskamp, R. G. Polcawich, M. Dubey, "Thin-film PZT lateral actuators with extended stroke," *J. MEMS*, **17**(4), 890-899, 2008.
- [10] K. Oldham, B. Hahn, B. Edamana, J. Pulskamp, R. Polcawich, "Low- power switching control schemes for piezoelectric micro-robotic actuators," *Proc. ASME Conf. on Smart Mat., Adaptive Struct., and Intelligent Syst.*, Ellicot City, MD, 2008.

- [11] W. C. West, J. F. Whitacre, E. J. Brandon, B. V. Ratnakumar, "Lithium micro-battery development at the Jet Propulsion Laboratory," *IEEE AESS Syst. Mag.*, 2001, 31- 33.
- [12] K. Oldham, B. Edamana, and B. Hahn, "Low-power control strategies for thin-film piezoelectric micro-robotic actuators," *Proceedings of the ASME 2009 Conference on Smart Materials, Adaptive Structures and Intelligent Systems*, Oxnard, CA, USA, 2009.
- [13] M. Karpelson, G.-Y. Wei, and R. J. Wood, "A review of actuation and power electronics options for flapping-wing robotic insects," *IEEE International Conference on Robotics and Automation*, Pasadena, CA, USA, pp. 779-786, May 2008.
- [14] J. A. Main, "Efficient power amplifiers for piezoelectric applications," *Smart Mat. and Struct.*, **5**(6), 766-775, 1996.
- [15] W. Bracke, P. Merkin, R. Puers, and C. Van Hoof, "Ultra-low-power Interface Chip for Autonomous Capacitive Sensor Systems," *Circuits and Systems I*, **54**(1), 130-140, 2007.
- [16] B. Borovic, F. L. Lewis, W. McCulley, A. Q. Liu, E. S. Kolesar, and D.O. Popa, "Control issues for microelectromechanical systems," *IEEE Control Systems Magzinen*, pp. 18-21, Apr. 2006.
- [17] A. Izadian, "Indirect adaptive trajectory control of MEMS LCR," *The 37th Annual Conference on IEEE Industrial Electronics Society*, Melbourne, Australia, pp. 4064-4068, 2011.
- [18] S. Bergbreiter, "Effective and efficient locomotion for millimeter-sized microrobots," *2008 IEEE/RSJ International Conference on Intelligent Robots and Systems*, Nice, France, pp. 4030-4035, 2008.
- [19] T. Ebefors, J. U. Mattsson, E. Kalvesten, and G. Stemme, "A walking silicon micro-robot," *The 10th Int. Conference on Solid-State and Actuators(Transducers '99)*, Sendai, Japan, pp. 1202-1205, 1999.
- [20] M. Isogai, "Locomotion mechanism and control method for a microrobot using the difference in the vibration characteristics of the legs (fabrication of a prototype microrobot; preliminary experiments and experiments in turning control)," *Int. Symposium on Micro-NanoMechatronics and Human Science (MHS)*, Nagoya, Japan, pp. 261-266, 2011.
- [21] F. Becker, V. Minchenya, K. Zimmermann, and I. Zeidis, "Single piezo actuator driven micro robot for 2-dimensional locomotion," *Micromechanics and Microactuators: Mechanisms and Machine Science*, vol. 2, pp. 1-10, 2012



- [22] B. R. Donald, C. G. Levey, C. D. McGray, I. Paprotny, and D. Rus, "An untethered, electrostatic, globally controllable MEMS micro-robot," *Journal of Microelectromechanical systems*, vol. 15, no. 1, pp. 1-15, Feb. 2012.
- [23] S. Bergbreiter and K. S. J. Pister, "Design of an autonomous jumping microrobot," *2007 IEEE Int. Conference on Robotics and Automation*, Roma, Italy, pp. 447-453, Apr. 2007
- [24] M. E. Karagozler, A. Thaker, S. C Goldstein, and D. S. Ricketts, "Electrostatic actuation and control of micro robots using a post-processed high-voltage SOI CMOS Chip," *2011 IEEE Int. Symposium on Circuits and Systems*, Rio de Janeiro, Brazil, pp. 2509-2512, May 2011.
- [25] S. Hollar, A. Flynn, C. Bellow, and K. S. J. Pister, "Solar powered 10mg silicon robot," *IEEE the 16th Annual Int. Conference on Micro Electro Mechanical Systems*, Kyoto, Japan, pp. 706-711, Jan. 2003.
- [26] M. Karpelson, R. J. Wodd, and G.-Y. Wei, "Low power control IC for efficient high-voltage piezoelectric driving in a flying robotic insect," *2011 Symposium on VLSI Circuits*, Kyoto, Japan, pp. 178-179, Jun. 2011.
- [27] L. Schenato, D. Campolo, and S. Sastry, "Controllability issues in flapping flight for biomimetic micro aerial vehicles (MAVs)," *Proceedings of the 42nd IEEE conference on Decision and Control*, Maui, Hawaii, USA, pp. 6441-6447, Dec. 2003.
- [28] J. Yan, R. J. Wood, S. Avadhanula, M. Sitti, R. S. Fearing, " Toward flapping wing control for a micromechanical flying insect," *Proceedings of IEEE Conference on Robotics and Automation*, Seoul, Korea, pp. 3801-3808, May 2001.
- [29] L. Schenato, X. Deng, and S. Sastry, "Fight control system for a micromechanical flying insect: architecture and implementation," *Proceeding of IEEE International Conference on Robotics and Automation*, Seoul, Korea, pp. 1641-1646, 2001.
- [30] R. N. DB, S. N. Nejad, M. Kabganian, and A. D. Djadid, "Adaptive control of a legged capsular microrobot based on Lyapunov stability criteria," *Proceedings of the Institution of Mechanical Engineers, Part C: Journal of Mechanical Engineering Science*, DOI: 10.1177/0954406211417940, Mar. 2012.
- [31] P. H. Saul, K. M. Brunson, and R. J. T. Brunyan, "Versatile high voltage level shift and driver for MEMS applications," *Electron. Lett.*, vol. 39, no. 2, pp. 185-186, 2003.

- [32] S. Chandrasekhar, D. Lindner, and R. Smith, "Optimized design of switching amplifiers for piezoelectric actuation," *Journal of Intelligent Materials, Systems, and Structures*, vol. 11, no. 11, pp. 887-901, 2000.
- [33] D. Campolo, M. Sitti, and R. S. Fearing, "Efficient charge recovery method for driving piezoelectric actuators with quasi-square waves," *IEEE Trans. Ultrasonics, Ferroelectrics and Frequency Control*, Vol. 50, No. 3, pp. 237-244, Mar. 2003.
- [34] G. Biancuzzi, T. Lemke, P. Woias, O. Ruthmann, H. J. Schrag, B. Vodermayr, T. Schmid, and F. Goldshmidtboeing, "Design and simulation of advanced charge recovery piezoactuator drivers," *Journal of Micromechanics and Microengineering*, vol. 20, no. 10, pp.1-12, Sep., 2010.
- [35] C.-S. Chao, P.-C. Huang, M.-K. Chen and L.-S. Jang, "Design and analysis of charge-recovery driving circuits for portable peristaltic micropumps with piezoelectric actuators," *Sensors and Actuators A: Physical*, vol. 168. no. 2, pp. 313-319, Aug. 2011.
- [36] D. Fang, H. -W. Qu, and H. -K. Xie, "A 1mW dual-chopper amplifier for a 50  $\mu\text{g}/\sqrt{\text{Hz}}$  CMOS-MEMS accelerometer," *2006 Symposium on VLSI Circuits*, pp. 2-6, 2006.
- [37] S.-Y. Peng, M. S. Qureshi, P. E. Hasler, A. Basu, "A charge-based low-power high-SNR capacitive sensing interface circuit," *IEEE Trans. Circuits and Systems - I*, vol 55, no. 7, pp. 1863-1872, Aug. 2008.
- [38] H. Danneels, K. Coddens, and G. Gielen, "A fully-digital, 0.3V, 270 nW capacitive sensor interface without external references," *Proceedings of the ESSCIRC*, Helsinki, Finland, pp. 287-290, Sep. 2011.
- [39] W. Singhose, Tarunraj Singh, and W. Seering, "On-Off control of flexible spacecraft with specified fuel usage," *Proceedings of the American Control Conference*, Albuquerque, New Mexico, pp. 2308-2312, Jun. 2009.
- [40] B. J. Driessen, "On-off minimum-time control with limited fuel usage: near global optima via linear programming," *Proceedings of the American Control Conference*, Chicago, IL, U.S.A., vol. 6, pp. 3875-3877, Jun. 2000.
- [41] C. Y. Kaya, J. L. Noakes, "Computations and time-optimal controls," *Optimal Control App. and Meth.*, **17**, pp. 171-185, 1996.

- [42] B. Edamana, K. Oldham, "An optimal on-off controller with switching costs using non-linear binary programming," *Proc. American Control Conf.*, St. Louis, MO, 4227-4232, 2009.
- [43] J. L. Noakes, C. Y. Kaya, "Computational method for time-optimal switching control," *J. Optimization Th. and App.*, **117**(1), pp.69–92, 2003.
- [44] D. G. Luenberger, *Linear and Nonlinear Programming*. Addison-Wesley, 1989.
- [45] W. E. Singhose, B. W. Mills, and W. P. Seering, "Closed-form methods for on-off control of multi-mode flexible structures," *Proc. 36<sup>th</sup> Conference on Decision and Control*, San Diego, CA, pp. 1381-1386, Dec. 1997.
- [46] C. -T. Chen, and C. Hwang, "Optimal on-off control for fed-batch fermentation processes," *Industrial Engineering and Chemical Research*, **29**, pp. 1869-1875, 1990.
- [47] K. Oldham, B. Hahn, and P. Park, "On-off control for low-power servo control in piezoelectric microrobotics", *Proc. 2008 ASME Dynamic Systems and Control Conference*, Ann Arbor, MI, U.S.A. 2008.
- [48] L. H. Ragan, "Radio receiver with adaptive on-off control," U.S. Patent 5,155,479, 1992.
- [49] P. V. Zhivoglyadov, R.H. Middleton, M. Fu, "Localization based switching adaptive control for time-varying discrete-time systems," *IEEE Trans. Automatic Control*, **45**(4), 752-755, 2000.
- [50] R. Breddermann, "Realization and application of a self-tuning on-off Controller," *Lecture Notes in Control and Information Sciences*, Springer Berlin, Berlin, Germany, pp.74-83, 1980.
- [51] M. Golob, B. Tovornik, and D. Donlagic, "Comparison of the self-tuning on-off controller with the conventional switching controllers," *1<sup>st</sup>. IEEE Conf. on Control Applications*, **2**, Dayton, OH, U.S.A. pp. 962-963, 1992.
- [52] J. C. Spall, "Model-free control of nonlinear stochastic systems with discrete-time measurements," *IEEE Trans. Automatic Control*, **43**(9), 1198–1210, 1998.
- [53] Z. Hou, and W. Huang, "The model-free learning adaptive control of a class of SISO nonlinear systems," *Proc. American Control Conference*, Albuquerque, NM, June, pp. 343-344 (1997).

- [54] C. -H. Wang, T. -C. In, T. -T. Lee, and H. -L. Liu, "Adaptive hybrid intelligent control for uncertain nonlinear dynamical systems," *IEEE Trans. Sys., Man and Cybernetics*, **32**(5), 583-587, 2002.
- [55] S. N. Huang, K. K. Tan, T. H. Lee, "Nonlinear adaptive control of interconnected systems using neural networks," *IEEE Trans. Neural Networks*, **17**(1), pp. 243-246, 2006.
- [56] T. H. Hayakawa, W. M. Haddad, N. Hovakimyan, "Neural network adaptive control for a class of nonlinear uncertain dynamical systems with asymptotic stability guarantees," *IEEE Trans. Neural Networks*, **19**(1), 80-89, 2008.
- [57] C. W. Lim, T. Y. Chung, and S. J. Moon, "Adaptive bang-bang control for the vibration control of structures under earthquakes," *Earthquake Engineering and Structural Dynamics*, **32**, pp. 1977-1994, 2003.
- [58] K. Ahn and S. Yokota, "Intelligent switching control of pneumatic actuator using on/off solenoid valves," *Mechatronics*, **15**(6), pp. 683-703, July 2005.
- [59] J. C. Spall, "Multivariate stochastic approximation using a simultaneous perturbation gradient approximation," *IEEE Trans. Automatic Control*, **37**(3), 332-341, 1992.
- [60] J. C. Spall, "An overview of the simultaneous perturbation method for efficient optimization," *J. Hopkins APL Tech. Dig.*, **19**(4), 482-492, 1998.
- [61] J. C. Spall, "A one-measurement form of simultaneous perturbation stochastic approximation," *Automatica*, **33**(1), 109-112, 1997.
- [62] J. C. Spall, "Implementation of the simultaneous perturbation algorithm for stochastic optimization," *IEEE Trans. Aerospace and Electronic Syst.*, **43**(3), 817-823, 1998.
- [63] Texas Instruments, "TMS320C5000 ultra-low-power DSPs," Datasheet, [www.ti.com](http://www.ti.com), 2012.
- [64] G. Gautschi, *Piezoelectric Sensorics*, Springer. 2002.
- [65] R. Horowitz, T. L. Chen, K. Oldham, X. Huang, R. Nagamune, and Y. Li, "Microactuators for dual-stage servo systems in magnetic disk files," *Springer Handbook of Nanotechnology Edited by B. Bushan*, part F.50, 2006.
- [66] Microchip Tech. Inc., "Driving capacitive loads with op amps," AN 884.

- [67] R. Grag and S. P. Khatri, *Analysis and Design of Resilient VLSI Circuits*, Springer, 2010.
- [68] J. P. Uyemura, *CMOS Logic Circuit Design*, Kluwer Academic Publisher, 2002.
- [69] H. Kam, T.-J. K. Liu, D. Markovic, and E. Alon, "Design, optimization, and scaling of MEM relays for ultra-low-power digital logic," *IEEE Trans. Electron Devices*, vol. 58. no. 1, pp. 236-250, 2011.
- [70] Texas Instruments, "Op amp noise theory and application," Available: [www.ti.com](http://www.ti.com).
- [71] National Semiconductor, "Select by operating voltage and supply current." Available: [www.national.com/en/amplifiers](http://www.national.com/en/amplifiers).
- [72] P. Kaur, M. Kaur, and G. Singh, "Low power low noise CMOS chopper amplifier," *International Journal of Electronics and Computer Science Engineering*, vol. 1, no. 2, pp. 734-740 (2012).
- [73] C. Chen and Z. Li, "A low-power CMOS analog multiplier," *IEEE Trans. Circuit and System*, **53**(2), pp. 100-104, 2006.
- [74] B. Hahn, and K. Oldham, "Model-free adaptive on-off step controller for piezoelectric micro-robotics," *Proc. 2009 ASME Dynamic Systems and Control Conference*, 2009.
- [75] S. K. Lucas, C. Y. Kaya, "Switching-time computation for bang-bang control laws," *2001 Proc. American Control Conf.*, 176-179, 2001.
- [76] F. Rezaayat, "On the use of an SPSA-based Model-free controller in Quality Improvement," *Automatica*, **31**(6), pp. 913-915, 1995.
- [77] V. Aksakalli, D. Ursu, "Control of nonlinear stochastic systems: model-free controllers versus linear quadratic regulators," *2006 Proc. The 45<sup>th</sup> IEEE Conf. Decision and Control*, 4145-4150, 2006.
- [78] Q. Zhang, Y. Zhou, X. Liu, X. Li, W. Gan, "A nonlinear ANC system with a SPSA-based recurrent fuzzy neural network controller," *2007 Proc. The 4<sup>th</sup> ISNN*, pp. 176-182, 2007.
- [79] D. C. Chin, "Comparative study of stochastic algorithms for system optimization based on gradient approximations," *IEEE Trans. Syst., Man, and Cybernetics*, **27**, 244-249, 1997.

- [80] P. Sadegh, J. C. Spall, "Optimal random perturbation for stochastic approximation using simultaneous perturbation gradient approximation," *IEEE Trans. Automatic Control*, **43**, 1480–1484, 1998.
- [81] P. Sadegh, "Constrained optimization via stochastic approximation with a simultaneous perturbation gradient approximation," *Automatica*, **33**(5), 889-892, 1997.
- [82] J. -C. Fort, and G. Pages, "convergence of stochastic algorithms: from the Kushner-Clark theorem to the Lyapounov functional method," *Adv. in Appl. Prob.*, **28**(4), 1072-1094, 1996.
- [83] L. Ljung, "Analysis of Recursive Stochastic Algorithms," *IEEE Trans. Automatic Control*, **22**(4), 551-575, 1977.
- [84] T. H. Gronwall, "Note on the derivatives with respect to a parameter of a system of differential equations," *Ann. of Mat.* **20**, 292-296, 1919.
- [85] N. Amann, D. H. Owens, and E. Rogers, "Iterative learning control for discrete-time systems with exponential rate of convergence," *IEEE Proc.-Control Theory Appl.*, Vol. 143, No. 2, pp. 217-224, 1996.
- [86] M. V. Solodov, 2003, "Convergence rate analysis of iterative algorithms for solving variational inequality problems," *Math. Program.*, A96, pp 513-528, 2003.
- [87] S. Hillenbrand and M. Pandit, "A discrete-time iterative learning control law with exponential rate of convergence," *Proceedings of the 38th Conference on Decision and Control*, Phoenix, AZ, USA, pp. 1375–1380, 1999.
- [88] S. Arimoto, S. Kawamura, F. Miyazaki, and S. Tamaki, "Learning control theory for dynamical systems," *Proceedings of the 24th Conference on Decision and Control*, Ft. Lauderdale, FL, USA, pp. 1375–1380, 1985.
- [89] T. Ishihara and H. Takeda, "A discrete-time design of robust iterative learning controllers," *IEEE Trans. Systems, Man, and Cybernetics*, Vol. 22, No. 1, pp. 74-84, 1992.
- [90] J.-X. Xu and Y. Tan, *Linear and Nonlinear Iterative Learning Control*, Springer, 2003.
- [91] B. Hahn and K. Oldham, "Sensing parameter selection for ultra-low-power system identification," accepted on *Proceedings of 2012 the American Control Conference*, Montreal, Canada.

- [92] B. Hahn and K. Oldham, "On-off iterative adaptive controller for low-power micro-robotic step regulation," *Asian Journal of Control*, published online, DOI: 10.1002/asjc.410, 2011.
- [93] B. Hahn and K. Oldham, "A model-free on-off iterative adaptive controller based on stochastic approximation," *IEEE Trans. Control System Tech.*, vol. 20, no. 1, pp. 196-204, 2012.
- [94] B. Hahn and K. Oldham, "Convergence rate estimation for iterative adaptive on-off control of a piezoelectric microactuator," *IEEE Trans. Control System Tech.*, Submitted on May 2012.
- [95] B. Hahn and K. Oldham, "Convergence rate estimation for iterative adaptive on-off control of a micro-robotic leg joint," accepted on *Proc. 2012 ASME Dynamics Systems and Control Conference*, Ft. Lauderdale, FL, USA, 2011.
- [96] Texas Instruments, "Noise Analysis in Operational Amplifier Circuits," Available: [www.ticom](http://www.ticom).
- [97] Analog Devices Corp., "OP490 low-voltage quad operational amplifier," Datasheet, [www.analog.com](http://www.analog.com), 2006.
- [98] L. Gerencser, "Convergence rate of moments in stochastic approximation with simultaneous perturbation gradient approximation and resetting," *IEEE Trans. Autom. Control*, Vol. 44, No. 5, pp. 894-905, May. 1999.
- [99] S. Sastry, *Nonlinear Systems: Analysis, Stability, and Control*, Springer, 1999.